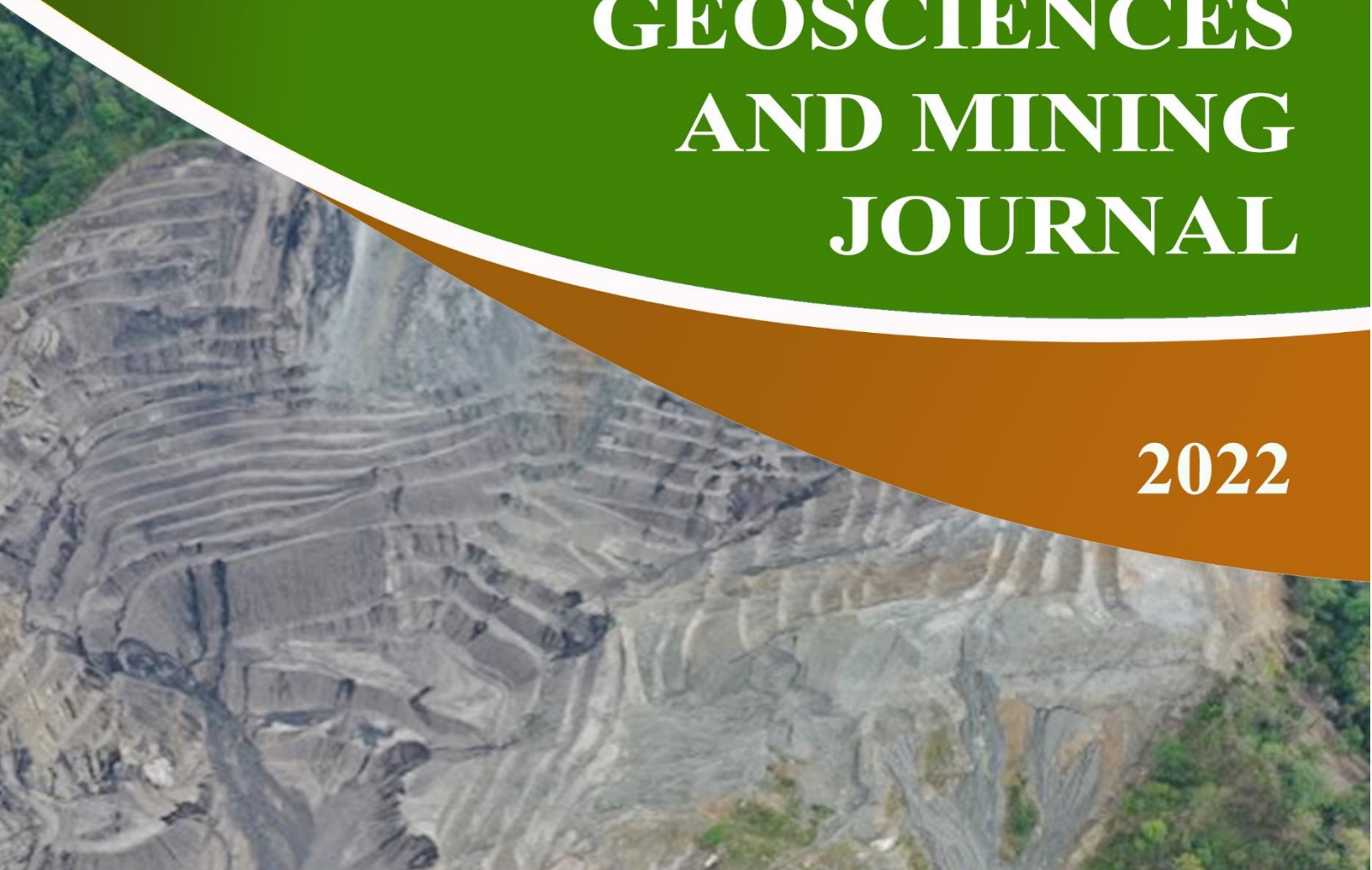




Series-03

GEOSCIENCES AND MINING JOURNAL

2022



Copyright © 2022 Department of Geology and Mines, MoEA

All rights reserved. No part of this book may be reproduced or used in any manner without the prior written permission of the copyright owner, except for the use of brief quotations in a book review.

To request permissions, contact the publisher at dgm@moea.gov.bt

Editorial Team:

Dr. Dowchu Drukpa, Chair

Mr. Ugyen Dorji, Member

Ms. Nityam Nepal, Member

Ms. Sonam Tshomo, Member

Pratik Bhattarai, Member

Pem Dorji Tamang, Member

Cover design by:

Mr. Kinley Norbu



དཔལ་ལྷན་འབྲུག་གཞུང་། བརྟན་རྒྱལ་ལྷན་ཁག།
ས་རིག་དང་ས་གཏེར་ལས་ཁུངས་ རྒྱལ་ཕྱི་ལྷན།
Department of Geology and Mines
Ministry of Economic Affairs
Royal Government of Bhutan
Thimphu



Foreword



On behalf of the Department of Geology and Mines, I am excited to bring the third edition of “Geosciences and Mining Journal 2022”. In this new edition of the journal series, the authors present their earnest work related to various subjects in the field of geosciences and mining.

The previous series presented a major overview of the mining sector. In this series, research-based articles covering various techniques ranging from **geophysical methods, remote sensing, and slope stability analysis methods** have been presented. The findings from Landslide inventory mapping carried out by the Department for 15 Dzongkhags are also presented. Bhutan is located in one of the most active tectonic regions, making the country highly vulnerable to geological hazards such as earthquakes and landslides. Due to growing land use and extreme weather patterns, the risk associated with these hazards is anticipated to rise.

A comprehensive knowledge of the geology is required for the growth and development of the mineral sector in the country. Today, the Department has completed regional geological mapping for about 50% of the country. A brief overview of precious and semi-precious stones is shared to disseminate the occurrence of such minerals in the country. The services provided by the chemical laboratory are also highlighted as information. Also, the taxation system in the mining sector in terms of various types of royalty systems and mineral rents have been discussed. Bhutan’s taxation in terms of the Ad-valorem-based royalty system implemented along with the mineral rents serve as a major contribution to the overall economy of the country. The mining sector at a glance presents the contribution of mining to the national economy.

With this, I would like to express my sincere appreciation to those who have contributed to this edition and encourage others in the Department to contribute to the future series.


23.11.2022

(Phuntsho Namgyal)
Director, DGM

Table of Contents

Application of Near-Surface Geophysical Methods for Imaging Active Faults in the Himalaya.....	1
Geophysical Prospecting Using Microtremors to Estimate 1-D Shallow Shear Wave Velocity Profiles in Thimphu, Bhutan.....	20
Use of Differential SAR Interferometry (DInSAR) and Offset Tracking in Estimation of Glacier Movement	28
Slope Stability Analysis using Limit Equilibrium Method.....	39
Mineral Royalties – a form of tax in mining sector	46
Mining sector at glance.....	54
Overview of gemstones in Bhutan.....	66
Toposheet wise Mapping Master Plan 2021	71
Landslide Inventory of 15 Dzongkhags.....	81
Overview of Geo-chemical Laboratory	87

APPLICATION OF NEAR-SURFACE GEOPHYSICAL METHODS FOR IMAGING ACTIVE FAULTS IN THE HIMALAYA

Dowchu Drukpa¹, Stéphanie Gautier², Rodolphe Cattin³

Abstract

Near-surface geophysical investigation is a relevant tool to provide quantitative constraints of the nature and the geometry of shallow fault zones. The strategy consists of combining results coming from different geophysical methods, including electrical resistivity, seismic and gravity measurements, to obtain a detailed characterization of the first 100s of m in terms of geometry (faults, stratigraphy, buried markers), cumulative deformation on the down throw, and quantification of the physical parameters around the fault. Integrating the new constraints on fault geometry and geomorphological and regional geodetic information allows one to estimate fault slip rate and to identify potential slip partitioning between horizontal and vertical displacement. The characterization of the seismic sources and slip partitioning has major implications in seismic hazard evaluation in the Himalaya area.

1. Introduction to near-surface geophysics

Geophysical methods have been widely used for the characterization of subsurface tectonic

features (Suzuki et al., 2000; Demanet et al., 2001; Morandi & Ceragioli 2002; Louis et al., 2002; Wise et al., 2003; Nguyen et al., 2005, 2007; Kaiser et al., 2009). Depending on the scale of investigation, geophysical methods can be divided into two categories (Mussett et al., 2000): deep surveys, with penetration depth ranges from 100 m to several km, which are mainly used to define regional seismotectonic models and, near-surface surveys which image structures at shallow depth (0-200 m) such as fault systems, lithological interfaces, landslide bodies as well as cumulative deformation. The same near-surface geophysical techniques are also deployed to quantify groundwater resources, to monitor active geohazards, for archeo-geophysical exploration and geotechnical site characterization (Telford et al., 1990; Reynolds, 1997). The success of any geophysical investigation is dependent on several factors, including the presence of strong contrasts in terms of physical properties, the availability of geological, geomorphological or hydrological information, and practical aspects for the

¹ *Dowchu Drukpa, Specialist, Department of Geology and Mines, Thimphu, Bhutan.
Doctor of Philosophy, University of Montpellier, France, Email: ddukpa@moea.gov.bt*

² *Stéphanie Gautier, University of Montpellier, France*

³ *Rodolphe Cattin, University of Montpellier, France*

deployment such as topography or site accessibility. Having good a priori information is critically important to choose relevant locations for the surveys and validate the geophysical investigations' outcome.

Various near-surface geophysical methods are particularly adapted to image internal structures and physical properties of fault zones, in a depth range between a few meters to a hundred meters (Demagnet et al., 2001; Villani et al., 2015). In particular, geophysical data can contribute to characterizing the geometry of the fault dip angle, the thickness of quaternary layers, and possible offsets at shallow depths. Those data can also help detect blind faults close to the surface and find the appropriate location for trench excavations. Despite promising results on many fault zones around the world (Nguyen, 2005), near-surface geophysical have been little implemented in the Himalayas.

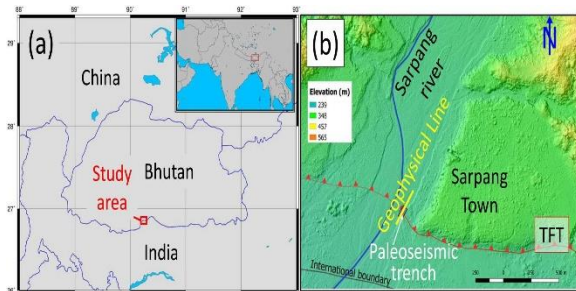


Figure 1. (a) Location of the Kingdom of Bhutan and the study area in south Central part of Bhutan. (b) High resolution Digital Elevation model (DEM) from satellite image of the study area showing the Topographic Frontal Thrust (TFT) fault trace, the location of the paleoseismic trench studied by Le Roux-Mallouf et al. (2016) and our geophysical profile (yellow line).

In this framework, near-surface geophysical investigations were carried out in central southern Bhutan for shallow subsurface

imaging of the Topographic Frontal Thrust (TFT) (Figure 1). At the front, a priori information of the exact location and estimated dip angle of the fault on the surface were gathered from previous geomorphological and paleoseismological studies (Berthet et al., 2014; Le Roux-Mallouf et al., 2016). Observations in the paleoseismic trench also confirmed rheological contrasts, suggesting strong physical parameters variations as usually described in fault zones (Boness & Zoback, 2004; Hung et al., 2009; Jeppson et al., 2010), which are in favor of geophysical imaging. Further, the case study site is located in the foothills, characterized by low elevation variations. This specific geographic feature ensures easy accessibility and feasibility of surveys. Geophysical data for the case study site is acquired along the east side of Sarpang river, where the east-west trending TFT trace was intersected by the previous paleoseismic trench study down to 1 m depth (Figure 2). Using various geophysical methods (Electrical Resistivity Tomography (ERT), seismic refraction, and gravity measurements) provides images of different physical properties at different depths of investigation. All geophysical data were collected along the same N-S profile, with varying lengths of spread depending on the methods. The midpoints of the geophysical surveys were positioned at the fault location at the surface deduced from the paleoseismic study.

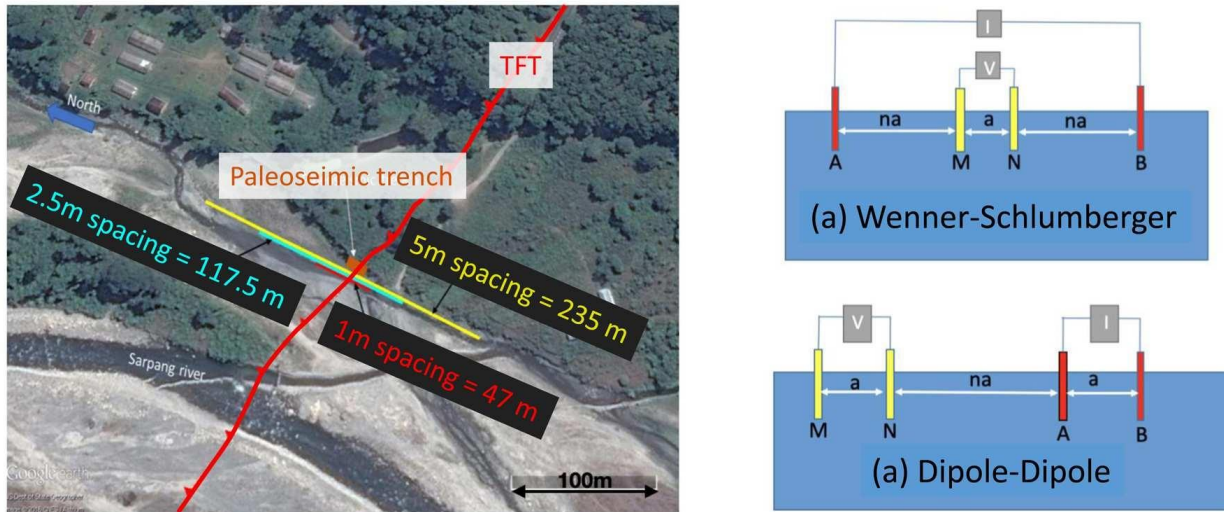


Figure 2. Location of both the Electrical Resistivity Tomography (ERT) surveys (yellow, blue, and red lines for the 5 m, 2.5 m and 1 m electrode spacing soundings, respectively) and the paleoseismic trench in Sarpang site (left) and geometric configurations used in the study (right).

2. Geophysical methods for fault mapping

2.1. Electrical resistivity tomography (ERT)

Low resistivity materials generally characterize fault zones. Hence, electrical resistivity tomography is widely used for near-surface fault imaging (Phillips & Kuckes, 1983). To obtain well-resolved images close to the surface as well as the deeper depth of investigation, combining ERT profiles with different electrode spacing is recommended (Nguyen et al., 2005; Gelis et al., 2010). Among the different geometric configurations available for ERT surveys, the commonly used Wenner-Schlumberger (WS) and Dipole-Dipole (DD) configurations (Figure 2) appears to achieve a good compromise between vertical and horizontal resolution and effect of noise (Dahlin & Zhou, 2004; Loke, 2015).

Accordingly, in south Bhutan, both WS and DD electrical resistivity soundings, with three different electrode spacings (1, 2.5, and 5 m), were carried out (Drukpa et al., 2017). The topography along the profile is relatively smooth, with variations less than 1.3 m. Therefore, no topographic correction was necessary for resistivity data analyses. The obtained ERT inverted sections (Figure 3) illustrate that an electrical resistivity survey is a valuable tool for characterizing faults in superficial layers from the ground surface. The different surveys provided consistent results. The WS electrical images appear to be more robust because of a greater sensitivity to both lateral and vertical variations (Nguyen et al., 2007). These resistivity images point out a major sub-vertical discontinuity, which is consistent with the prolongation of the fault towards the surface.

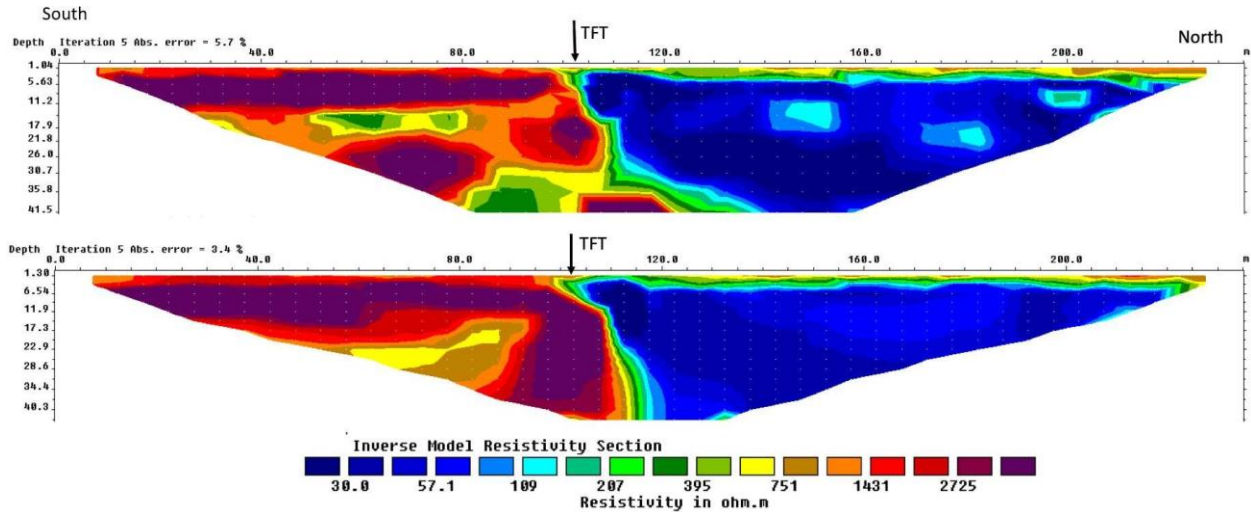


Figure 3. 2D 5m-spacing Dipole-Dipole ERT model (top) and Wenner-Schlumberger model (bottom) inverted with RES2DINV (Loke, Barker 1996). Both images represent models obtained after 5 iterations. The RMS corresponds to the misfit between observed and computed data. The TFT label indicates the location of fault.

More precisely, the fault zone is marked by high electrical resistivity contrasts (~1:100) with a nearly vertical contact down to ~40 m depth. The north side shows a uniform apparent resistivity layering with a thin upper layer resistivity of 200-1000 Ωm overlying a very low resistivity layer < 100 Ωm. The south side shows relatively constant resistivity values (1000-4000 Ωm) with a very high resistivity zone located at 5-15 m depth at the southern end of our profile. A thin upper layer of low resistivity is also observed southward.

2.2. Seismic Tomography

The seismic tomography technique is an additional method for characterizing near-surface fault zone (Demagnet et al., 2001; Villani et al., 2015) by usually estimating P-wave velocity models from travel times. Like ERT, data acquisition layout design for seismic tomography should obtain high-resolution images and achieve the target

depth of investigation. These targets can be achieved by maintaining appropriate receiver spacing and roll-along where ever needed to increase the spread length and, therefore deeper depth of investigation.

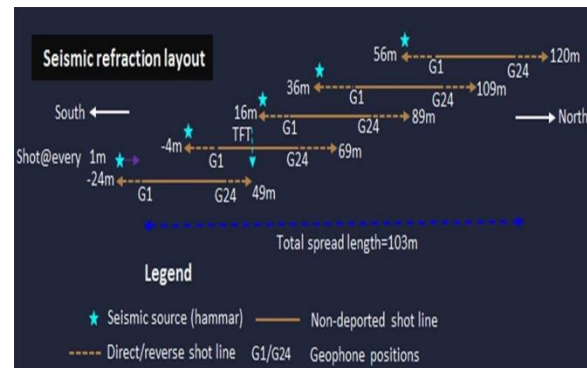


Figure 4. Seismic data acquisition layout plan.

A seismic survey co-located with ERT profiles was carried out for the case study. The seismic layout comprises of 1 m receiver spacing and five roll-along (shift of 20 geophones and overlap of 4 geophones each time) to finally acquire a 103 m long seismic profile (Figure 4) (Drukpa et al., 2017). Seismic sources were generated by hitting a

10 kg sledgehammer on an iron plate at each geophone along each seismic line. A total of 5,760 first-arrivals travel times were manually hand-picked (Figure 5). As for ERT, no topographic correction was implemented.

Seismic refraction images show that the TFT fault implies an abrupt transition of the travel times resulting in a strong contrast of both the ray distribution and the velocity values (Figure 5). The velocity model confirms the presence of a shallow interface on the northern side.

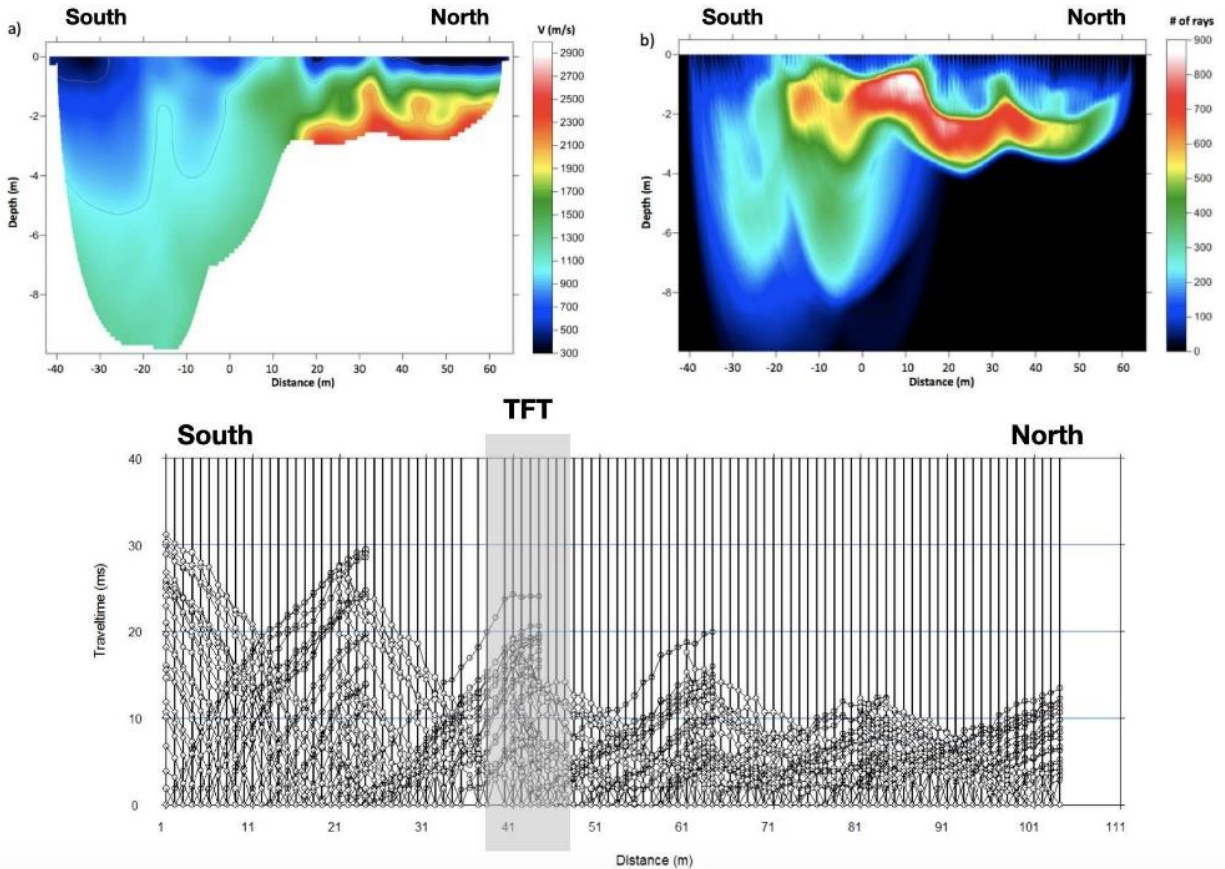


Figure 5. Top: a) Seismic tomographic refraction image showing the velocity variations of the both sides of the TFT obtained using RAYFRACT software; The TFT fault trace is located at 0 m. b) Ray coverage illustrating the resolved area. Bottom: Hodochrones of the traveltimes along the seismic line

2.3. Microgravity

The gravity method is a versatile geophysical technique to determine density contrast within the Earth. Variations of the gravitational field due to the density contrasts are measured using extremely sensitive instruments to identify anomalies at depth. This technique allows determining and locating the presence of a deficit or an excess of mass in the subsurface, which corresponds to negative or positive anomalies. In near-surface geophysics, micro-gravimetry is carried out for various investigations such as detection of karsts and voids, measurements of sediment thickness, archaeological surveys or mineral exploration (Telford et al., 1990).

In southern Bhutan, gravity measurements were recorded along the same South-North profile as the ERT and seismic lines (Drukpa et al., 2017). From the center point of the survey line positioned at the paleoseismic trench, gravity readings were acquired at every 5 m on either side of the profile covering a distance of 30 m and 105 m to the south and the north, respectively. Spatially denser gravity points were collected in the vicinity of the fault area. Using the GravProcess software (Cattin et al., 2015), network adjustment was performed and topographic effect was corrected from accurate elevation data gathered along the same profile assuming a constant density of $2,670 \text{ kg/m}^3$. A regional trend of $-1.58 \text{ } \mu\text{Gal/m}$ obtained by Hammer et al. (2013), is also taken into account. The final dataset consists of 139 corrected gravity measurements, which highlight variations along the profile (Figure 6). No change at the fault trace is observed, but a transition occurs

at around 27 m north of the fault. The southern part of the profile is characterized by a moderate northward increase of ca. $4 \text{ } \mu\text{Gal/m}$. The northern part shows an increase twice as large with a northward increase of ca. $450 \text{ } \mu\text{Gal}$ at 65 m.

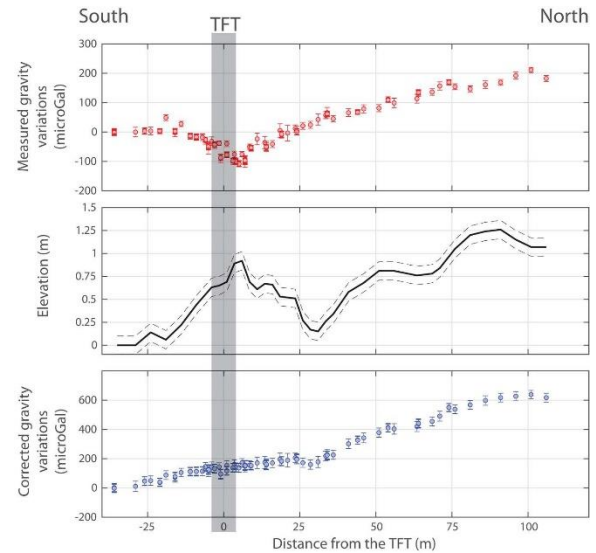


Figure 6. Measured gravity (top), elevation (middle) and gravity variations corrected for both topographic effect and regional trend (bottom) along the study profile. Data uncertainty is associated with both accuracy of the CG5 gravimeter and error in elevation measurement.

3. Inversion technique and its application to geophysical data from Sarpang

Geophysical inversion is a mathematical and statistical tool used to recover physical properties models from field observations and information on geological structures (Tarantola, 2005). Inversion methods can be divided into deterministic and stochastic approaches. Deterministic inversion is a conventional linear approach that consists in gradually updating the model parameters to minimize the differences between observed

and theoretical data computed inside the output model (Ellis & Oldenburg, 1994). It is a model-driven inversion approach, relatively easy to implement. Still, strong a priori constraints are required to converge towards the best acceptable model. Unlike the deterministic approach (Ramirez et al., 2005), the stochastic inversion is a statistical process in which prior information and forward modeling are combined to produce different output models consistent with the available data. This approach provides a more complete description of the possible acceptable solutions but can be time consuming. In this framework, Drukpa et al. (2017) propose a novel common stochastic approach to invert the near-surface geophysical data. Following Mosegaard & Tarantola (1995), a Markov Chain Monte Carlo technique is used to pseudo-randomly generate a large collection of models according to the posterior probability distribution.

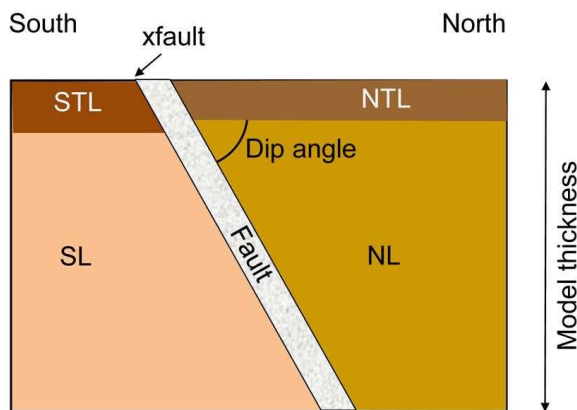


Figure 7. Geometry of the model used in the stochastic inversion. STL - South Top layer, NTL - North Top Layer, SL - South Layer and NL - North Layer. *xfault* is the prior location of the fault as observed in the field. Model thickness is associated with the thickness investigated by each geophysical method.

This approach was applied to shallow geophysical data for the case study site in south Bhutan. Assuming a simplified geometry (Figure 7), each model is associated with only five bodies, including a south (STL) and north (NTL) top layers, a south (SL) and north (NL) shallow layers and a fault layer. Based on this formulation, a set of models results for a given dataset combines ten parameters estimations that include either the velocity, the resistivity, or the density of each body, as well as the thickness of layers, the fault location, and the fault dip angle. In order to fix the limit of the solution-space, *a priori* parameters ranges for resistivity and velocity values are obtained from preliminary deterministic inversion using RES2DINV (Loke & Barker, 1996) and RAYFRACT (Schuster, 1993; Sheehan et al., 2005; Pasquet et al., 2015), respectively. Assuming prior density contrasts between NL and the other bodies in the -500 to 500 kg/m^3 . Concerning the geometry, prior information comes from structural and geomorphological observations (Long et al., 2011; Le Roux-Mallouf et al., 2016), which yield top layers thickness less than 5 m and a fault dip angle between 10° and 80° .

The pseudo-random walk through this multidimensional parameter space is controlled by the following rules for the transition between model m_i to model m_j :

If $L(m_j) \geq L(m_i)$ then accept the proposed transition from i to j

If $L(m_j) < L(m_i)$ then accept the proposed transition from i to j with the probability $\frac{L(m_j)}{L(m_i)}$

where $L(m_i)$ and $L(m_j)$ are the likelihood of the old and the new model, respectively. Here we assume that the likelihood function can be written as

$$L(m_i) = \exp \left(-\frac{1}{n_{obs}} \sum_{n=1}^{n_{obs}} \frac{|calc_n(m_i) - obs_n|}{\sigma_n} \right)$$

where n_{obs} is the number of data points, obs is the data vector and σ^2 is the total variance, i.e., the uncertainties associated with each data point. $calc(m_i)$ is the forward modeling function associated with the model m_i . This function is obtained using the different forward modeling depending on the considered datasets described below.

Two-dimensional geoelectrical modeling is performed with the software package R2 (Binley & Kemna, 2005; Binley, 2015). The current flow between electrodes is obtained using a quadrilateral mesh with an exponentially increasing node at depth and a constant node spacing in the horizontal direction. For seismic refraction, synthetic travel times are computed using the real receiver-shot configuration and solving the Eikonal equation with a finite-difference algorithm (Podvin & Lecomte, 1991). Rays are traced in the obtained time field with the a posteriori time-gradient method. More precise travel times are then estimated along ray paths (Priolo et al., 2012). The model is discretized on a regular grid. The velocity field is parametrized by trilinear interpolation between grid nodes. Gravity variations along the profile are calculated from the 2D formulations of Won & Bevis (1987), which provide the gravitational acceleration due to n-sided polygons. Here the polygons are associated with the geometry of the five

bodies described above. The model is extended southward and northward to avoid edge effects at the two terminations.

The posterior probability of each model parameter is then obtained from the final collection of the 5×10^5 sampled models. Compared to the commonly deterministic approach, which leads to the more acceptable model, the main advantages of stochastic inversion include its ability (1) to assess the fault geometry because no smoothing is applied, (2) to provide a measurement of the uncertainties on the obtained dip angle, and (3) to allow the study of trade-off analysis between geometric and either electrical resistivity, velocity or density properties. Using parallelism, the computation time associated with electrical, seismic, and gravity inversion on a ten-core workstation is between ca. 10 and 24.5 hours.

4. Geophysical results from south Bhutan

4.1. Electrical Resistivity Tomography

All Dipole-dipole and Wenner-Schlumberger data were separately inverted using the stochastic approach. The set of most likely models derived from the stochastic approach explains the main features of the observed apparent resistivity pattern, except southward where some residual differences persist (Figure 8). It points out a high fault dip angle of ca. 70° (Figure 8).

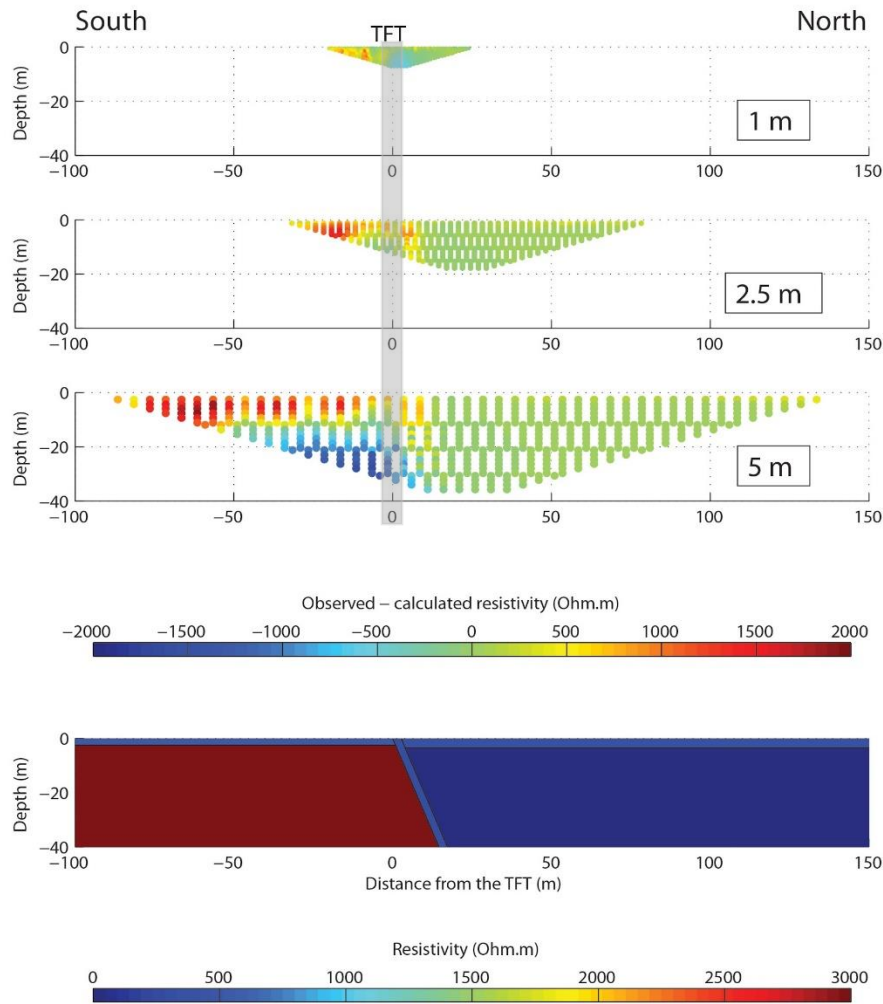


Figure 8. Misfit between observed and calculated ERT pseudo-sections for electrode spacing of 1 m, 2.5 m and 5 m using WS configuration. This misfit is defined as the difference between the observed and calculated resistivities using the electrical model plotted at the bottom.

Bivariate frequency histograms indicate no tradeoff between dip angle and the other geometric and electrical parameters. This figure constrains the model parameters and discusses the robustness and relevance of the results.

In southern Bhutan, the histograms suggest a 2.5 m thick fault zone. However, the resistivity of this unit remains poorly resolved. The inversion approach images thin

low-resistive top layers, both on the southern (~2.5 m, ~550 $\Omega \cdot m$) and northern sides (~3.5 m, ~350 $\Omega \cdot m$). The small resistivity contrasts between those two top layers can prevent the estimation of the fault geometry at a very shallow depth (< 5 m). On the contrary, due to the very high resistivity contrast between the two deeper bodies (SL~3,300 $\Omega \cdot m$ vs. NL~30 $\Omega \cdot m$), we consider the obtained fault dip angle as a

4.2. Seismic tomography

well-constrained parameter down to 40 m depth. This assumption is confirmed by the narrow posterior distribution obtained for dip angle. Finally, there exist some discrepancies between the observed and calculated pseudo-sections on the south part. Based on the simplified geometry of the model assuming horizontal layering, the stochastic inversion procedure cannot explain the north-south resistivity variations in the footwall of the TFT.

Altogether, this information on both geometry and resistivity contrast suggests an apparent resistivity contrast between both sides of the fault and a constant dip angle of $\sim 70^\circ$ over a depth ranging between ca. 5 m and ca. 40 m (Figure 9).

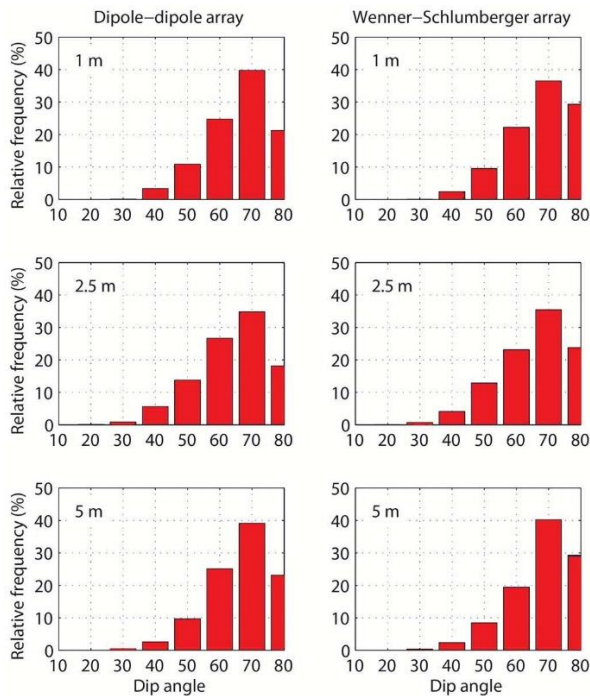


Figure 9. Distribution of TFT dip angle from ERT sections using both dipole-dipole and Wenner-Schlumberger arrays. Electrode spacing ranges from 1 m (top) to 5 m (bottom).

The set of final velocity models resulting from the stochastic inversion approach provides low travel-time residuals of ± 3 ms in average for most of the source-receiver (Figure 10). This suggests that assuming simple geometry captures most of the main features of the velocity field. Furthermore, travel-time residuals show a relatively homogeneous pattern, except close to the fault trace between -5 and 15 m, where residuals abruptly increase from -5 ms to 4 ms northward. This result demonstrates that the presence of the fault influences seismic data.

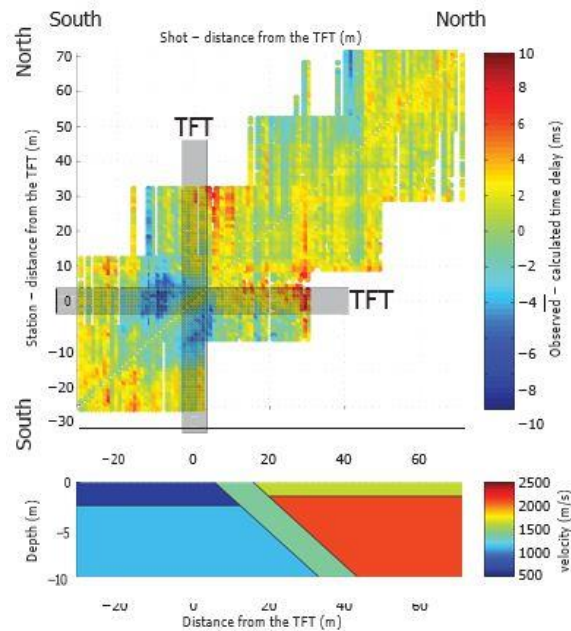


Figure 10. Misfit between observed and calculated time delay corresponding to the traveltime residuals. This misfit is defined as the difference between the observed and calculated travel time using the velocity model plotted at the bottom. Compared to resistivity model (Figure 8), one can noted the limit of the y-axis, which corresponds to a lower depth of investigation.

Ray coverage (Figure 5) indicates a shallower resolution depth compared to ERT investigations. Resolution depth varies

between the two sides of the fault, from ca. 8 m to ca. 5 m in the south and north, respectively. At these depths, the velocity models resulting from both the stochastic inversion (Figure 10) and tomography (Figure 5) point out high velocity variations of about 50% at the transition of the fault zone. The 2D seismic model also emphasizes strong vertical velocity changes on both sides of the fault. High velocity contrasts between top and bottom layers induce a concentration of rays at a depth between 2 and 4 m, which prevents deeper investigations, in particular in the north.

Taking into account this shallow investigation depth, the velocity field can be characterized by two deeper units of $V_p \sim 1,100$ m/s (SL) and $V_p \sim 2,100$ m/s (NL) below by two superficial low-velocity layers (STL: ~ 5 m, ~ 900 m/s and NTL: ~ 3 m, $\sim 1,600$ m/s). The stochastic inversion procedure also reveals that seismic data are sensitive to the dip angle parameter (Figure 11). The 2D seismic inversion result suggests a northward dipping fault with a very low-angle of ca. 20° - 30° at depths down to ca. 5 m, which is consistent with field observations in the trench (Le Roux-Mallouf et al., 2020). This observation is also in agreement with both ERT profile (Figure 3) and the related stochastic ERT results, which displays a change in dip angle with a gentler slope of the TFT fault near the surface. Without information on the near-surface geometry of the fault, a constant fault dip angle was assumed and the same model was used for the different ERT configurations. Thereby the inversion procedure could not image this dip

angle change near the surface with resistivity data only.

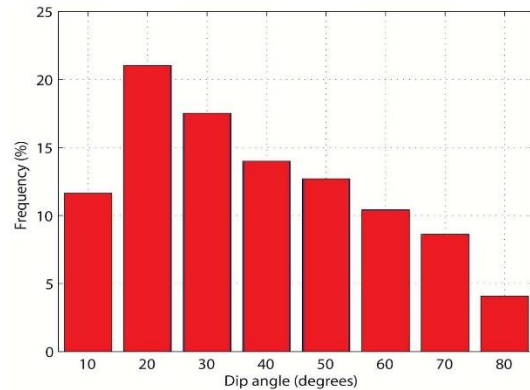


Figure 11. Distribution of TFT dip angle obtained from seismic measurements.

Hence, seismic data inversion with field observations confirms a northward dipping fault with a low angle of ca. 20° - 30° at very shallow depth. Seismic and electrical resistivity images together suggest a dip angle that increases gradually up to ca. 70° at a depth of 5-10 m.

4.3. Micro-gravity

Since gravity measurements are affected mainly by the deeper part of the model, the focus of the study is on the long wavelength of the gravity profile associated with the two south-north gravity gradients (Figure 6). The result of the stochastic inversion suggests that the observed northward increase of gravity measurements is mostly related to both Δ (the density contrast between SL and NL) and α (the fault dip angle) (Figure 12). As indicated in Figure 12, gravity measurements cannot be used to assess the other density and geometric parameters, which remain poorly constrained.

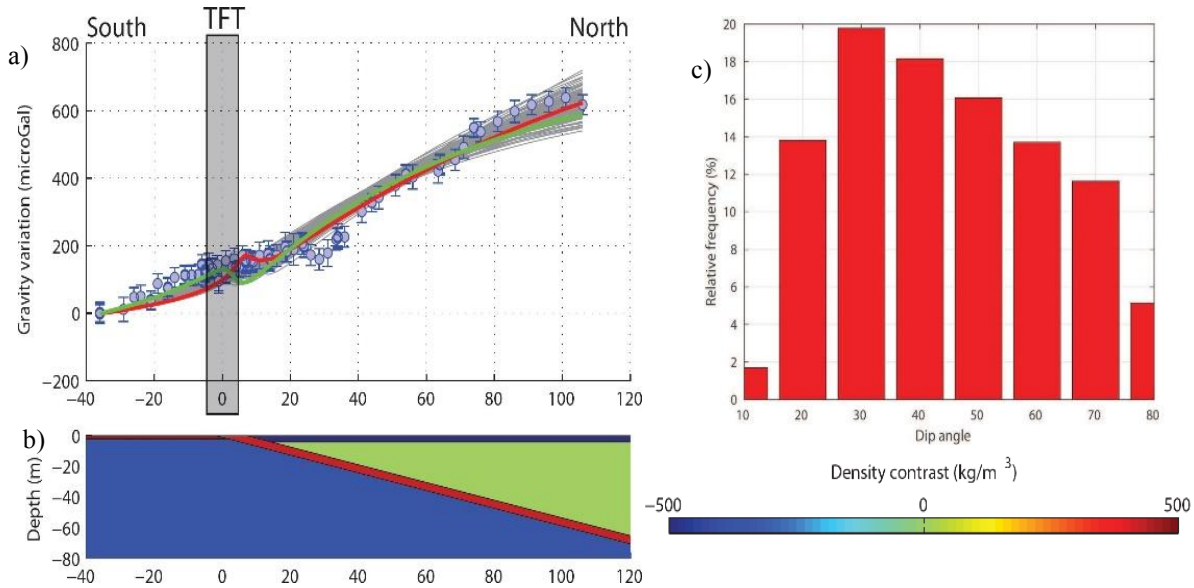


Figure 12. a) Comparison between observed (blue circles) and calculated (gray lines) gravity variations along the study profile obtained for the 100 best-fitting models. b) Density contrast models associated with the red (30° dip angle) plotted above. c) Distribution of TFT dip angle obtained from gravity stochastic inversion.

The gravity model result reveals a tradeoff between Δ and α : the higher the density contrast, the lower the fault dip angle. For $\Delta = -350 \text{ kg/m}^3$ the fault dip angle is ca. 30°, whereas for $\Delta = -200 \text{ kg/m}^3$ the fault dip angle is ca. 60° (Figure 12). This leads to a wide distribution of the fault dip angle (Figure 12c). The maximum of the distribution obtained at $\alpha \sim 30\text{-}40^\circ$ and the most likely model thickness down to 80 m depth suggests a fault that flattens at depths below 40 m.

5. Implications of near-surface geophysical findings

The geometry of the fault, especially at shallow depth, is a crucial parameter for better understanding deformation kinematics and accommodation at crustal scale. In particular, the slip rate can be estimated by combining the subsurface dip angle and

terrace dating results. The new constraints for the TFT geometry deduced from near-surface geophysical techniques allow studying stress partitioning at the frontal thrust zone and its associated seismic hazard implications in south central Bhutan.

5.1. Subsurface imaging

Taking advantage of the various scales of investigation coming from ERT, seismic and gravity methods, an accurate description of shallow structures and fault geometry at depth is obtained in the case study. The subsurface can be subdivided in three main zones:

1. a very shallow part up to 5 m depth well-constrained by both field observations and seismic data considering the ray coverage;

2. an intermediate depth part well-imaged by ERT sections between 5 and 40 m depth due to high resistivity contrasts,
3. a deeper part documented by gravity measurements below 40 m depth.

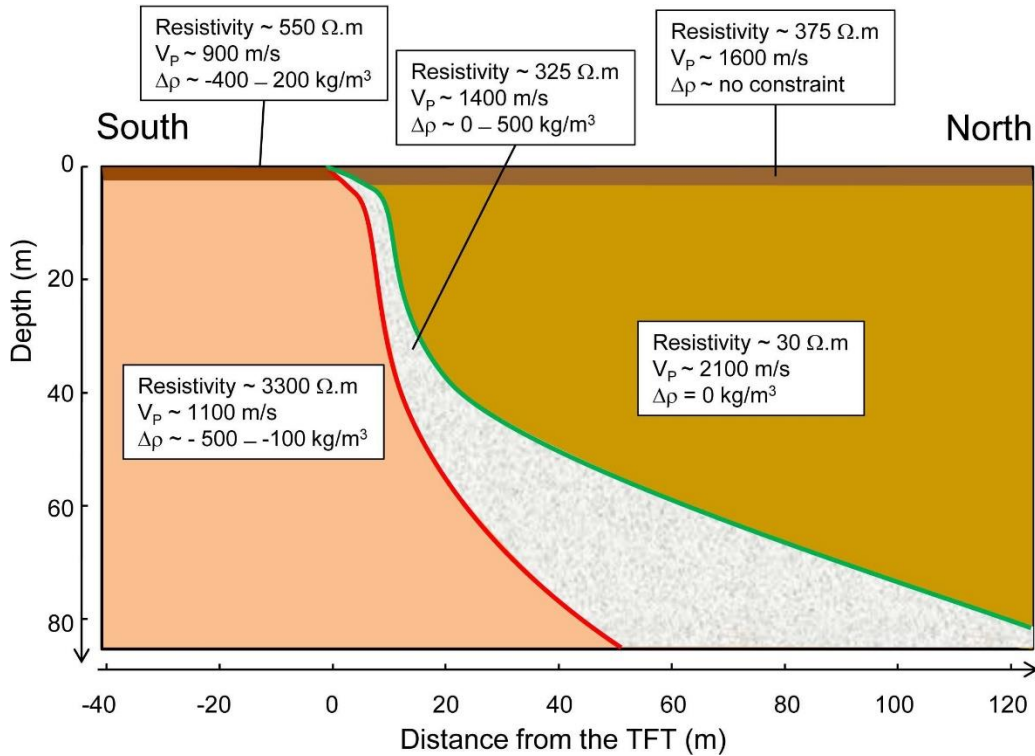


Figure 13. Simplified cross section showing the main geophysical results obtained from electrical resistivity tomography, seismic refraction and gravity measurements. Together these results suggest a TFT with a flat and ramp geometry, with a surface dip angle of $\sim 20^\circ$ reaching $\sim 70^\circ$ at 20 m depth and flattening in its deeper part. Note that dashed area is bounded by the two end-member models of fault geometry given by the green and the red lines. Hence, this area does not represent the fault thickness, which is estimated to 2.5 m.

The fault geometry discussed here arises from the integration of these three surface sensitivities.

In terms of lithological setting and water content, the geophysical datasets suggest a thin layer ($\sim 3\text{-}5$ m) that appears to be present on both sides of the fault trace and probably corresponds to recent alluvial deposits. Along the profile, resistivity and velocity variations at shallow depth may be due to a northward decrease of water saturation. Below these superficial layers, in the hanging

wall of the TFT, the obtained very low-resistivity values ($< 30 \Omega \cdot m$), the high V_p of ca. 2,100 m/s and the relatively low densities probably underline a phyllite unit, which can be observed in the field.

Overall, the geophysical methods image a more complex fault geometry than proposed by earlier studies (Berthet et al., 2014; Le Roux-Mallouf et al., 2016). The geophysical results show a TFT with a flat and listric-ramp geometry with a low dip angle of 20° - 30° at shallow depth, steeply dipping at

~70° in the middle and gradually flattening to a shallower dip angle of 30°- 40° in its deeper part (Figure 13).

5.2.Overthrusting slip rate assessment

Berthet et al. (2014) estimated a Holocene vertical slip rate of 8.8 ± 2.1 mm/yr by dating two uplifted river terraces in Sarpang area. Assuming a dip angle of 20-30°, a slip rate of 20.8 ± 8.8 mm/yr, which is consistent with the GPS convergence rate of 17mm/yr obtained across central Bhutan (Marechal et al., 2016). Finally, they conclude that the TFT mainly accommodates the Himalayan convergence. However, this major conclusion can be revisited in light of our new constraints on the TFT geometry.

First, assuming a constant overthrusting slip rate along the TFT, a vertical velocity profile is calculated from this observed uplift rate (Okada, 1985). As expected, this calculated profile depends on TFT geometry: a higher fault dip angle implies a higher uplift rate. More surprisingly, it also depends on the distance between the TFT and the location of dated samples. For instance, a distance of 5 m from the TFT yields two very different vertical velocity profiles associated with the two end-member models for the fault geometry. On the contrary, if the uplift rate is measured about 10 m north from the TFT, the uplift rate difference drastically reduces. In other words, due to the flat and listric-ramp geometry of the shallow TFT, the uplift rate measured on the top of river terraces is spatially variable and cannot be constant. This result questions the validity of commonly used approaches for which a mean uplift rate is obtained by combining several

uplifted terraces located at various distances from the front. Furthermore, assuming that the far-field GPS shortening rate corresponds to an upper limit for the uplift rate, our calculation shows that part of the models is unrealistic. This suggests that both the convergence rates derived from GPS and the uplift measurements can be used to reduce the a priori geometric parameter ranges tested in our stochastic approach.

Second, assuming no prior information on the relative location of uplift rate measurements, one can deduce the overthrusting slip rate from the TFT geometry. The slip rate associated with a rigid block model with a constant dip angle α can be easily estimated from:

$$\text{Slip rate} = \frac{\text{Uplift rate}}{\sin(\alpha)}$$

As previously proposed by Berthet et al. (2014), this simple approach gives a minimum dip angle of 30° for which most of the convergence across central Bhutan is accommodated along the TFT. However, the steeper is the dip angle; the greater is the chance for slip partitioning with other faults. Assuming a constant uplift rate of 8.8 ± 2.1 mm/yr associated with no information on the sampling location, the slip rate can be estimated from less straightforward modeling based on the obtained geometry. In that case, using dislocations embedded in a homogeneous half-space (Okada, 1985), the obtained slip rate exhibits high variations along the profile from 20-40 mm/yr above the very shallow part of the fault to 10-20 mm/yr in the northern part of the profile. Using the convergence rate as a maximum value for the slip, this result suggests a

minimum distance of 8 m for the steepening of the TFT and an accommodation of at least 10 ± 2 mm/yr of the 17 mm/yr of convergence at the TFT.

The obtained uncertainties associated with this slip rate estimate arise mainly from both the location of samples for terrace dating and the fault geometry inferred from geophysical inversion.

5.3. Deformation at the topographic front

Based on new constraints on the TFT geometry and the resulting slip rate, it is proposed that at least 60% of the convergence rate due to ongoing underthrusting of India beneath the Himalaya is accommodated by the TFT.

It results that additional faults must be active in this area, which is consistent with results obtained by Dey et al. (2016) in the Kangra section of the Indian Himalayas where, besides the MFT, other out-of-sequence faulting such as the Jwalamukhi Thrust (JMT) accommodates part of the Sub-Himalayan shortening. In the case study area in south Bhutan, one can mention either the north-propagating emerging thrust front (FBT) documented by Dasgupta et al. (2013) in the Brahmaputra plain, and the Main Boundary Thrust (MBT), which accommodates the present-day deformation in eastern Bhutan (Marechal et al., 2016).

Based on recent studies, it is now well-established that at least two major earthquakes have occurred on the TFT in the past, the last one having occurred about 300 years ago in 1714 (Le Roux-Mallouf et al., 2016;

Hetényi et al., 2016). Thus, a slip deficit of 3-5 m has accumulated on the TFT during this inter-seismic period, and could potentially be released in a large magnitude earthquake with high probability of rupture reaching the surface.

6. Conclusion

This study presents high-resolution near-surface geophysical imaging results based on a joint approach, including electrical resistivity, seismic, and gravity data to constrain the TFT geometry in south central Bhutan.

Our results show that a flat and listric-ramp geometry characterizes the upper part of the TFT with high variations of dip angle. This geometry differs from the constant fault dip angle inferred from surface observation only. Estimating the slip rate without additional depth constraints can induce significant errors, arising from the terrace dating to determine the uplift rate and the projection of the fault dip angle based on surface observations.

By combining information from surface observations with our new constraints on the fault geometry, we estimate that at least 60% of the Himalayan convergence is accommodated by the TFT, making this fault a high seismic hazard zone.

The hypothesis of slip partitioning cannot be totally ruled out. Other faults such as the FBT emerging in the Brahmaputra plain, and the MBT can also be active. Therefore, further studies combining geomorphology and near-surface geophysics along the Himalayan front, especially towards the eastern part of Bhutan, will be helpful to study potential

lateral variations in the fault geometry and its implication on the present-day strain partitioning. Moreover, local variability

across the TFT may be assessed by exploring areas within a few 100s of meters along strike with respect to the Sarpang study area.

References

- Berthet, T., Ritz, J. F., Ferry, M., Pelgay, P., Cattin, R., Drukpa, D., Braucher, R., Hetényi, G. (2014). *Active tectonics of the eastern Himalaya: New constraints from the first tectonic geomorphology study in southern Bhutan*, *Geology*, 42(5), 427–430.
- Binley, A. (2015). *Tools and Techniques: Electrical Methods, Vol. 11*, Elsevier B.V. Binley, A., Kemna, A. (2005). *Electrical Methods*, p. 129-156. In Hubbard, S., Rubin, Y. (eds.), *Hydrogeophysics*. Springer.
- Boness, N. L., Zoback, M. D. (2004). *Stress-induced seismic velocity anisotropy and physical properties in the SAFOD Pilot Hole in Parkfield, CA*, *Geophysical Research Letters*, 31(15).
- Cattin, R., Mazzotti, S., Baratin, L. M. (2015). *GravProcess: An easy-to-use MATLAB software to process campaign gravity data and evaluate the associated uncertainties*, *Computers and Geosciences*, 81, 20–27.
- Dahlin, T., Zhou, B. (2004). *A numerical comparison of 2D resistivity imaging with 10 electrode arrays*, *Geophysical Prospecting*, 52(5), 379–398.
- Dasgupta, S., Mazumdar, K., Moirangcha, L. H., Gupta, T. D., Mukhopadhyay, B. (2013). *Seismic landscape from Sarpang re-entrant, Bhutan Himalaya foredeep, Assam, India: Constraints from geomorphology and geology*, *Tectonophysics*, 592, 130–140.
- Demant, D., Pirard, E., Renardy, F., Jongmans, D. (2001). *Application and processing of geophysical images for mapping faults*, *Computers and Geosciences*, 27(9), 1031–1037.
- Dey, S., Thiede, R. C., Schildgen, T. F., Wittmann, H., Bookhagen, B., Scherler, D., Strecker, M. R. (2016). *Holocene internal shortening within the northwest Sub-Himalaya: Out-of-sequence faulting of the Jwalamukhi Thrust, India*, *Tectonics*, 35(11), 2677–2697.
- Drukpa, D., Stephanie, G., Rodolphe, C., Kinley, N., Nicolas, L. M. (2017). *Impact of near-surface fault geometry on secular slip rate assessment derived from uplifted river terraces: Implications for convergence accommodation across the frontal thrust in southern Central Bhutan*, *Geophysical Journal International*, 212(2), 1315–1330.
- Ellis, R. G., Oldenburg, D. W. (1994). *Applied geophysical inversion*, *Geophysical Journal International*, 116(1), 5–11.
- Gelis, C., Revil, A., Cushing, M., Jougnot, D., Lemeille, F., Cabrera, J., de Hoyos, A., Rocher, M. (2010). *Potential of electrical resistivity tomography to detect fault zones in limestone and*

- argillaceous formations in the experimental platform of tournemire, france*, *Pure and Applied Geophysics*, 167, 1405–1418.
- Hammer, P., Berthet, T., Hetényi, G., Cattin, R., Drukpa, D., Chopel, J., Lechmann, S., Moigne, N. L., Champollion, C., Doerflinger, E. (2013). *Flexure of the India plate underneath the Bhutan Himalaya*, *Geophysical Research Letters*, 40(16), 4225–4230.
- Hetényi, G., Cattin, R., Berthet, T., Le Moigne, N., Chopel, J., Lechmann, S., Hammer, P., Drukpa, D., Sapkota, S. N., Gautier, S., Thinley, K. (2016). *Segmentation of the Himalayas as revealed by arc-parallel gravity anomalies*, *Scientific Reports*, 6 (September), 33866.
- Hung, J.-H., Ma, K.-F., Wang, C.-Y., Ito, H., Lin, W., Yeh, E.-C. (2009). *Subsurface structure, physical properties, fault-zone characteristics and stress state in scientific drill holes of Taiwan Chelungpu Fault Drilling Project*, *Tectonophysics*, 466(3), 307–321.
- Jeppson, T. N., Bradbury, K. K., Evans, J. P. (2010). *Geophysical properties within the San Andreas Fault Zone at the San Andreas Fault Observatory at Depth and their relationships to rock properties and fault zone structure*, *Journal of Geophysical Research: Solid Earth*, 115(B12).
- Kaiser, A. E., Green, A. G., Campbell, F. M., Horstmeyer, H., Manukyan, E., Lan-gridge, R. M., McClymont, A. F., Mancktelow, N., Finnemore, M., Nobes, D. C. (2009). *Ultrahigh-resolution seismic reflection imaging of the Alpine Fault, New Zealand*, *Journal of Geophysical Research: Solid Earth*, 114(11), 1–15.
- Le Roux-Mallouf, R., Ferry, M., Cattin, R., Ritz, J., Drukpa, D. (submitted). *A 2600-yr-long paleoseismic record for the Himalayan Main Frontal Thrust (Western Bhutan)*, *Solid Earth*, 11, 2359–2375
- Le Roux-Mallouf, R., Ferry, M., Ritz, J.-f., Berthet, T., Cattin, R., Drukpa, D. (2016). *First paleoseismic evidence for great surface-rupturing earthquakes in the Bhutan Himalayas*, *Journal of Geophysical Research: Solid Earth*, 121(10), 7271–7283.
- Loke, M., Barker, R. D. (1996). *Rapid least-squared inversion of apparent resistivity pseudosections by a quasi-Newton method*, *Geophysical prospecting*, 44(1), 131–152.
- Loke, M. H. (2015). *Tutorial: 2-D and 3-D electrical imaging surveys*, *Geotomo Software Malaysia*, (July), 176.
- Long, McQuarrie, N., Tobgay, T., Grujic, D., Hollister, L. (2011). *Geologic map of Bhutan*, *Journal of Maps*, 7(1), 184–192.
- Louis, I. F., Raftopoulos, D., Goulis, I., Louis, F. I. (2002). *Geophysical imaging of faults and fault zones in the urban complex of Ano Liosia neogene basin, Greece: synthetic simulation approach and field investigation*, *International Conference on Earth Sciences and Electronics*, 2002, (October), 269–285.

- Marechal, A., Mazzotti, S., Cattin, R., Cazes, G., Vernant, P., Drukpa, D., Thinley, K., Tarayoun, A., Roux-Mallouf, L., Thapa, B. B. et al. (2016). Evidence of inter- seismic coupling variations along the bhutan himalayan arc from new GPS data, *Geophysical Research Letters*, 43, doi:10.1002/2016GL071163.
- Morandi, S., Ceragioli, E. (2002), *Integrated interpretation of seismic and resistivity images across the «Val d’Agri» graben (Italy)*, *Annals of Geophysics*, 45(2).
- Mosegaard, K., Tarantola, A. (1995). Monte Carlo sampling of solutions to inverse problems, *Journal of Geophysical Research: Solid Earth*, 100(B7), 12431–12447.
- Mussett, A., Khan, M., Button, S. (2000). *Looking Into the Earth: An Introduction to Geological Geophysics*, Cambridge University Press.
- Nguyen, F. (2005). *Near-surface Geophysical Imaging and Detection of Slow Active Faults*, Department of Georessources, Geotechnologies and Construction Materials, Doctorate, (May), 359.
- Nguyen, F., Garambois, S., Chardon, D., Hermitte, D., Bellier, O., Jongmans, D. (2007). Subsurface electrical imaging of anisotropic formations affected by a slow active reverse fault, Provence, France, *Journal of Applied Geophysics*, 62(4), 338–353.
- Nguyen, F., Garambois, S., Jongmans, D., Pirard, E., Loke, M. H. (2005). Image processing of 2D resistivity data for imaging faults, *Journal of Applied Geophysics*, 57(4), 260–277.
- Okada, Y. (1985). Surface deformation due to shear and tensile faults in a half-space, *Bulletin of the seismological society of America*, 75(4), 1135–1154.
- Pasquet, S., Bodet, L., Dhemaied, A., Mouhri, A., Vitale, Q., Rejiba, F., Flipo, N., Guérin, R. (2015), ‘Detecting different water table levels in a shallow aquifer with combined p-, surface and sh-wave surveys: Insights from vp/vs or poisson’s ratios’, *Journal of Applied Geophysics*, 113, 38–50.
- Phillips, W. J., Kuckes, A. F. (1983). ‘Electrical conductivity structure of the san andreas fault in central california’, *Journal of Geophysical Research: Solid Earth*, 88(B9), 7467–7474.
- Podvin, P., Lecomte, I. (1991). ‘Finite difference computation of traveltimes in very contrasted velocity models: a massively parallel approach and its associated tools’, *Geophysical Journal International*, 105(1), 271–284.
- Priolo, E., Lovisa, L., Zollo, A., Böhm, G., D’Auria, L., Gautier, S., Gentile, F., Klin, P., Latorre, D., Michelini, A. et al. (2012). The Campi Flegrei Blind Test: Evaluating the Imaging Capability of Local Earthquake Tomography in a Volcanic Area, *International Journal of Geophysics*, 2012.
- Ramirez, A. L., Nitao, J. J., Hanley, W. G., Aines, R., Glaser, R. E., Sengupta, S. K., Dyer, K. M., Hickling, T. L., Daily, W. D. (2005). Stochastic inversion of electrical resistivity changes

- using a Markov Chain Monte Carlo approach, *Journal of Geophysical Research: Solid Earth*, 110(B2).
- Reynolds, J. (1997). *An Introduction to Applied and Environmental Geophysics*, John Wiley.
- Schuster, G. T. (1993). *Wavepath eikonal travelttime inversion: Theory*, *Geophysics*, 58(9), 1314.
- Sheehan, J. R., Doll, W. E., Mandell, W. a. (2005). *An Evaluation of Methods and Available Software for Seismic Refraction Tomography Analysis*, *Journal of Environmental & Engineering Geophysics*, 10(1), 21–34.
- Suzuki, K., Toda, S., Kusunoki, K., Fujimitsu, Y., Mogi, T., Jomori, A. (2000). 'Case studies of electrical and electromagnetic methods applied to mapping active faults beneath the thick quaternary', *Engineering Geology*, 56(1), 29–45.
- Tarantola, A. (2005). *Inverse problem theory and methods for model parameter estimation*, *Society for Industrial and Applied Mathematics*.
- Telford, W. M., Geldart, L. P., Sheriff, R. E. (1990). *Applied geophysics, Vol. 1*, Cambridge university press.
- Villani, F., Tulliani, V., Sapia, V., Fierro, E., Civico, R., Pantosti, D. (2015). *Shallow subsurface imaging of the Piano di Pezza active normal fault (central Italy) by high-resolution refraction and electrical resistivity tomography coupled with time- domain electromagnetic data*, *Geophysical Journal International*, 203(3), 1482– 1494.
- Won, I.J., Bevis, M. (1987). *Computing the gravitational and magnetic anomalies due to a polygon: Algorithms and Fortran subroutines*, *Geophysics*, 52(2), 232–238.
- Wise, D. J., Cassidy, J., Locke, C. A. (2003). *Geophysical imaging of the Quaternary Wairoa North Fault, New Zealand: A case study*, *Journal of Applied Geophysics*, 53(1), 1–16.

GEOPHYSICAL PROSPECTING USING MICROTREMORS TO ESTIMATE 1-D SHALLOW SHEAR WAVE VELOCITY PROFILES IN THIMPHU, BHUTAN

Nityam Nepal¹, Takumi Hayashida^{2,3}, Toshiaki Yokoi³

Abstract

Microtremor measurements were conducted at 25 sites in Thimphu to obtain 1-D shallow shear wave velocity (V_s) profiles. The V_s profiles were obtained from the inversion of the phase velocities using the microtremor Spatial Autocorrelation method. The averaged V_s values in the upper 30 m (V_{s30}) obtained at sixteen sites are categorized under “Class C (dense soil and soft rock)” of the NEHRP classification. The horizontal-to-vertical (H/V) spectral ratios of the observed microtremors were also obtained and compared to the theoretical ones calculated from the inverted V_s profiles. Almost all sites showed a flat characteristic of the spectral ratios between 1 Hz and 15 Hz. The computed site amplifications showed most sites in Thimphu having predominant frequencies above 4 Hz.

We also performed microtremor array surveys at six sites in South Ibaraki, Japan, using the same method and sensors used in Thimphu to corroborate the applied methods and to understand the effects of geology/geomorphology on the results

obtained. The results obtained in Thimphu and South Ibaraki showed clear distinctions in the V_s profiles and predominant frequencies. Thimphu City, located on mountainous terrain, showed higher values of V_{s30} and dominant frequencies than most sites in South Ibaraki, which is located on a deep sedimentary basin.

Keywords: Microtremors, Thimphu, SPAC method, V_{s30} , H/V spectral ratio.

1. Introduction

The seismicity of Bhutan is low in normal times, but the recent paleoseismic studies revealed the existence of a significant event with a magnitude of 8 ± 0.5 in the 18th century (Le Roux Mallouf et al., 2016). Since then, the only noticeable event was the 2009 Mongar earthquake (Mw 6.1) in the east, which caused local damage and claimed 12 lives. Significant events located outside the territory, such as the 2011 Sikkim earthquake (Mw 6.9), have caused considerable damage in the country (Diehl et al., 2017). Bhutan falls under the “category Zone V (highest risk zone)” in the Indian seismic zonation system, indicating a Peak Ground Acceleration value

¹ Nityam Nepal, Senior Geologist, Department of Geology and Mines, Thimphu, Bhutan.

Masters of Disaster Management, National Graduates Institute for Policy Studies, Japan, Email: nnepal@moea.gov.bt

² Takumi Hayashida, International Institute of Seismology and Earthquake Engineering, Building Research Institute

³ Toshiaki Yokoi, International Institute of Seismology and Earthquake Engineering, Building Research Institute

of 0.36g. However, this estimation is much lower than the recent hazard results (Stevens et al., 2020). Most of the buildings in Bhutan consist of traditional styled rammed earth and stone masonry houses, and these structures do not follow any building code.

Generally, significant seismic risks arise from the probable collapse of buildings and other structures. For this reason, Bhutan faces high vulnerability in terms of both hazard and risk. Seismic hazards need to be understood well to eliminate risks as far as possible. Seismic wave amplification occurs depending on local geological conditions (e.g., thickness and physical properties of subsurface sedimentary soils), and effects of amplification at the subsurface soil are different from site to site and are controlled by the geological condition. Studying local site effects and understanding the subsurface profiles is essential for understanding the impact of subsurface geology on strong ground motion for earthquake hazard assessment and risk mitigation.

Geophysical exploration using microtremors (ambient seismic noise) is a reliable and straightforward technique to understand subsurface structures and deduce soil characteristics. In this study, we will use the microtremor array data measured in the city of Thimphu to construct 1-D subsurface Vs profiles. The study also uses microtremor array data measured in South Ibaraki, where geological information, PS loggings and Vs30 information are available, to validate the techniques applied and confirm the results. The geological and geomorphological difference of Thimphu and South Ibaraki will also be helpful to

understand the effects of different environments on microtremors.

2. Methodology

2.1.SPAC method

The primary method used in this study is the Spatial Autocorrelation (SPAC) method, which uses microtremor array recordings to estimate the characteristics of the subsurface Vs profile from the Rayleigh-wave phase velocities. The technique was first proposed by Aki (1957, 1965) and completed by Okada (2003).

The coherence function between sensor pairs is derived based on a stochastic approach. This approach assumes that: 1) Microtremor propagates as a sum of the individual sources and reaches the array as a plane wave. For this assumption, the sources of microtremors are located distant from the array; 2) Microtremors propagate uniformly and continuously from all directions, and the distribution of signals from source to sensors is uniform (Aki, 1957). Based on the assumptions, the SPAC coefficient between a sensor pair can be linked by fitting it to the Bessel function of the first kind of zero order.

$$\rho_{AB}(r, \omega) = \frac{1}{2\pi} \int_0^{2\pi} \frac{Re[S_{AB}(r, \omega)]}{\sqrt{|G_A(\omega)||G_B(\omega)|}} d\theta \cong J_0 \left\{ \frac{\omega r}{c(\omega)} \right\} \quad (1)$$

where $\rho_{AB}(r, \omega)$ is the coherence function between sensors A and B, $S_{AB}(r, \omega)$ is the cross-spectrum of the sensor pair, $G(\omega)$ are the power spectrum of the microtremor, and r , ω , and $c(\omega)$ are the sensor-to-sensor distance, the angular frequency, and the phase velocity, respectively. After we obtain the dispersion curves of Rayleigh-wave, we

apply a heuristic inversion technique to estimate 1-D subsurface Vs profiles. An initial velocity model consisting of horizontal layers is assumed and each layer thickness and Vs values are determined. After the inversion we obtain a Vs structure model which optimally fits the observed phase velocities.

2.2.H/V spectral ratio (HVSR) method

The horizontal-to-vertical (H/V) spectral ratio of microtremors is calculated using three-component microtremor data at a single station. This method was first developed by Nakamura (1989), which described that the spectral ratios of the horizontal to vertical component corresponds to the site amplification characteristics. There are discussions regarding the physical interpretation of the H/V ratios, and recent works show that the H/V represents the predominant frequency of the subsurface soil (Pierre-Yves et al., 2008). The H/V spectral ratio can be defined as

$$\frac{H}{V}(f) = \sqrt{\frac{P_{NS}(f)+P_{EW}(f)}{P_{UD}(f)}} \tag{2}$$

where P_i indicates the power spectrum.

3. Data

The Thimphu city expands in the N-S direction along the valley and is divided by Wang River that runs from north to south. The populated area is entirely located within the valley deeply carved by Wang River, with the settlements built on the valley slopes.

The microtremor array measurements were carried out in the northern region of Thimphu at twenty-five sites (Figure 1). For most

measurements, a triangular array with four sensors was applied. We measured microtremors using arrays with radii of 5 m and 10 m. At sites where space was restricted for the 10 m array measurement, linear arrays consisting of two sensors were deployed. The regional geological map of Bhutan categorizes all arrays to be on the Lower metasedimentary unit of the Greater Himalayan Zone (Neoproterozoic-Cambrian) (Long et al., 2011), which mainly consists of metasedimentary rocks such as quartzite, biotite-muscovite-garnet schist, and paragneiss (Long & McQuarrie, 2010).

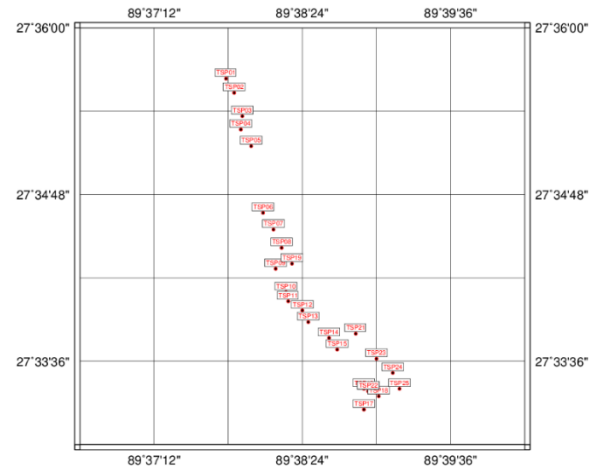


Figure 1. Location of microtremor array sites in Thimphu.

South Ibaraki Prefecture, Japan, is situated in the northeastern corner of the Kanto Basin, the largest sedimentary basin in Japan. The maximum depth of sediments reaches approximately several hundred meters to ~1 km in the region. Mt. Tsukuba lies to the north of the basin, whose geology is mainly comprised of mainly gabbro and granite rocks. The sedimentary soil thickness gradually decreases from south to north, and recorded ground motions show areal

variations of seismic wave amplification. We took microtremor measurements at six different sites in South Ibaraki (Figure 2).

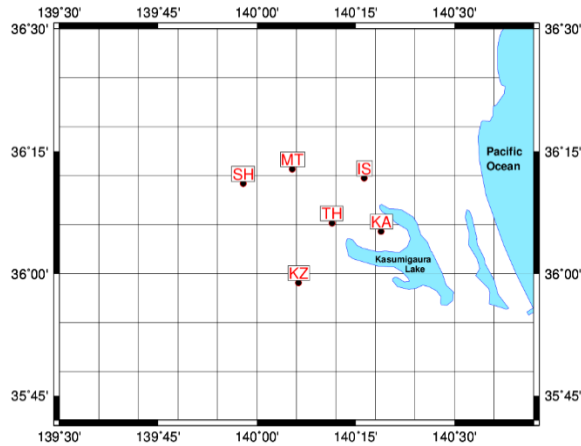


Figure 2. Location of microtremor array sites in South Ibaraki

The six sites were distributed on different geomorphological units. Except for site MT (Mt. Tsukuba), which was located on a hillside at an elevation of 170 m above sea level, the other five sites, IS, KZ, KA, SH, and TH were located on a low-lying sedimentary basin. Strong-motion observation stations operated by National Research Institute for Earth Science and Disaster Resilience (NIED) (KiK-net: sites KA, MT, KZ; K-net: sites SH, IS) or Japan Meteorological Agency (JMA) (site TH) were installed at all sites. PS-logging data are available at four sites; IS, KA, MT, and SH. The calculated V_{s30} values and the PS-logging data for these sites will be used to corroborate the results of observed values obtained from the array measurements and validate the microtremor survey technique applied in this study. The measurements were

taken using four array radii: 5 m, 10 m, 15 m, and 20 m.

4. Results And Discussion

4.1. South Ibaraki

In this study, data processing of the SPAC method is carried out using software SPAC2021 developed by Toshiaki Yokoi (2021), and horizontal-to-vertical spectral ratio analysis was carried out using software Prochv developed by Takumi Hayashida (2021).

The observed phase velocities at South Ibaraki sites were compared with the theoretical ones computed using available PS-logging information (see Figure 3). The PS-logging values were available down to 20 m depth at sites IS and SH, 400 m at site KA, and down to 92 m at site MT. The comparisons between the observed and the theoretical phase velocities dispersion curves are similar at sites IS, KA, and SH in the higher frequency side, representing the phase velocities in shallow depth soils (Figure 3). In the lower frequency side, the theoretical curves show discrepancies; the observed phase velocities are much higher than the theoretical ones, possibly due to a lack of deeper structural information in the logging data. At site MT, the dispersion curve shows similarity in the lower frequency side but discrepancies in the higher frequency side. This could be due to the soft velocity layers of the PS logging (~ 100 m/s) for the top 2 m layer. All sites show rough correlations between the observed and theoretical phase velocities.

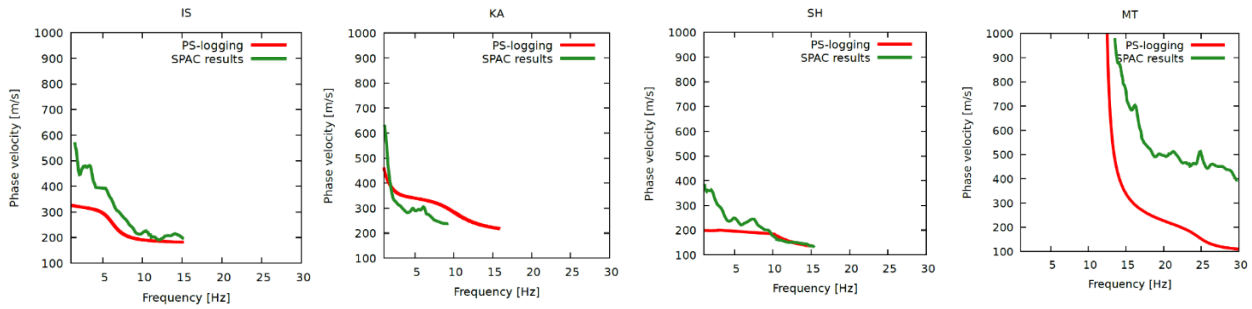


Figure 3. Comparison of the observed phase velocities obtained from SPAC analysis and the theoretical phase velocities obtained from PS-logging data.

The 1-D Vs profiles obtained at the five sites in the basin (IS, KA, KZ, SH, and TH) represent the dispersive characteristics of the Rayleigh-wave phase velocities. The Vs profiles obtained from the microtremors were compared to the theoretical ones derived from PS-logging data. Both data show good correlations. These results suggest that the inversion process was efficient, and the obtained results were reliable.

Table 1. Vs30 values obtained from observed data and PS logging.

SITE ID	VS PROFILE S	PHASE VELOCITIES	SPAC COEFFICIENTS	PS LOGGING
IS	285	293	299	246
KA	304	317	301	No logging
KZ	274	274	209	301
SH	671	667	702	692
MT	222	226	221	206
TH	305	370	329	No logging

The Vs30 values were calculated at all sites using various methods such as CEN (2004), Vs30 values from SPAC coefficients (Hayashida and Yokoi, 2021), and Lamda – 40 m method (Konno and Kataoka, 2000). The Vs30 values obtained from the observed data were also compared to the theoretical values obtained from PS-logging data (Table

1). All the Vs30 values show good correlations with those of the estimated ones from Vs profiles. According to the National Earthquake Hazards Reduction Program (NEHRP) site classification, MT falls under Class C (soft rock) while the rest of the sites fall under Class D (stiff soil).

The predominant frequencies of H/V and site amplifications were also calculated. The theoretical site amplifications computed from the Vs profiles at three sites were compared to the amplification models provided by the National Institute for Land and Infrastructure Management (NILIM), Japan. For all the sites, the predominant frequencies of the theoretical site amplifications are roughly similar to the frequency of the dominant peaks obtained around 1 Hz in the NILIM models. Theoretical H/V obtained from PS logging and Vs profiles were compared to the observed H/V. All values showed a good correlation for all sites and have almost flat characteristics except for site MT. However, the predominant frequencies of site amplification did not match those of H/V.

4.2.Thimphu

The phase velocities obtained for most sites in Thimphu are lower than South Ibaraki. The frequency ranges and the phase velocities of the dispersion curves varied

among sites in Thimphu. Phase velocities below 5 Hz are observed only at three sites. In the lower frequency side, the phase velocities have high variations among the sites.

Vs models in Thimphu are obtained at twenty-two sites out of twenty-five sites. The average maximum depth obtained for all sites is about 24 m. The depth reached 30 m at only eight sites.

The Vs30 values were also computed in Thimphu for twenty-two sites using the same methods in South Ibaraki. Following the National Earthquakes Hazards Reduction Program (NEHRP) classification, six sites in Thimphu are categorized under Class D (stiff soil) and sixteen sites are classified under Class C (dense soil/soft rock).

The theoretical H/V ratios for most sites in Thimphu have flat characteristics. At site TSP016, the theoretical ratios have a dominant peak at 6.6 Hz, whereas the observed H/V ratio has a dominant peak at 5.5 Hz. Site TSP022 has a clear dominant peak for the theoretical ratios at 8.5 Hz, but in contrast the observed ratios have a peak at 1 Hz. The predominant frequencies of site amplification had considerable variation (2-12 Hz) among the sites in Thimphu. This might suggest large range heterogeneity of the shallow subsurface layers in the area. Conducting microtremor measurements with larger array might result in deeper Vs profiles. However, due to constraints in the availability of the open surface in the area, the use of larger arrays is not possible. At most of the sites, the predominant peaks have higher values than those observed at sites in South Ibaraki. Similar to the results in South Ibaraki, the dominant frequencies of site amplification did not match those of H/V at sites in Thimphu either.

4.3. Limitations

The power spectral densities, which indicate microtremor amplitude levels, hold the information of the available frequency range for the analysis. The power spectral densities for the sites in Thimphu were compared to the power spectral densities of the sites in South Ibaraki. The population of Thimphu city is almost 1/10 of South Ibaraki. South Ibaraki is a neighboring region of the capital city, Tokyo, and traffics can be the primary source for the generation of ambient vibrations. Unlike Japan, Bhutan does not use railway transport; trains are also a major source of tremors that are detectable even up to 100 km away (e.g., Brenguier et al., 2019). Therefore, the source of ambient vibrations is much weaker in Thimphu.

The lower limit of the phase velocity dispersion curves was set at frequencies for which the SPAC coefficient curves reached their peaks at all sites. This limited the range of phase velocities in the dispersion curves at around 5 Hz. As a result, information about the deep layers could not be obtained at most sites. Using larger arrays, the information of the deeper parts may be obtained. However, as the availability of space is restricted in the current study area, larger arrays could not be observed in this study.

5. Conclusions

Microtremor measurements were conducted at twenty-five sites in Thimphu city and six sites in South Ibaraki. The observed phase velocity dispersion curves, Vs profiles, Vs30, H/V, and site amplifications obtained for South Ibaraki are well compared to theoretical ones. This implies that the results obtained in Thimphu using the same methods are acceptable. The effects of different geology and geomorphology on

microtremors are also clearly shown by the results obtained. For sites located on the sedimentary basin, reliable phase velocities are possibly obtained in the lower frequency side (~1 Hz) due to deeper sediments. For site MT and the sites in Thimphu, reliable phase velocities were obtained only in the higher frequency range (> 4 Hz), and the obtained Vs profiles were shallow in depth. This implies that the predominant frequencies for Thimphu sites could not be well justified, and a more detailed study of the geology and geomorphology of the area might help corroborate the results obtained. The observed phase velocities in Thimphu ranged from ~180 to 930 m/s in the frequency range of 4 Hz to 30 Hz. In South Ibaraki, a wide range of phase velocities were obtained from 130 to ~2500 m/s in the same frequency range. The observed values in South Ibaraki vary widely owing to the variability in the geomorphology of the sites. According to the NEHRP classification, six sites in Thimphu

were located on Class D (stiff soil), and sixteen sites were located on Class C (dense soil and soft rock).

The dominant frequencies of site amplification could also be well explained. The dominant frequencies of site amplification at sites located on the basin in South Ibaraki have dominant peaks below 2 Hz. Site MT had the dominant peak at ~8 Hz. At sites in Thimphu, the dominant peaks were observed within a wide range frequency (2–12 Hz), and hence the correlation of the dominant frequencies among the sites in Thimphu could not be determined. The observed and theoretical H/V ratios of most sites in Thimphu had almost flat features. They do not match the predominant frequency of site amplification. The shallow depth of the Vs profiles obtained in this study might not properly constrain the characteristics of Thimphu.

References

- Aki, K. (1957). *Space and time spectra of stationary stochastic waves, with special reference to microtremors*, *Bulletin Earthquake Research Institute Tokyo University*, Vol. 25, pp. 415-457.
- Aki, K. (1965). *A note on the use of microseisms in determining the shallow structure of the Earth's crust*. *Geophysics*, 30, 665-666.
- Brenguier, F., Boué, P., Ben-Zion, Y., Vernon, F., Johnson, C. W., Mordret, A., Coutant, O., Share, P.E., Beaucé, E., Hollis, D., Lecocq, T. (2019). *Train Traffic as a Powerful Noise Source for Monitoring Active Faults with Seismic Interferometry*. doi:10.1029/2019GL083438.
- CEN. (2004). *Eurocode 8- design of structures for earthquake resistance. Part 1: general rules, seismic actions and rules for buildings*. European standard EN 1998–1, December 2004. European Committee for Standardization, Brussels.
- Diehl, T., Singer, J., Hetényi, G., Grujic, D., Clinton, J., Giardini, D., & Kissling, E. (2017). *Seismotectonics of Bhutan: Evidence for segmentation of the Eastern Himalayas and link to foreland deformation*. *Earth and Planetary Science Letters*. <https://doi.org/10.1016/j.epsl.2017.04.038>

- Hayashida, T. & Yokoi, T. (2021). *Can Vs30 be estimated directly from SPAC and CCA coefficients? – examinations using measured microtremor array data- The 6th IASPEI/IAEE International Symposium: Effects of Surface Geology on Seismic Motion, GS2-P12.*
- Konno, K. & Kataoka, S. (2000). *An estimating method for the average S-wave velocity of ground from the phase velocity of Rayleigh wave. Proceedings of JSCE., 647, 415–423.*
- Nakamura, Y. (1989). *A method for dynamic characteristics estimation of subsurface using microtremor on the ground surface, Q. Rep. Railw. Tech. Res. Inst. 30, no. 1, 25-33.*
- Okada, H. (2003). *The microtremor survey method, Geophysical Monograph Series No. 12, Society of Exploration Geophysicists.*
- Sanchez-Sesma, F. J., Rodríguez, M., Iturrarán-Viveros, U., Luzón, F., Campillo, M., Margerin, L., García-Jerez, A., Suarez, M., Santoyo, M. A., Rodríguez-Castellanos, A. (2011). *A theory for microtremor H/V spectral ratio: application for a layered medium, Geophys. J. Int. 186, 221–225. doi:10.1111/j.1365-246X.2011.05064.*
- Stevens, Victoria & Risi, Raffaele & Le Roux-Mallouf, R., Drukpa, D., & Hetényi, G. (2020). *Seismic hazard and risk in Bhutan, Natural Hazards. 104. 1-29. 10.1007/s11069-020-04275-3.*

USE OF DIFFERENTIAL SAR INTERFEROMETRY (DINSAR) AND OFFSET TRACKING IN ESTIMATION OF GLACIER MOVEMENT

Jampel Gyeltshen¹

Abstract

The emergence of freely available space-borne synthetic aperture radar (SAR) data and processing software has made surface deformation probes remotely possible. In other words, free SAR data have leveraged the use of RADAR technology for studying ice and glaciers. This study applied the differential interferometry and offset tracking methods to estimate the glacier surface deformation in the Himalayan region of Bhutan. The result obtained from this study show velocities for the lake terminating glacier in the minimum range of 0 - 3 cm/day to a maximum range of 24 - 134 cm/day and is comparable with other accurate methods of the field-based survey and optical images (ASTER) for the same area

Keywords—Himalaya, Bhutan, glaciers, RADAR, offset tracking, SAR, differential interferometry.

1. Introduction

The mountain glaciers account for the world's 75% of freshwater supply and blanket 10% of Earth's surface (Leibowitz, 2009). The glaciers in the Himalayas are natural reservoirs of freshwater. They are the only perennial source of the major river

systems in South Asia including Bhutan. The livelihoods downstream hinge on these supplies for everyday sustenance. In the fragile ecological setting of the Bhutan Himalaya, they are an indispensable part of the ecosystem (Mool, 2001). Most essentially glaciers form core elements in the hydrological regime. The glacial-fed rivers are an important source of hydropower and contribute significantly to the economy of the country (Dharmadhikary, 2015). Its mysticism, uniqueness, and aestheticism of being the third pole on the planet earth are identities in themselves which bring along another economic aspect of tourism into the equation. They are the natural indicator of global climate change due to their sensitivity toward variability in climate regimes (Lewis, 2009).

Associated with such tangible and intangible aspects, the mountain glaciers are the most important landforms. However, the glacial retreat is happening at a very disturbing scale and unprecedented rate since the turn of the 20th century (Bello & Aina, 2014). Owing to their sensitivity and susceptibility they are the hardest hit landforms on the globe by the current trends of climate change. Global warming increased the rate of ablation and

¹ *Jampel Gyeltshen, Dy. Chief Survey Engineer, Department of Geology and Mines, Thimphu, Bhutan. Masters of Geo-Informatics, Bharati Vidyapeeth Deemed University, India, Email: jgyeltshen@moea.gov.bt*

hence the glacier retreat too. The melting of the glaciers leads to the formation of numerous supraglacial or alpine lakes. Almost all the lakes are at the headwater or upper region of the river catchment. These lakes are often loosely held by the fragile moraine dams (Strozzi et al., 2002). In the growing face of fast glacier retreats, the number of new lake formations are increasing and the existing ones are expanding. They are the time bombs waiting to unleash their demonic force of catastrophic proportion. Such phenomena take an unprecedented toll not just on the economy but also on lives, infrastructures, and ecosystems alike (Sheng et al., 2012) (Gourmelen et al., 2018).

The unfolding of the GLOF events was examined in the past both through in-situ field surveys and optical remote sensing investigations. As uncovered by the preceding probes all the incidents of GLOF were clustered along the regions of major river systems in Bhutan. Given the intricate dynamics, numerical models like spatial principal component analysis (SPCA) coupled with Geographical Information System (GIS) and remote sensing (RS) technologies are employed to unlock the underlying principles and mechanisms at operation. The differential GPS surveys are also being used to study the thinning of the glaciers in the Himalayan region of Bhutan (Schubert et al., 2013). These findings have a strong suggestion that thinning of glaciers will only accelerate progressively with time eventually resulting in an accelerated glacial lake formation and expansion. The rate of thinning at the lake-terminating glacier is

found to be $(-4.67 \pm 0.02$ m per year) which is as much as 3 times the rate of the land-terminating glacier $(-1.40 \pm 0.02$ m per year) (Tsutaki et al., 2018). The Glacier velocities in Bhutan Himalaya were evaluated using the fusion of DEMs from the Shuttle Radar Topography Mission (SRTM) and Advanced Spaceborne Thermal Emission and Reflection Radiometer (ASTER) (Ferretti et al., 2001). The surface velocities of glaciers determined from this method are in the order of 100–200 m per year. Ever since its inception in 1986 for topographic mapping, the synthetic aperture radar interferometry (Hooper & Zebker, 2007) has found its way into a myriad of earth surface deformation studies. One of its niche application domains has been the glacier investigation. The advent of the SAR space-borne mission of European Space Agency (ESA) and subsequent free SAR data products has spurred SAR interferometry in various fields and glaciology in particular. Also, SAR data of ERS-I&II, optical imagery of SPOT-5, and other ancient aerial photographs are used to solve the complex puzzle of glacier dynamics and lake formation in Tibet (China) and Nepal Himalaya (Kampes, 2018) (Hooper, 2018) (Zebker & Villasenor, 1992). Hence, SAR data have added essential resources for studying ice and glaciers. The differential SAR interferometry is one of the SAR techniques that can determine glacier surface displacements at the centimeter level. In SAR interferometry, the phase difference of the two SAR images with both spatial and temporal separation is exploited. The phase of the interferometric image pair is sensitive to both surface topography and coherent displacement along the radar line of sight.

The topographic induced phase is eliminated using interferograms with similar displacement generated from an interferometric pair or DEM simulated interferogram to obtain an actual displacement map. The use of differential SAR interferometry is restricted by the noise in the phase, normally indicated by the coherence. The coherence over the glaciers is influenced by the flow and meteorological circumstances. The increasing temporal separation between the SAR interferometric pairs also increases the coherence loss. Other sources of SAR signal decorrelation are melting of ice and snow, snowfall and dispersion of the ice and snow by wind. An offset tracking method is an alternative or can be used in complement with DInSAR for monitoring glacier surface deformations.

2. Materials and methods

2.1. Study Area

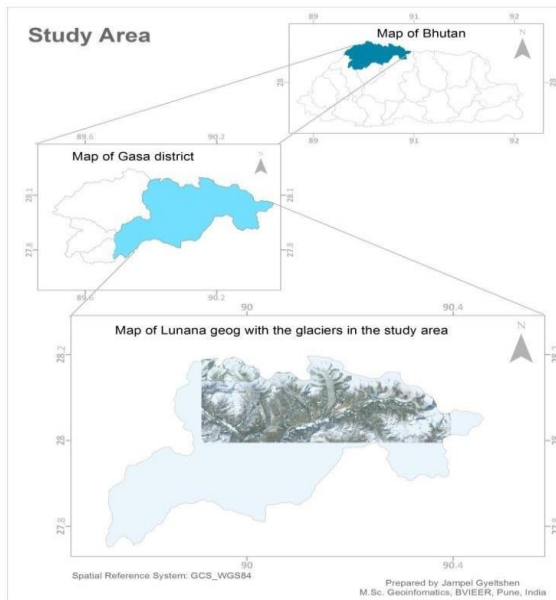


Figure 1. The map of the study area in northern Bhutan

The glacial complex in the study region has different kinds of glaciers: active, lake terminating, and land-terminating glaciers. The entire complex is at the headwaters of one of the most important rivers running major hydropower plants. Given its extent and activeness, they are most susceptible to GLOF in the entire catchment and areas downstream (Usai, 2003). The study area spans approximately 800 square kilometers encompassing the glaciers in northern central Bhutan. The glaciers in the study area stretch from the top right corner $28^{\circ}13'7.30''\text{N}$ and $89^{\circ}55'48.34''\text{E}$ to the bottom left corner $28^{\circ}1'45.74''\text{N}$ and $90^{\circ}19'59.19''\text{E}$. The mountain ranges in the area are mostly oriented in the north-south direction. The slopes in the area are also facing southeast, south, or west. The glaciers in the study area are an important source of the rivers. It also houses the most potentially dangerous glacial lakes in Bhutan. Against such backdrops, the study area is identified for the current probe.

2.2. Dataset and software

For DInSAR a single look complex (SLC) SAR images acquired by Sentinel-1A (S1A) and Sentinel-1B (S1B) satellites in interferometric wide swath (IW) mode are used. The image used corresponds to the acquisition date of September 10, 2018 (master image from S1A) and September 22, 2018 (slave image from S1B). The image pair is chosen in such a way that there is a minimum temporal separation between the two acquisitions (here 12 days) to minimize the coherence loss. The two satellites are 180 degrees apart in the sun's synchronized polar orbit. The Sentinel sensors operate at c-band with 5.405 GHz frequency which

corresponds to a wavelength of 5.55 cm. The IW mode spans 250 km swath with a spatial resolution of 5 m by 20 m (range and azimuth) with three IW sub-swaths and a series of bursts. For the feature tracking the Ground Range Detected (GRD) of the same period and platform but with different spatial resolution, 20 m X 22 m (range X azimuth) is used. The SLC image has phase information whereas the GRD image has information on radar backscattered signal strength represented by intensity. The Sentinel Application Platform (SNAP) toolbox and the QGIS software were used for data processing and visualization.

2.3. Methodology

2.3.1 Differential SAR Interferometry

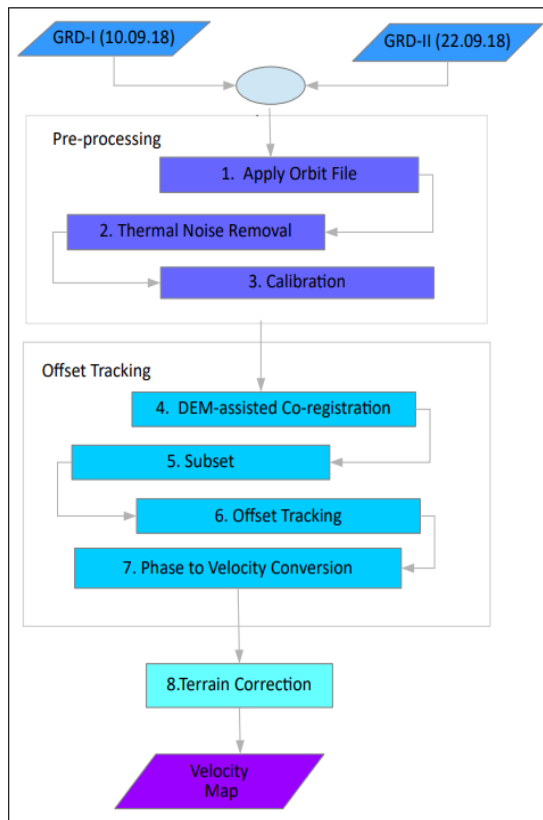


Figure 2. DInSAR flow chart

The formation of the interferogram is achieved through cross-multiplication of the master image with the complex conjugate of the slave image. In other words, a complex image formed by cross-multiplying the two SAR images yields an interferometric fringe known as the phase of the SAR interferogram. The interferometric processing eliminates other sources of error like the flat-earth phase which is present in the interferometric phase/signal due to the curvature of the reference surface (in the current case WGS84 ellipsoid). The removal of the flat earth phase ensures that the interferogram is related only to the surface deformation (in this case the glacier). The estimation of the flat-earth phase is done using the metadata and orbital information. It is estimated for the grid points are distributed over the entire image and the polynomial surface fitting of the grid points are generated using a least square method. For the SAR scene of 100 by 100 km, a polynomial of degree five usually is enough to model the reference phase. While for smaller images a lower degree can be opted. Like the flat-earth phase is the error in the interferogram generated from the SAR image pair, the topographic phase introduced by the variation in the topography is another error. To remove the phase due to topographic variation, an external DEM is used to simulate the interferometric phase. This simulated phase is subtracted from the processed interferogram or the phase generated from the SAR image pair. The resultant interferometric phase (the difference between the processed interferogram from the SAR image pair and the DEM-simulated interferogram) is known

as a differential interferogram, hence the term differential SAR interferometry. It is achieved by using the Topographic Phase Removal operator in the SNAP.

2.3.2 Feature offset Tracking

The Offset Tracking feature use Sentinel-1 Level-1 GRD products. Offset Tracking is a method that measures feature (proxy intensity) motion between two images using patch intensity cross-correlation optimization. Level-1 GRD image is a focused SAR data that is detected, multi-looked, and projected to the ground range using the WGS84 Earth ellipsoid model. They are like optical RS images with DN values as intensity but in SAR geometry. Unlike SLC image GRD image does not have phase information. Just like the differential SAR interferometry, feature (intensity) tracking requires two images with temporal separation. The pre-date image is selected as the master image and the post-date the slave.

Apply orbit File: An identical pre-processing has to be applied to both SAR scenes participating in the feature tracking. The image pair is batch-processed in SNAP to not just avoid the cumbersome nature of step by step and image-by-image process but to ensure identical processing. In batch processing, only the final product is physically saved on the disk thereby saving the memory. The orbital information in the metadata of SAR products is usually not accurate so as to provide accurate position and velocity information of the satellite precise orbit files are applied to the processing images.

Thermal Noise Removal: Like any imaging system, the system or the sensor also generates background energy and in the case of the SAR imagery background energy generated by the receiver itself is called thermal noise. The thermal noise skews the radar reflectivity to larger values thereby diluting the correct estimates of the radar reflectivity. The Thermal Noise Removal tool in the SNAP helps to mitigate the effects of noise. **Calibration:** The electromagnetic energy reflected by the target element on the ground is what the sensor on board has to record. Since the SAR images are acquired by different sensors or by the same sensor at different times and modes, to ensure that the pixel values of the SAR image are truly the corresponding backscattered radar values of the reflecting surface or target element the radiometric correction is done through calibration tool in the SNAP.

DEM-assisted co-registration: The correct geometric alignment of the two SAR images is very important in feature tracking to ensure that each pixel of the images represents the same area on the surface of the earth. The co-registration can be achieved using only orbital files however offset tracking requires precise co-registration so the DEM assisted co-registration tool in SNAP is used to get the desired level of precision.

Subset: Since the study area or Area of Interest (AOI) is small the image needs to be subset to reduce the computation time and storage.

Offset tracking: The movement of the feature between two co-registered images can be estimated both in the direction of range

and azimuth by running a cross-correlation between the selected Ground Control Point (GCP). Based on the offsets estimated by the cross-correlation the velocity of the movement of the feature is calculated. For the offset tracking, GCP grid spacing in terms of the pixels for both range and azimuth directions has to be set. Setting the grid spacing to 60 pixels ($60 \times 10 = 600$ m, 10 is the resolution cell size) in directions, level of detail (velocity vectors) and smoothness is optimum. The grid spacing can be reduced but comes at the expense of longer processing time and dense velocity vectors.

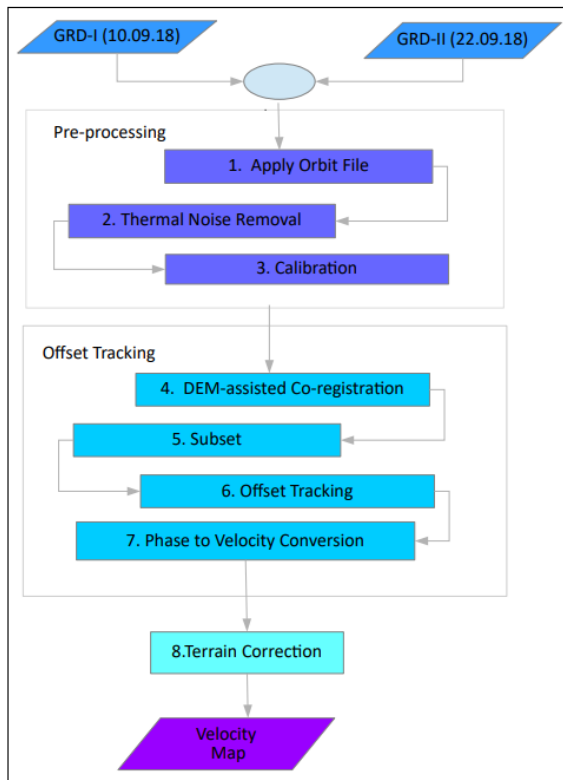


Figure 3. Feature tracking flow chart

Setting the registration window dimensions whose size depends on the maximum velocity of the glacier per day between the two imagery dates is explained here. In the case of SAR acquisitions with 12 days apart

and with a maximum speed of 5 m/day the glacier surface will move by a maximum of $12 \times 5 = 60$ m. So, the default SNAP setting of 128 pixels ($1280 \text{ m} \times 1280 \text{ m}$) can be used. If the maximum glacier velocity of the area under study is known then it can be set to filter out incorrect high values.

Terrain correction: The velocity map generated from offset tracking is radar geometry and to bring it on to the geographic projection system the SAR image is reprojected using the Range-Doppler Terrain Correction tool of the SNAP. The process is similar to the ortho-rectification in optical image processing to assign the pixels with their corresponding geographic coordinates. The range-Doppler terrain correction is basically applied only to SAR images as the SAR images are in the slant or range geometry which is different from the optical remote sensing geometry.

3. Result

3.1.LOS Displacement

The displacement along the Line of Sight (LOS) or in the range direction determined by DInSAR is shown in the map below. The LOS or the range direction is the direction perpendicular to the direction of the satellite (or azimuth direction). The displacement map is generated using SAR images taken at the descending mode. Here the azimuth direction is from north to south and the range direction is east-west in the displacement map below. The positive and negative signs before the magnitude of the displacement are just to indicate the direction of displacement.

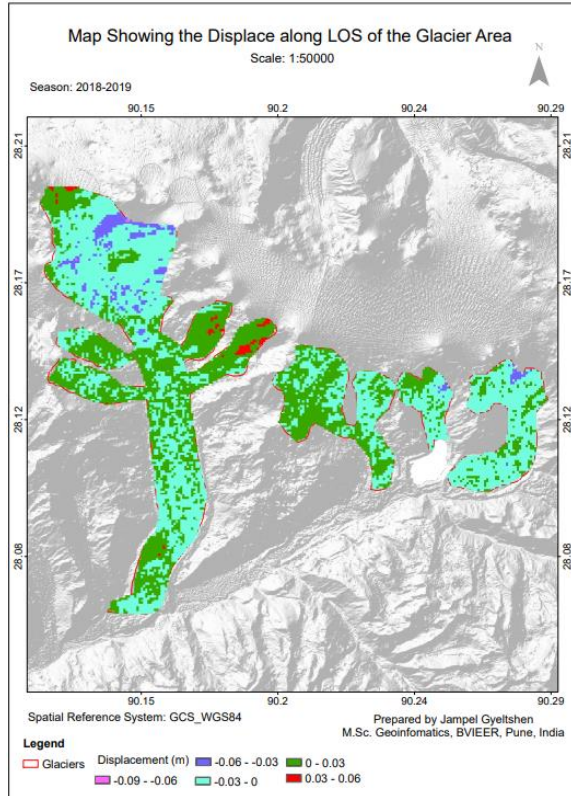


Figure 4. The LOS displacement overlaid on hill shade

The displacement away from the sensor is shown by a negative sign and towards the sensor is indicated by a positive sign. As shown in Figure 4, the maximum displacement of the glacier in 12 days’ time period along LOS away from the sensor and towards the sensor is 6 cm each. The minimum LOS displacement in both directions is 1 cm. The maximum LOS displacement is 9 cm away from the sensor but in the mountain peaks or in the region outside the glacier demarcation.

3.2.Velocity

The velocity determined using feature tracking method from the SAR GRD image shows glacier velocity of the area for the 12 days’ time period (September 10 and 22,

2018) is 134 cm/day (max) to 0-3 cm/day (min) as shown in Figure 5.

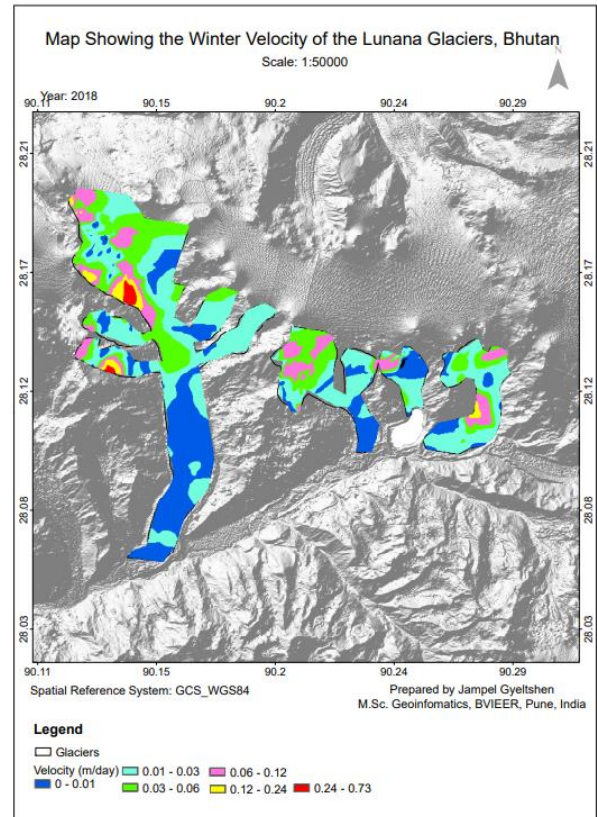


Figure 5. The winter velocity of glacier by feature tracking against hill shade

The glacier velocity in the summer as depicted in Figure 6 is in the range of 400-500 cm/day (max) to 0-50 cm/day (min).

In winter the glacier velocity drops to a range of 1-73 cm/day as shown in Figure 5.

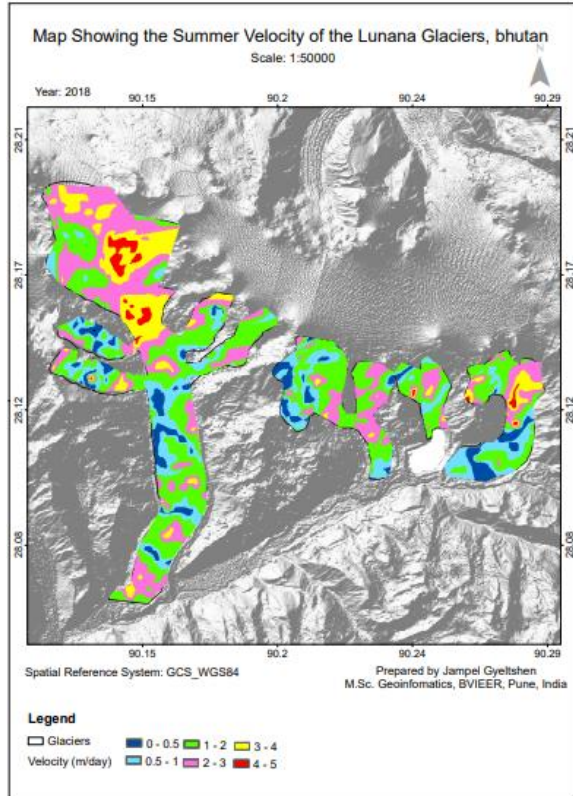


Figure 6. The summer velocity of glacier by feature tracking with hill shade as backdrop

4. Discussion

The earlier work on the Bhutan glacier has uncovered the signs of glaciers' recession. These retreating glaciers are characterized by the thickening of ice in the upstream regions and thinning at debris-covered terminus or snout. Also, they are active glaciers associated with motion and deformation (Tsutaki et al., 2018). This study determines the glacier deformation and its surface velocity over the glaciers in Bhutan Himalaya. Based on the temporal resolution of the Sentinel-1 products the investigation spans over a period of one year from October 2017 to October 2018. The entire time period is divided into the 12-day time period, summer and winter both separated by six months. The result shows glacier velocities in

winter are stable or minimal while in summer the velocity of the glaciers triples indicating seasonal variation in the surface velocities. Although many glacier deformation studies in the Himalayan region are carried out employing SAR methods, Bhutan segment has no record of glacier studies using such techniques. One of the studies in the area using image matching technique and optical image of Advanced Spaceborne Thermal Emission and Reflection Radiometer (ASTER) has estimated the surface velocity of the land-terminating glaciers in the range of 100-200 cm/year which corresponds to 2.74-5.48 cm/day (Kääb, 2005). The current velocity estimation using SAR offset tracking has yielded the velocities for the lake terminating glacier in the minimum range of 0-3 cm/day to a maximum range of 24-134 cm/day as shown in Figure 5. The result is in sync with the one determined by the pattern matching technique using optical images for the same area. The velocity is determined for a 12-day time period which corresponds to September 10 and 22, 2018 SAR acquisitions. The glacier velocity in the summer as depicted in Figure 6 is in the maximum range of 4-5 m/day and minimum range of 0-50 cm/day.

In winter the glacier's velocity drops to a range of 1-73 cm/day as shown in Figure 5. In the land-terminating glaciers, the glacier's velocity is very minimal, augmenting the fact that the Himalayan glaciers are summer melting type (Tsutaki et al., 2018) (Kääb, 2005) (Venkataraman, 2005) (Kumar et al., 2011) (Luckman et al., 2007).

The highest glacier velocities are found to be as high as 73 cm/day on the glacier on higher

slopes which could be attributed to fresh snowfalls and their movements. Otherwise, land-terminating glaciers are stagnant in winters. On the contrary, all the glaciers both lake and land-terminating, have high summer movement with peak velocities in the order of 300-500 cm/day. Also, the surface velocities of the debris-covered glaciers are slower.

Similarly, LOS displacement obtained from DInSAR is 9 cm away from the sensor with a minimum of 1 cm. Similarly, LOS displacement toward the sensor is 6 cm maximum and the minimum is 1 cm. The maximum displacement of the glacier in the upper regions is mainly attributed to the high slope (Kääb, 2005) (Ageta et al., 2000). The glaciers in the current study area lie in the slope range of 0-20° and are valley glaciers. The velocity of the glaciers is higher in the upper regions of the slope which are in tune with the finding from the deformation rates uncovered using the optical or ASTER image matching technique (Kääb, 2005). It also points to the fact that the glacier movement in these regions is basal sliding proportional to the slope change and summer precipitation.

5. Conclusion

Both the SAR techniques; DInSAR and offset tracking are found capable of determining the glacier surface deformation rates. The results are not only promising but are in tune with other accurate methods of the field-based survey as demonstrated in the other regions of the Himalayas. Such encouraging results are not only economical with the potential to replace the cost-

intensive, rugged terrain and hostile-laden field surveys but can be adopted with increased frequency for regular monitoring of the glaciers and their dynamics. The glaciers' deformation trends can also be studied for all seasons as SAR imaging is not impeded by the cloud and night covers. The examination of glacier dynamics can be achieved in detail like between inter-annual variations and inter-seasonal variations.

Leveraged by the free data and processing software, such techniques are within the reach of many users, scientists, researchers, decision-makers, planners, and most essentially disaster management agencies. In the fragile geological and ecological setting of the Himalayan region, the GLOF remains the single largest threat to the economy, livelihood and lives. Uncovering the glacier's dynamics through such a method will help the disaster mitigation plan to be put in place. It can also be applied for time-series monitoring of the glacier without having to visit the field or in complementary to the in-situ observation.

References

- A geta, Y., Iwata, S., Yabuki, H., Naito, N., Sakai, A., Narama, C., et al. (2000). *Expansion of glacier lakes in recent decades in the Bhutan Himalayas*. IAHS-AISH Publication.;264.
- Bello, O. A., Aina, YA. (2014). *Satellite remote sensing as a tool in disaster management and sustainable development: towards a synergistic approach*. Elsevier Ltd.
- Dharmadhikary, S. (2015). *International Rivers. Hydropower in Bhutan - Time for a Rethink?* Retrieved from www.internationalrivers.org: <https://archive.internationalrivers.org/blogs/328-5>.
- Ferretti, A., Prati, C., Rocca, F. (2001). *Permanent Scatterers in SAR Interferometry*. *Ieee Transactions on Geoscience And Remote Sensing*; 39(1):13.
- Gourmelen, N., Amelung, F., Lanari, R. (2018). *Interferometric synthetic aperture radar–GPS integration: Interseismic strain accumulation across the Hunter Mountain fault in the eastern California shear zone*. *Journal of Geophysical Research*;115(B9). Available from: <http://doi.wiley.com/10.1029/2009JB007064>.
- Hooper, A. (2008). *A multi-temporal InSAR method incorporating both persistent scatterer and small baseline approaches*. *Geophysical Research Letters [Internet]*;35(16). Available from: <https://agupubs.onlinelibrary.wiley.com/doi/full/10.1029/2008GL034654>.
- Hooper, A., Zebker, HA. (2007). *Phase unwrapping in three dimensions with application to InSAR time series*. *J Opt Soc Am A, JOSAA*;24(9):2737–47.
- Kääb, A. (2005). *Combination of SRTM3 and repeat ASTER data for deriving alpine glacier flow velocities in the Bhutan Himalaya*. *Remote Sensing of Environment*;94(4):463–74.
- Kampes, BM. (2018). *Radar Interferometry: Persistent Scatterer Technique [Internet]*. Springer Netherlands; (*Remote Sensing and Digital Image Processing*). Available from: [//www.springer.com/in/book/9781402045769](http://www.springer.com/in/book/9781402045769).
- Kumar, V., Venkataramana, G., Høgda, KA. (2011). *Glacier surface velocity estimation using SAR interferometry technique applying ascending and descending passes in Himalayas*. *International Journal of Applied Earth Observation and Geoinformation*;13(4):545–51.
- Leibowitz, E. (2009). *WWF*. Retrieved from www.worldwildlife.org: *Ten Interesting Facts about Glaciers | Blog Posts | WWF [Internet]*. Available from: <https://www.worldwildlife.org/blogs/good-nature-travel/posts/ten-interesting-facts-about-glaciers>.
- Lewis, S. (2009). *Remote sensing for natural disasters: Facts and figures*. Retrieved from www.scidev.net: <https://www.scidev.net/global/features/remote-sensing-for-natural-disasters-facts-and-figures/>.

- Luckman, A., Quincey, D., Bevan, S. (2007). *The potential of satellite radar interferometry and feature tracking for monitoring flow rates of Himalayan glaciers. Remote Sensing of Environment*;111(2–3):172–81.
- Mool, P. W. (2001). *Inventory of Glaciers, Glacial Lakes and Glacial Lake Outburst Floods: Monitoring and Early Warning Systems in the Hindu Kush-Himalayan Region - Bhutan. Kathmandu, Nepal: International Centre for Integrated Mountain Development (ICIMOD); United Nations Environment Programme (UNEP).*
- Schubert, A., Faes, A., Kääh, A., Meier, E. (2013). *Glacier surface velocity estimation using repeat TerraSAR-X images: Wavelet- vs. correlation-based image matching. ISPRS Journal of Photogrammetry and Remote Sensing*; 82:49–62.
- Sheng, Yaobin & Wang, Yunjia & Ge, Linlin & Rizos, Chris. (2012). *Differential radar interferometry and its application in monitoring underground coal mining-induced subsidence.*
- Strozzi, T., Luckman, A., Murray, T., et al. (2002). *Glacier motion estimation using SAR offset-tracking procedures, IEEE Transactions on Geoscience and Remote Sensing* ;40(11):2384–91.
- Tsutaki, S., Fujita, K., Nuimura, T., Sakai, A., Sugiyama, S., Komori, J., et al. (2018). *Contrasting thinning patterns between lake- and land-terminating glaciers in the Bhutan Himalaya. The Cryosphere Discussions*;1–29.
- Usai, S. (2003). *A least squares database approach for SAR interferometric data. Geoscience and Remote Sensing, IEEE Transactions on*;753–760.
- Venkataraman, G., Rao, Y. S., & Rao, K. S. (2005). *Application of SAR Interferometry for Himalayan Glaciers. Fringe Workshop; 2006ESASP.610E..28V.*
- Zebker, H.A. & Villasenor, John. (1992). *Decorrelation in Interferometric Radar Echoes. Geoscience and Remote Sensing, IEEE Transactions on.* 30. 950 - 959. 10.1109/36.175330.

SLOPE STABILITY ANALYSIS USING LIMIT EQUILIBRIUM METHOD

Yonten Phuntsho¹

Abstract

Bhutan is susceptible and vulnerable to slope failure due to its adverse topographical, geological and environmental factors. Many possible factors affect slope stability, such as soil and slope conditions. In this study, circular slip failure analysis based on the limit equilibrium theory was conducted to understand the influence of various factors. Firstly, Aieslip, a landslide case study, was carried out for groundwater level to elucidate the slope failure mechanism. Then, a sensitivity analysis using soil and slope parameters assumed in Bhutan was carried out. As a result, it was confirmed that the groundwater level has the most significant influence on the stability than other factors.

1. Introduction

As part of the fragile Himalayan geological region with high elevation, gradient and heavy precipitation, Bhutan is a hotspot of slope failures. The anthropogenic activities exacerbate the condition of slope stability. According to Tayler and Burns (2005), "Earthquakes are the greatest threat to long term stability of slope in active earthquake zones." Similarly, according to Thielen et al. (2005), "The combination of intense rainfalls, steep topography and soil conditions are critical." Bhutan has been

facing challenges of many landslides/slope failures, primarily along the roadway. The landslide inventory report showed 480 landslides in the four districts i.e., one landslide every 11.5 sq. km and according to the audit report (RAA, 2018), the government spends around Nu. 2,666.54 million annually only on road maintenance due to slides.

The primary purpose of slope stability analysis is to contribute to safe and economical excavations and provide uninterrupted services like traffic movement, power production, and similar infrastructure. With Bhutan on the development path, the demand for engineered cut and fill slopes will increase, increasing the need to understand the analytical and investigative methods to solve slope stability problems. The key to understanding the slope stability principle lies in understanding the geological, topographical and environmental factors. The study area, Aieslip, is located 9 km from Gelephug Town towards Zhemgang on the left side of the Primary National Highway (PNH) (Figure 1).

¹ *Yonten Phuntsho, Senior Geologist, Department of Geology and Mines, Thimphu, Bhutan
Masters of Engineering, Nagoya University, Japan, Email: yphuntsho@moea.gov.bt*

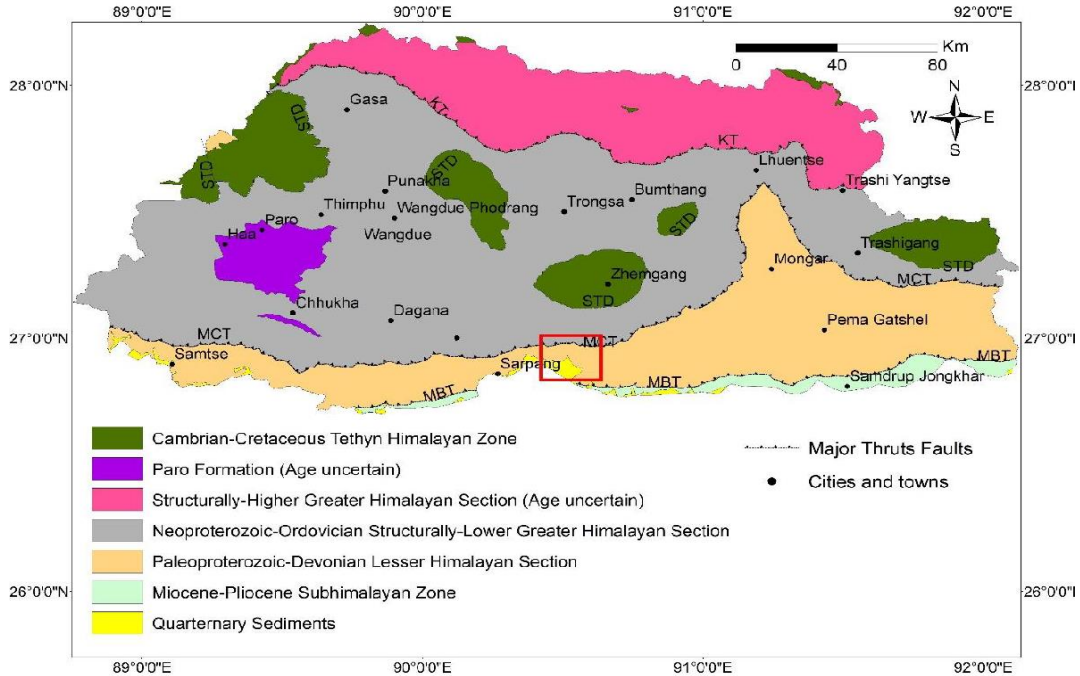


Figure 1. Simplified Geological Map of Bhutan modified from Long et al. 2011. The red square shows the location of the study area

2. Objective

The increase in the construction projects, together with the country’s development, increases the need to understand the analytical and investigative methods to solve the slope stability problems. However, given the significant impact of slope failure on the economy and life of the people, slope stability studies are of paramount importance. The primary objectives of this study are as follows: -

1. To evaluate the slope stability conditions at the Aieslip as a case study;
2. Compare the most common limit equilibrium methods (LEMs); and
3. Carry out the sensitivity analysis due to Material parameters

3. Methodology

SLIDE2 software is a 2D slope stability program developed by Rocscience Inc Toronto, Canada, for evaluating the safety of factor or probability of failure of circular or non-circular failure surfaces in soil. Different conditions like external loading, groundwater and support are modeled in different ways. SLIDE2 utilized the LEMs to analyze the stability of slip surfaces using both vertical and non-vertical slices.

3.1.Principle of the Limit Equilibrium method

The LEM assumes the material as linear and utilizes the Mohr-Coulomb criterion to determine the shear strength of the slip surface. The computation of Factor of Safety

(FoS) using several limit equilibrium equations is called the limit equilibrium procedure (Duncan, 2005).

$$F = \frac{s}{\tau} \dots\dots\dots(1.1)$$

where *s* is shear strength and τ is the equilibrium shear stress. Using Mohr-Coulomb equation shear strength is expressed as Eq. (1.2)

$$\tau = \frac{c + \sigma \tan \phi}{F} \dots\dots\dots (1.2)$$

where *c* and ϕ are the cohesion and friction angle respectively for the soil and σ is the total normal stress on the shear plane.

The shear strength expressed in terms of effective stress

$$\tau = \frac{c' + (\sigma - \mu) \tan \phi}{F} \dots\dots\dots (1.3)$$

where *c'* and ϕ' represent the shear strength parameters in terms of effective stresses, μ is the pore water pressure and *F* is the FoS.

3.2.LEMs

There are two methods to fulfill the static equilibrium in the limit equilibrium analysis. The first approach considers the equilibrium for the entire soil mass bounded beneath an assumed slip surface and above by the slope. In this approach, the equilibrium equations are solved for a single free body. In the other procedure, the soil mass is divided into several horizontal or vertical slices, and equilibrium equations are solved for each slice (Duncan, 2005).

3.3.Data collection

Most of the data required for the LEM analysis is gathered from the Reports of

studies carried out by the Department of Geology and Mines (DGM) and the detailed Geotechnical Investigation report by Alpha Geotech and Company.

Index Properties

The soil ranges from silt to gravel with silt ranging from 5 - 12%, sand ranging from 50-70% and gravel ranging from 25-42% (Table 1).

Table 1. Summarized index soil properties of Aieslip

Test no.	Moisture content	Unit weight	Specific Gravity	Permeability	Grain size distribution (%)		
					Fines	Sand	Gravel
					w (%)	Yb kN/m ³	G _s
TP-A1	16.08	16.37	2.71	1.03E-04	5.59	52.29	42.12
TP-A2	23.69	17.36	2.41	1.22E-05	12.37	62.15	25.48
TP-A3	15.46	16.33	2.64	1.03E-04	5.28	57.32	37.4
TP-A4	28.44	17.65	2.5	1.22E-05	10.78	69.49	19.73

Shear Strength Parameters

The shear strength of the soil from the landslide area is determined using direct shear box tests. Table 2 shows the summarized shear strength properties for four soil samples collected from the four trial pits. The cohesion of the soil ranges from 2.93 - 22.12 kPa and the friction angle from 22.12-33.5°.

Table 2. Shear parameter of Aieslip using shear box test

Test no.	Direct shear		
	c		Phi
	kg/cm ²	kPa	deg
TP-A1	0.03	2.93	33.5
TP-A2	0.25	24.63	24.84
TP-A3	0.02	2.42	2.42
TP-A4	0.23	22.12	22.12

Data for Parametric analysis

The soil data for the sensitivity analysis is compiled from the past geotechnical reports that DGM had undertaken and the average soil data from ten districts are shown in Table 3.

Table 3. Material input parameter for the sensitivity analysis

Parameter	Min	Mean	Max
Friction angle (degree)	27	30	33
Cohesion (kPa)	0.5	6.8	13.03
Unit weight (N/m ³)	12	14	16
GWT (m)	0	7	14

4. Result and interpretation

The result for the study is presented in three parts, the first being the result for the Aieslip Landslide and the second, the results for the comparison among LEMs and third for the sensitivity analysis on the FoS.

4.1.LEM analysis for Aieslip landslide

Based on drilling, the dry season groundwater table is defined at the boundary between the overlying soil layer and the underlying phyllite bedrock. The groundwater table may change from the current location in the future. However, the main objective in the current study is only to determine the FoS. Figure 2(a) shows the FoS and the critical slip surface when the groundwater is at the minimum, indicating dry season. The FoS is greater than 1 for all the selected LEMs indicating a stable slope. Similarly, Figure 2(b) shows the FoS for all the LEMs along with the critical slip surface when the groundwater is at the ground level. The FoS is less than 1 for all the LEMs, indicating eminent slope failure.

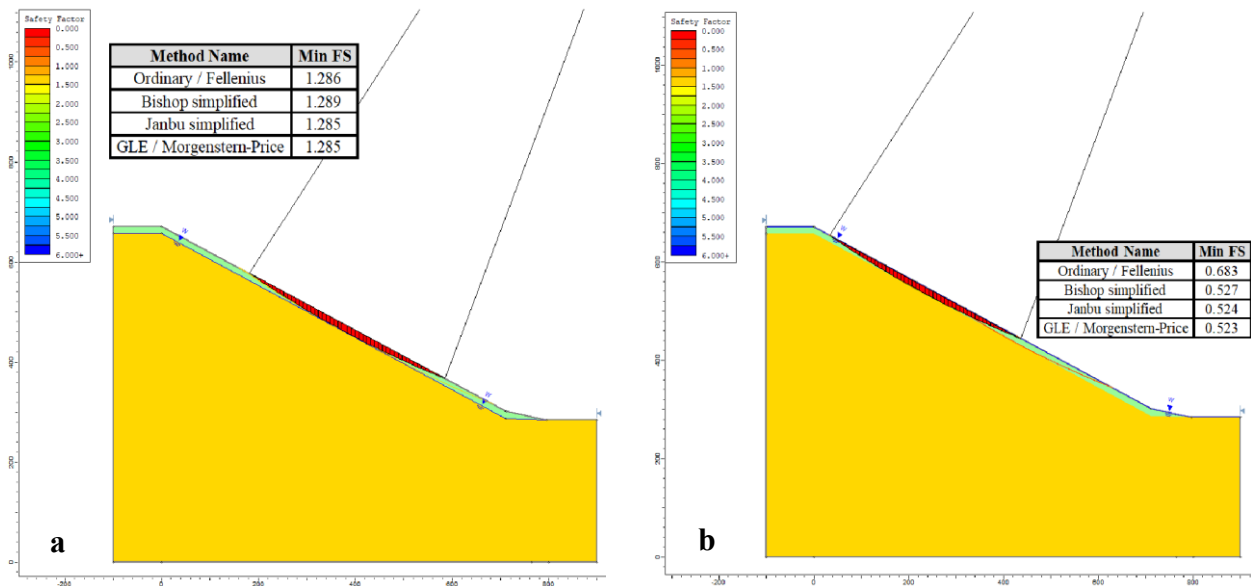


Figure 2. The result of SLIDE2, a) FoS during dry season, b) FoS during the wet season

4.2. Comparison of LEMs

The difference among the LEMs is based on assumptions about the position and inclination of the interslice forces, as shown in Table 4. Some methods compute the FoS by force equilibrium (Janbu's simplified method) or moment equilibrium (Bishop & Fellenius method). Similarly, the advanced LEM satisfy both force and moment equilibriums (Morgenstern-Price method).

Table 4. Assumption made for different LE methods for fulfilling moment & force equilibrium (modified from Duncan & Wright, 1979)

Procedure	Equilibrium conditions satisfied				Equation and unknown	Shape of slip surface
	Overall moment	Individual moment	Interslice vertical force	Interslice horizontal force		
Fellenius method	Yes	No	No	No	1	circular
Bishop's simplified method	Yes	No	Yes	No	N+1	circular
Janbu's simplified method	No	No	Yes	Yes	3N	any
Morgenstern-Price method	Yes	Yes	Yes	Yes	3N	any
Spencer's method	Yes	Yes	Yes	Yes	3N	any

Table 5 and Figure 3 show the summarized FoS for different LEMs for different groundwater conditions. For unsaturated conditions, the slope is analyzed to be stable with a FoS > 1. However, for saturated conditions, the slope indicates failure. The FoS for all the LEMs deviate by < 1%; however, there is significant deviation in case of saturated loading conditions.

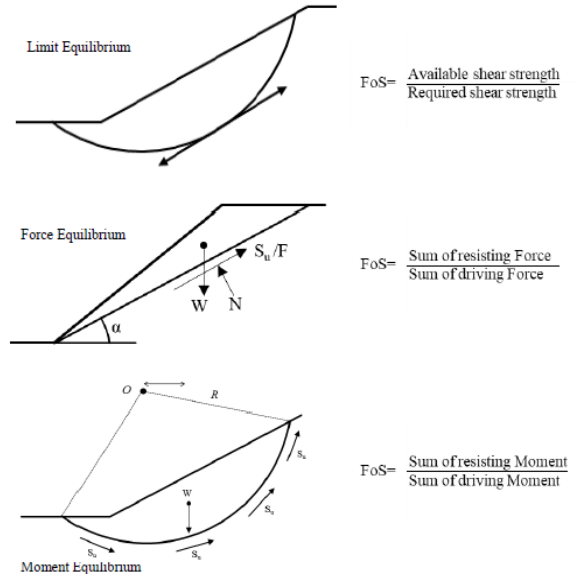


Figure 3. Various definitions of Factor of Safety (Abramson et al., 2002)

Table 5. The FoS for different loading conditions & LE methods

Method	FoS			
	Unsaturated	Saturated	Pseudostatic 0.1	Pseudostatic 0.2
Fellenius	1.286	0.683	1.031	0.847
Bishop simplified	1.289	0.527	1.034	0.850
Janbu simplified	1.285	0.524	1.031	0.847
M-P	1.285	0.523	1.031	0.847

4.3. Parametric Analysis

The sensitivity analysis gives an overview of the significance of different input parameters on the FoS of the slope. This study divides the input parameters into material parameters based on the minimum and maximum groundwater level.

The sensitivity analysis allows for the determination of the sensitivity of the FoS to variation in the input data variable. This is done by varying one variable while keeping all other variables constant. In the material sensitivity analysis, the parameters taken into

consideration are unit weight, friction angle and cohesion, and groundwater location (Table 6).

Table 6. Material input parameter for the sensitivity analysis

Parameter	Min	Mean	Max
Friction angle (degree)	27	30	33
Cohesion (kPa)	0.5	6.8	13.03
Unit weight (N/m ³)	12	14	16
GWT (m)	0	7	14

Table 7 shows the FoS analyzed for the Morgenstern-Price method when the groundwater is at the minimum. In the minimum groundwater condition, the FoS > 1 for all the material parameters. The friction angle and cohesion have a positive influence on the FoS. However, unit weight has a negative influence on the FoS.

Table 7. FoS for sensitivity analysis for M-P method

Parameter	FoS		
	Min	Mean	Max
Friction angle	1.11	1.24	1.38
Cohesion	1.12	1.24	1.36
Unit Weight	1.26	1.24	1.22

Table 8 shows the result for the slope's FoS in the presence of the groundwater table. In the presence of mean groundwater (7 m), the FoS < 1 for all the material parameters indicating a slope failure. Similar to the minimum groundwater conditions, the friction angle and cohesion positively influence the FoS. However, in the case of unit weight, it shows a positive influence, unlike the minimum groundwater conditions.

Table 8. Change in FoS in the presence of Ground Water Table

	FoS		
	Min	Mean	Max
Friction angle	0.79	0.88	0.98
Cohesion	0.76	0.88	1.01
Unit Weight	0.85	0.88	0.91
GWT	1.23	0.88	0.25

5. Conclusion and Recommendation

5.1. Conclusion

The objective of the study is to determine the slope stability of Aieslip as the case study based on the groundwater level. The second objective is to compare different limit equilibrium methods. Accordingly, the most common limit equilibrium methods are compared with the advanced Morgenstern-Price method. Finally, the sensitivity analysis for material and slope parameters is carried out to determine its influence on the FoS.

The key findings from the study are summarized as follows:

1. The slope stability of Aieslip area showed stability when the groundwater is at the minimum and failure with the rise in groundwater;
2. In the case of saturated loading conditions, Bishop, Janbu and Morgenstern-Price methods yield similar FoS. However, the Fellenius method shows significant deviation of 30.59% from the Morgenstern-Price method;
3. In the absence of the groundwater, the change in friction angle has the most significant influence on the FoS,

followed by the cohesion. And in the presence of groundwater, the height of the groundwater has the most significant influence on the FoS.

5.2.Recommendation

Limit equilibrium analysis of slope stability is an effective, reliable and widely used method in excavation and embankment slopes design. The accuracy of an equilibrium analysis of slope stability depends on the accuracy with which the strength properties and geometric conditions can be defined on the inherent accuracy of the Griffiths analysis method. Within these

perspectives, following recommendations are made:

1. The Finite Element Method is recommended to compare the FoS from the LEM.
2. Based on the result, extra care should be given to the height of the groundwater and angle of the slope while carrying out the slope stability analysis; and
3. The accuracy of an equilibrium analysis depends on the accuracy with which the strength properties are defined. Equipment with high precision and accuracy like triaxial must be used for the determination of the shear parameter.

Reference

- Abramson et al. (2002). Slope stability and stabilization methods*
- Alpha, G. (2020). Detailed Geotechnical Investigation & Design of Countermeasure Structures for Mitigation of Landslide at Aieslip on Trongsa - Gelephu PNH. September.*
- DiPietro, J. A., & Pogue, K. R. (2004). Tectonostratigraphic subdivisions of the Himalaya: A view from the west. Tectonics*
- Duncan, J. M., & Wright, S. G. (1980). The accuracy of equilibrium methods of slope stability analysis. Engineering Geology*
- Duncan, J. Michael. (2005). Soil Strength and Slope Stability.*
- Duncan, James Michael. (1996). State of the Art: Limit Equilibrium and Finite-Element Analysis of Slopes. Journal of Geotechnical Engineering*
- Griffiths, D. V., & Lane, P. A. (2001). Slope stability analysis by finite elements. Géotechnique*
- Kellett, D. A., Grujic, D., & Erdmann, S. (2009). Miocene structural reorganization of the South Tibetan detachment, eastern Himalaya: Implications for continental collision*
- Le Fort, P. (1975). Himalayas: the collided range. Present knowledge of the continental arc. In American Journal of Science*
- Rocscience. (2002). Slide 5.0 User's Guide. Slide 5.0 User's Guide, 90.*
- Searle, M. (2005). Colliding Continents.*

MINERAL ROYALTIES – A FORM OF TAX IN MINING SECTOR

Karma Chophel¹

Mineral Taxation in General

Minerals have become the basic building blocks of civilized life and are an essential segment of economies of a country. The minerals are mined by human for development purposes.

Mineral sector is generally subjected to a special taxation and Royalty regime, in addition to the range of taxes normally imposed on all business sectors in the economy. The reason being the depletion of non-renewable resources and the desirability to generate a return to the State as the owners of natural resources.

All governments, in the process of determining the structure and nature of the taxes they impose on mining and on the mineral sector in general, encounter the following public policy issues.

Optimal level of taxation on mining

The more the taxes imposed on the mineral sector, the greater is the share of wealth created by mining to the government. However, increasing tax rates undermines companies' incentives to carry out mineral exploration, develop new mines or increase the productions. On the other hand, low tax rates leave the state with only the non-tax benefits that flow from mining and mineral production. Thus, between these two extremes is an optimum level of taxation which is a critical issue for public policy.

Optimal mix of taxes

Many different types of taxes can be, and are, imposed on the mineral sector. Each, including the various forms of royalties, has its own set of advantages and disadvantages with respect to economic efficiency, the division of risks between the state and companies, ease of administration, and other considerations. Mining is a particularly risky activity. This is partly because of the long gestation period associated with the development of most new mines and the difficulty of anticipating the potential technical, geological, economic, and political problems. In addition, most mineral commodity markets are highly volatile over the business cycle, with wide price fluctuations.

Some economists claim that royalties imposed on each metric ton of mineral mined introduce inefficiencies in production decisions. It is a cost of production and it impacts the profitability of some projects especially low-grade ores. Therefore, many argue that a tax on corporate income or profits is more efficient, because such a tax does not alter the optimal output of companies striving to maximize profits, and marginal ore will remain profitable to exploit. However, corporate profit taxes and royalties based on profits also have distorting effects on firms' behavior.

¹ Karma Chophel, Executive Engineer, Department of Geology and Mines, Thimphu, Bhutan
Master of Professional Engineering, The University of Western Australia, Email: kchophel@moea.gov.bt

A corporate profits tax and royalties based on profitability tend to distribute the risk of mining evenly between the state and companies. A unit or value-based royalty shifts more of the risk to companies. Even when prices are depressed and companies are at loss, the government continues to receive a certain amount for each metric ton of metal produced and sold.

The mix of taxes also affects the flow of government revenues over time. Revenues from a unit or value-based royalty comes at the time of production whereas corporate profits tax or profit-based royalty once the project is profitable. Moreover, with a corporate profits tax, provisions allowing the accelerated depreciation of capital equipment can postpone the flow of tax revenues for years.

Another important consideration in determining the mix of taxes is the difficulty of tax administration and the possibilities for evasion. Some taxes, including many types of royalties, are easy to administer and difficult to evade. Government officials simply need to know a company's total sales or production to determine its tax liability. This not only reduces administrative costs; it reduces the incentives that the firms have to devote to tax reduction efforts.

Specificity or uniformity

Another policy issue concerns the specificity of the tax code. For tax purposes, many countries consider the mining and the mineral sector special. This is in part because, for some countries, this sector plays a dominant role in the economy, accounting for a large share of all government revenues and foreign exchange earnings. In such instances, it is not unusual

for the government to negotiate specific agreements covering a variety of issues, including taxation for individual large-scale, or "mega," projects. In addition, there is widespread perception that the mineral sector is different, and so should be taxed differently, because it exploits a non-renewable resource.

Tax regime stability

Companies that are deciding whether to invest in a mineral project are largely influenced by the expected return after taxes and risks involved. An important component of any assessment of risk is the perceived stability of the existing tax regime. Companies that plan to invest hundreds of millions of dollars or even billions of dollars in a new mine and mineral complex are very wary of possible changes in the tax burden after their investment is made and no longer mobile.

However, for both companies and governments, stability of tax regime is hard to guarantee. One reason is the difficulty of binding future governments to the current promises and agreements. Changes in the tax regime undermine the investors' perception of stability, raising the perceived risk of investment in the country.

Distribution and use of tax revenues

One of the conclusions emerging from what is called the resource curse debate is that mineral production can both foster and hinder economic growth, with the outcome being largely determined by how governments use the taxes and other funds they receive from the mineral sector.

Given the volatility of mineral prices and profits over the business cycle, one issue in the debate concerns the usefulness of a

commodity stabilization fund. When mineral taxes are high, the government deposits some of its revenue into such funds. Revenues are then withdrawn when mineral prices and taxes are low. Such arrangements exist, or have existed, in Chile, Namibia, Nauru, Norway, Papua New Guinea, and other mineral producing countries; they have worked well in some countries and not so well in others. An associated issue is what to do with the money while it is in the fund. Investing profits abroad, rather than domestically, helps insulate the domestic economy from the adverse microeconomic effects that a mineral boom can cause, thereby reducing the prospect of what is commonly called the Dutch disease from occurring (Otto, et al., 2006)

Mineral Royalties

A Dictionary for Mining, Minerals and Related Terms compiled and edited by the staffs of US Bureau of Mines defines Royalty as “(a) A lease by which the owner or lessor grants to the lessee the privilege of mining and operating the land in consideration of the payment of a certain stipulated royalty on the mineral produced. Ricketts (b) Ownership of mineral rights under restricted terms. Wheeler, R.R. (c) Eng. The mineral estate or area of a colliery, or a portion of such property. A field of mining operations. (d) The landowner's share of the value of minerals produced on a property. It is commonly a fractional share of the current market value (oil and gas) or a fixed amount per ton (mining).”

In the majority of nations, minerals are owned by the state, by the people generally, or by the crown or ruler. In other instances, mainly European civil law nations, the

owner of the land where the minerals occur owns the minerals. The owner of minerals, like the owner of any other form of real property, has an interest in receiving payment. Such a payment, can affect ownership transfer tax that is often used as the justification for a royalty.

In Bhutan, the mineral is owned by the State. The section KA 11-1 of the Thrimshung-Chhenpo spells that all rights of ownership of minerals are vested exclusively in the Government whether occurring in private or government land. The ownership of mineral is enshrined in the Article 1(12) of the Constitution of the Kingdom of Bhutan 2008 as the properties of the State.

Justification for Royalties

The structure and rates of mineral royalties vary widely, and are collected firstly, for the payment to the owner of the mineral resources in return for the extraction of the minerals from the land. The royalty, as the instrument for compensation, is payment in return for the permission that gives the mining company access to the minerals and the right to develop the resource for its own benefit (Otto, et al., 2006).

Second, mineral resources are non-renewable on any time scale of relevance to the human race. As a result, an opportunity cost is incurred in consuming mineral resources today, since once exploited they are no longer available for use in the future. This means that future production will have to rely on inferior quality resources and, consequently, more expensive resources, or use alternative materials.

Third, although there are mines failing to earn a competitive rate of return on their capital or are, at best, just marginally

profitable, a few are highly profitable. Inevitably, the latter tend to attract the attention of the public and raises many questions.

Economists have justified mineral royalty payments as the owner's share of differential returns on certain mines given their higher productivity (economic rent) or as payments to the owner for minerals removed (user cost) (Hein & Cecot, 2017).

Types of Royalties and Assessment Methods

The evolution of royalty instruments has become more complex over time as the legal description of mineral rights ownership developed alongside the separate tenure for mineral developers under mineral law. The owner of the mineral rights is defined in property law, which varies from country to country. An owner could be a community as a group of people, whose communal ownership stems from ancient customary law; an individual, as is the case in countries where there are traces of civil law; or a government exercising sovereignty over the mineral resources within its territory in terms of international law.

The various types of royalties have merits and demerits which impacts both investors and governments. Some royalties are relatively easy to assess and monitor, and others are more difficult. There are wide varieties of approaches across the globe in royalty taxation in different countries with no clear trend for global convergence. However, the royalty tax system globally can be classified as one of the three types:

1. Unit based;
2. Ad Valorem (value based); and

3. Profit based.

Few nations apply hybrid systems that combine two or three methods. Though the unit based and Ad Valorem systems of royalty are more prevalent, the profit-based systems are increasingly being applied in the developed countries.

Unit-based Royalties

The oldest form of royalty assessment is based on a fee levied per unit volume or weight and is termed a *unit-based* or *specific* royalty (the latter used mainly in Australia). For example, the royalty may be calculated based on Nu. 160 per cubic meter or Nu. 50 per metric ton. Although volume-based unit royalties used to be applied in some nations, primarily to industrial minerals and crude oil, they have largely been re-placed by weight-based unit royalties that are easier to monitor and assess. A unit-based royalty is most often applied to minerals that are more or less homogeneous, such as industrial minerals (sand, gravel, cobbles, limestone, dimensional stone) or sold in bulk (coal, iron ore, salt, phosphate, potash, sulfur). The most prevalent forms of unit-based royalty are based on making the measurement (weight or volume) at the mine mouth, before significant treatment or processing takes place. However, the concept can be applied at any stage of the mineral preparation process.

Unit-based royalties are straightforward compared with most other assessment methods because parameters subject to dispute, such as price, value, and costs, do not come into the calculation. However, they are not without their quirks. For instance, weight-based measures may change depending on the degree to which

the mineral undergoes treatment. For metallic minerals sold as ore or in concentrate, the weight basis may be linked to the weight of the ore or concentrate, the weight of the metal contained in the ore or concentrate, or the weight of the metal that can be recovered.

Unit-based royalties are not as easily applied to non-homogeneous mineral products. For example, a typical copper concentrate from a massive sulfide deposit may contain marketable copper, but also zinc, lead, gold, and platinum, each of which has a very different intrinsic value. A unit-based royalty based on copper content alone would not recognize the value potential of by-products or co-products. The rate of the royalty for different mineral are mostly different.

Value-based Royalties

Value-based royalties are also known as Ad Valorem royalties. The royalty is calculated by multiplying the royalty rate with the value of the mineral. The royalty rate may be uniform for all sales of that mineral or may vary according to a sliding scale based on the volume or cumulative value of material sold. Value can be determined in many ways, with the most common being the value of the mineral in the following circumstances:

- Contained in the ore at the mine mouth;
- Contained in the first product sold (such as a concentrate);
- Recoverable;
- Determined by the gross revenues derived from sales;
- Determined by the gross revenues derived from sales minus certain

allowable costs, such as transportation, insurance, and handling;

- As reflected in a net smelter return (adjusted for smelter and refining charges).

Like unit-based royalties, value-based royalties are payable irrespective of whether the mine is making a profit or not. However, unlike unit-based royalties, value-based royalties fluctuate following commodity prices. Thus, when prices are high, the government will enjoy more revenue than when prices are low.

Value-based royalties should be easy to calculate but often are not. The degree of complexity will depend largely on how value is defined. If value is defined simply as revenue received from a sale (gross value, invoice value, billed value), the calculation is straightforward. However, some governments are concerned that the value received from a sale may be less than the market value. This suspicion may arise from experiences with “transfer pricing” tax avoidance situations, sales to vertically integrated affiliates at abnormally low prices, poor guessing with regard to futures contracts, long-term sales agreements where prices are out of sync with the market, and so forth. Companies may argue that invoice value does not reflect market value, because market value would take into account certain expenses, for example, transportation, insurance, and handling to the point of export. In response, some countries have moved to more complicated systems that take into account a hypothetical market value. Governments define market value in a number of ways. For instance, value may be calculated by first determining the amount of the physical mineral contained in the product and then

applying a reference price to that amount. Reference prices, such as a London Metals Exchange daily quotation for copper cathode, are available for some but not all minerals. An inherent problem with reference price systems is that quite often what is being sold, such as a concentrate, is not the same product as is being referenced, such as cathode.

The picture becomes more complicated when the value begins to be adjusted to subtract out specified costs, usually not directly related to mineral extraction or beneficiation. The most common adjustment is to deduct from the sales value all costs such as transportation, insurance, and handling that are incurred from the mine site to the point of sale. Another common value is net smelter return, in which the taxable amount takes into account the return to the producer after smelting and refining charges and penalties are taken out.

Profit-based and income-based Royalties

Most investors favor taxation systems that are based on the ability to pay, that is, some measure of profitability or adjusted income. Unit-based and value-based royalties do not take into account the relative profitability of an operation because they simply look at the quantity of mineral produced or at some measure of the value of mineral produced or sold. Ad Valorem royalties in their purest forms look only at value, although cost-adjusted valuation methods do to some extent account for some non-production-related costs. Distinct from unit-based and Ad Valorem approaches are a variety of methods that in some way include deducting a broader set of costs, including production and capital costs, in the royalty calculation. Some nations have moved

away entirely from assessing royalty and rely instead only on the general income tax (for example, Greenland, Mexico, Sweden, and Zimbabwe do not impose a royalty).

Many nations have applied to royalty assessment the concept of taxation based on the ability to pay. The approaches vary but are grounded in the concept that both the value of the mineral produced and certain allowable costs (such as capital costs, production costs, marketing costs, transportation costs, handling costs, and insurance costs) should be taken into account. According to Green, quoted in Faber 1997, the ideal approach to royalty assessment is described as follows:

“A mineral royalty is a compensation to the owner for the exhaustion of an asset and ideally, therefore, should be fixed at a figure bearing some relation to the value of the mineral as it lies in the ground, i.e., the sale of the mineral recovered less a reasonable charge for the extraction, treatment and transport to the point of sale, sufficient to cover all costs and overheads including a reasonable return on the capital expenditure, together with the provision for the amortization of that capital.

In practice, the assessment and auditing challenges posed by a royalty based on the concept of resource rent have proved too great, and today few, if any, governments attempt it. However, simpler profit-based or income-based royalty systems have been adopted that include in the calculation the sales revenues less allowable costs but ignore return on capital. Profit-based royalties go by many names, including net profit royalty, net interest royalty, net proceeds royalty, mining tax, and so forth.

The net profit royalty is complex and often difficult to understand or confirm, requiring a lot of information and often the services of an accounting professional to calculate and confirm it. Conceptually, and if determined equitably by a payor, the net profit royalty is good for all concerned. The recipient will probably receive a relatively large percentage of net profit and so may see a high return from a successful venture. He must, however, be prepared to wait to realize this return and to share with the payor in the risks of the venture by permitting the payor to recoup at least a goodly portion of his costs before sharing. He must also be prepared to spend time and money for expert professional advice to be sure that he receives his proper share. Above all, he must be prepared to run the risk that the project, even if it is brought into commercial production by a generous and equitable payor, may never see a “net profit,” in which event he will never see a royalty payment.”

Hybrid systems

A variety of approaches combine the concept of profitability with value or unit-based royalties. For example, a measure of profits can be calculated and, depending on that measure perhaps a ratio of costs to sales revenue, a rate of return, or a ratio of price per unit to a reference price, the Ad Valorem royalty rate is adjusted up or down. This type of system thus takes into account profitability and distinguishes low-profit mines from high-profit mines, while maintaining a royalty flow from all mines.

In another hybrid system, the taxpayer calculates both an Ad Valorem and a profit-based royalty and then pays the higher of the two, or pays both, but in the latter case is able to credit the Ad Valorem payment

against the profit-based royalty liability. In such systems the Ad Valorem royalty acts as a minimum tax.

Conclusion

The majority of the world’s nations have initiated regulatory reform of their mineral sector over the last decade. One of the main reforms were targeted towards examination of the fiscal system imposed on mining sector.

Most governments impose a royalty tax on producers of minerals. Those nations that do not impose royalty may be reluctant to do so because of the desire to apply non-discriminatory taxation principles across economic sectors or to present favorable investment conditions to attract investment in a globally competitive market place.

Most royalty methods applied by various nations can be classified as one of three types: unit based, value based (Ad Valorem), or profit-based. Some nations, but only a few, apply hybrid systems that combine two of the three methods. The most prevalently used methods are the unit-based and value-based systems, but profit-based systems are increasingly being applied, particularly in diversified economies.

Due to geological, economic, social, and political circumstances that make each nation unique, an approach to royalty taxes that is optimal for one nation may be impractical for another. However, while designing mineral sector taxation systems, policy makers must carefully seek to balance tax types, rates, and incentives that satisfy the needs of both the nation and the mining investor. When determining taxes and levels of taxes to apply in the mining sector, policy makers should not only

consider ways to achieve individual tax objectives but also take into account the cumulative impact of all taxes. Such awareness must include recognizing the importance of each tax type for achieving

specific objectives. The overall tax system should be equitable to both the nation and the investor and should be globally competitive.

References

- Hein, J. F., & Cecot, C. (2017). *Mineral Royalties: Historical Uses and Justifications*. SSRN Electronic Journal.
- Hund, Kirsten; Porta, Daniele La; Fabregas, Thao P.; Liang, Tim; Drexhage, Jogn;. (2020). *Minerals for Climate Action: The Mineral Intensity of the Clean Energy Transition*. Washington DC: The World Bank.
- Indian Bureau of Mines. (2011). *Mineral Royalties*. Nagpur.
- Otto, J., Andrews, C., Cawood, F., Doggett, M., Guj, P., Stermole, F., . . . Tilton, J. (2006). *Mining Royalties: A Global Study of Their Impact on Investors, Government and Civil Society*. Washington DC: The World Bank.
- The Constitution of the Kingdom of Bhutan*. (2008).
- US Bureau of Mines. (1996). *Dictionary for Mining, Minerals and Related Terms*. US Department of the Interior.

MINING SECTOR AT GLANCE

Sangay Dendup¹

Mining in Bhutan

The mining sector has been identified as one of the five jewels of economy of the country due to its potential for economic growth and diversification. The Mines and Mineral Management Act (MMMA) 1995 and Mines and Mineral Management Regulations (MMMR) 2022 (amended) provides guidance to the sector to ensure scientific management of mineral resources and maximize the benefit to the nation and community. Further, the Economic Development Policy (EDP) 2016 and Mineral Development Policy (MDP) 2017 provides policy direction to the sector.

Given the rugged topography of the country, the mining in Bhutan is limited to open cast mining. In this context, the commonly adopted mining method is of drilling and blasting for extraction of minerals, while excavator-truck combination is used for loading and transportation of minerals and wastes.

Current Mining Scenario

Out of 84 mines and quarries, only 25 mines and 32 stone quarries in the country are currently in operation. Remaining mines and quarries are non-operational due to market issues and few quarries are recently leased. The regional distribution of the mines and quarries is shown in Figure 1. Further, there are total of 30 permit holders

for collection of minerals from the riverbeds and surface (mostly land developemnt). Four different types of minerals collected under the permit of Department of Geology and Mines (DGM) is as shown in the Figure 2.

Some of the minerals mined in Bhutan are gypsum, dolomite, quartzite, talc, limestone, marble, coal, iron ore, calc tufa, phyllite and construction stones. The Table 1 shows distribution of mines and quarries in each Dzongkhag. The allocation of mines generally follows first-come, first-serve principle while government allocate those strategic mines to State Own Enterprise.

The Dolomite mine in Chunaikhola, Gypsum mine in Khothakpa and Coal mine in the Eastern Bhutan are three large scale mines in Bhutan. These mines were auctioned for a period of 15 years. However, upon completion of auction periods, government allocated these mines to State Mining Corporation Limited (SMCL).

¹ Sangay Dendup, Mining Engineer, Department of Geology and Mines, MoEA, Thimphu, Bhutan
B.E. Mining Engineering, Acharya Institute of Technology, India. Email: sangaydendup@moea.gov.bt

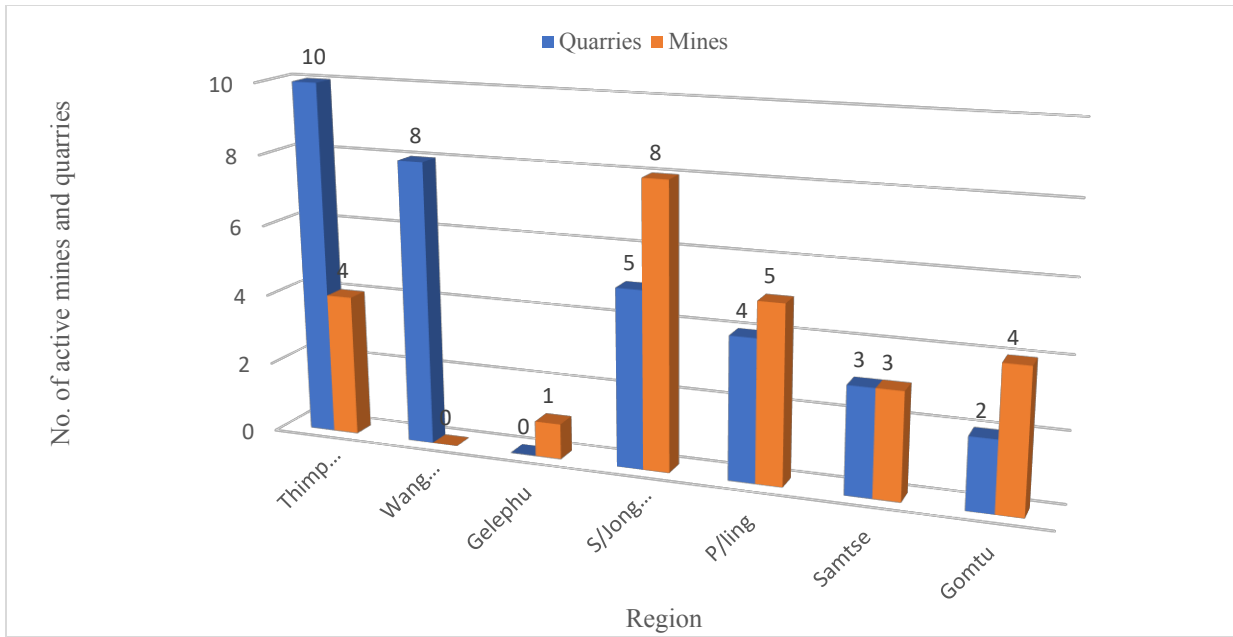


Figure 1. No. of active mines and quarries based on the Regions

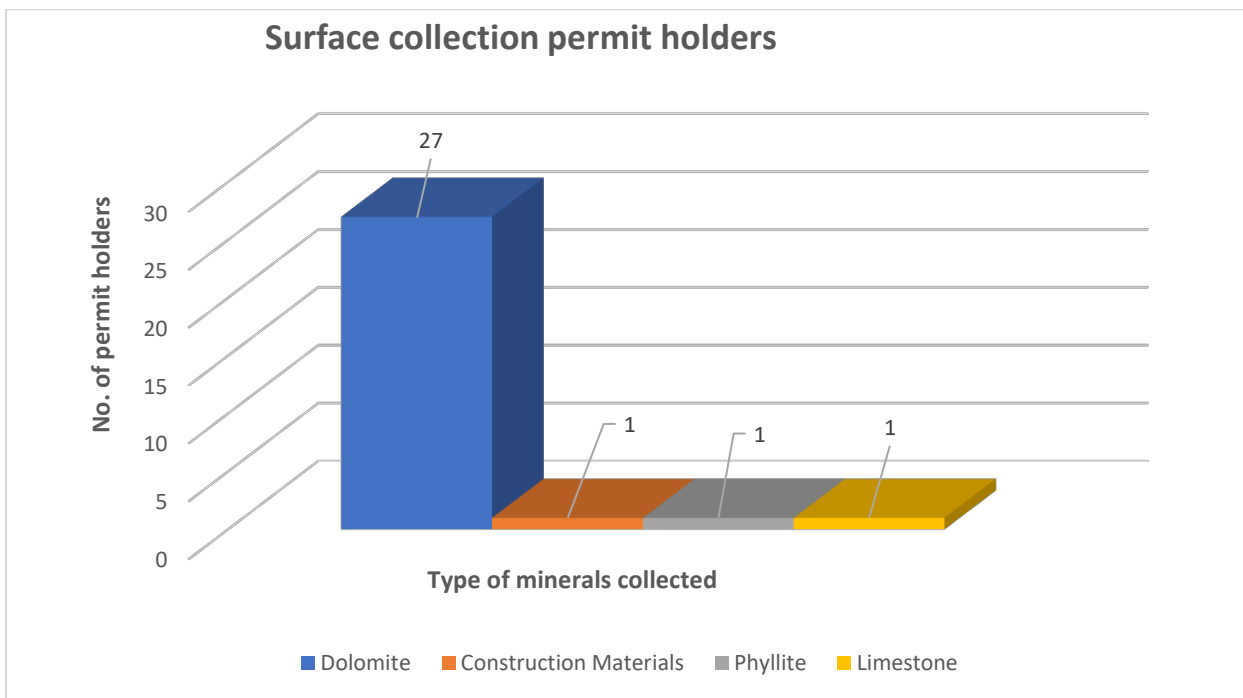


Figure 2. No. of permit holders

Table 1. Dzongkhag wise distribution of mines and quarries

Dzongkhag	Types of Minerals												
	Calc Tufa	Coal	Construction	Dolomite	Granite	Gyp-sum	Lime-stone	Marble	Iron Ore	Phyllite	Quartzite	Talc	Total No.
Bumthang			4										4
Chhukha			4								5	1	10
Dagana			3						1		1		5
Gasa													0
Haa													0
Lhuentse													0
Monggar			4										4
Paro			5				1						6
Pemagatshel			4			3	2						9
Punakha													0
Samdrup Jongkhar		5	0										5
Samtse	1		9	1			3				4		18
Sarpang													0
Thimphu			4				1	2					7
Trashigang			3										3
Trashi Yangtse			1										1
Trongsa			1										1
Tsirang			1										1
Wangdue Phodrang			9		1								10
Zhemgang			0										0
Total													84

Revenue contribution from Mining

Mining sector is the backbone of economic development. The economic growth of any nation is primarily driven by its richness in mineral resources and mining (e.g. Australia, Canada, Middle east countries, Mongolia, South Africa, US, etc.). It not only provides raw materials for industrial development, but it is also one of the main sources of foreign exchange through sale of minerals and its products.

The mineral wise production for the last five years (2017-2021) is shown in Table 2. The quantity of the mineral sale in domestic and export market in 2020 and 2021 is as shown in Figure 3 and Figure 4, respectively.

Revenue from mining is generated in form of royalty, mineral rent, land lease rent, auction fees (license), Corporate Income Tax, Business Income Tax and other forms of taxes. Its contribution has been increasing over the period. Royalty contribution (both domestic and export) in 2021 is shown in Figure 5. However, like any other sectors, the Mining has affected a lot by pandemic and the royalty contributions from Mining Sector is decreased to Nu. 312.79 million in 2021 from Nu. 456.70 million in 2020. This sector is reported as top ten major revenue contributors in 2017-18 as shown Figure 6.

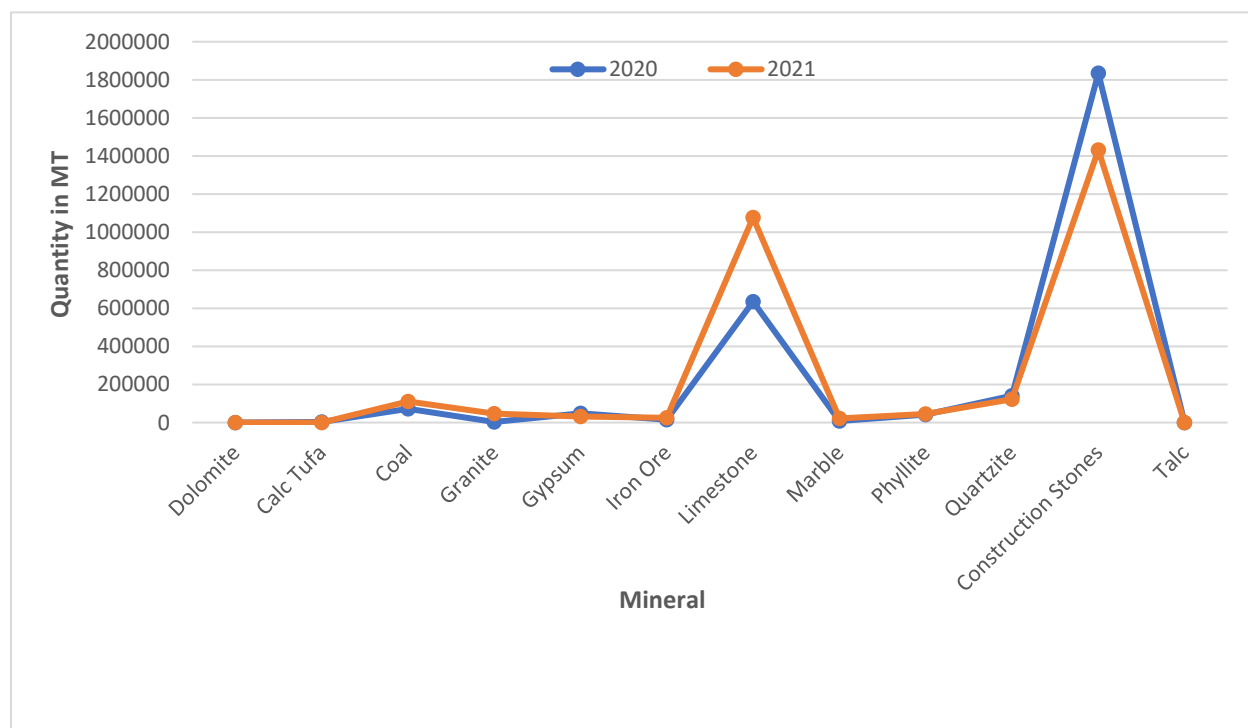


Figure 3. Sale of minerals in domestic market in 2020 & 2021

Table 2. Mineral production for the last five years

Sl. No.	Mineral in MT	Year					Total
		2017	2018	2019	2020	2021	
1	Calc Tuffa	0.00	12,323.80	22,079.10	3,753.12	0.00	38,156.02
2	Coal	161,526.74	186,823.75	184,784.50	72,838.11	111,544.69	717,517.79
3	Construction stones	3,828,254.00	3,730,975.36	3,325,418.60	2,157,386.97	1,806,488.88	14,848,523.81
4	Dolomite	2,536,693.31	2,821,116.44	3,027,517.70	1,232,106.76	2,041,154.90	11,658,589.11
5	Granite	26,364.04	6,293.33	3,391.30	3,568.01	47,334.35	86,951.03
6	Gypsum	328,127.99	461,128.12	490,595.50	331,049.57	403,752.98	2,014,654.16
7	Iron ore	32,974.37	37,843.08	36,864.20	14,734.12	25,916.73	148,332.50
8	Limestone	1,235,161.67	1,344,037.86	1,546,302.10	817,458.68	1,295,516.90	6,238,477.21
9	Marble	96,567.10	188,900.53	94,318.30	8,874.40	84,034.55	472,694.88
10	Phyllite	61,910.29	53,188.53	78,246.40	42,178.12	45,083.43	280,606.77
11	Quartzite	175,501.08	145,713.93	141,065.90	150,131.31	123,320.32	735,732.54
12	Talc	1,293.20	2,042.46	1,374.80	972.09	677.88	6,360.43

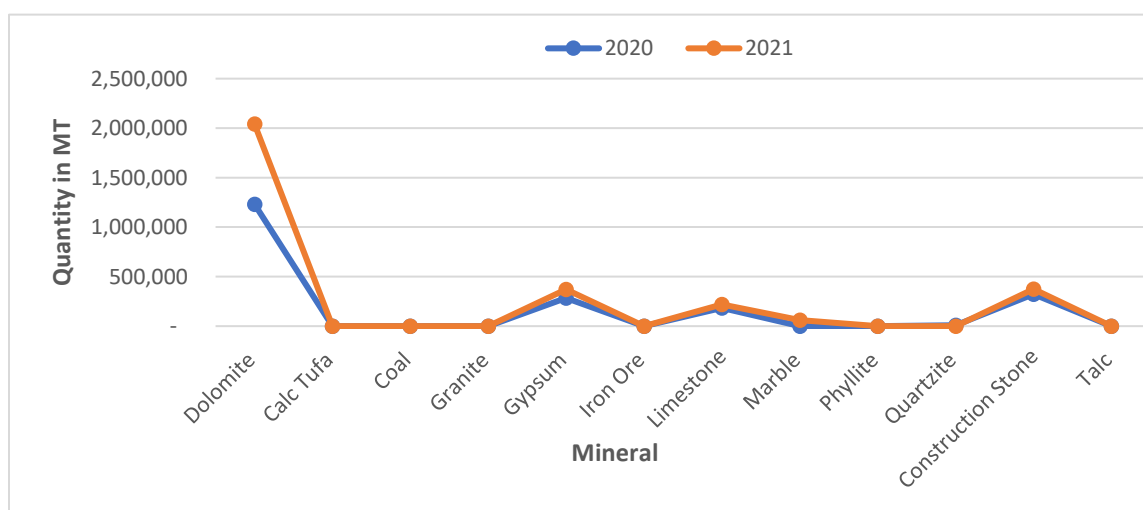


Figure 4. Export of minerals in 2020 & 2021

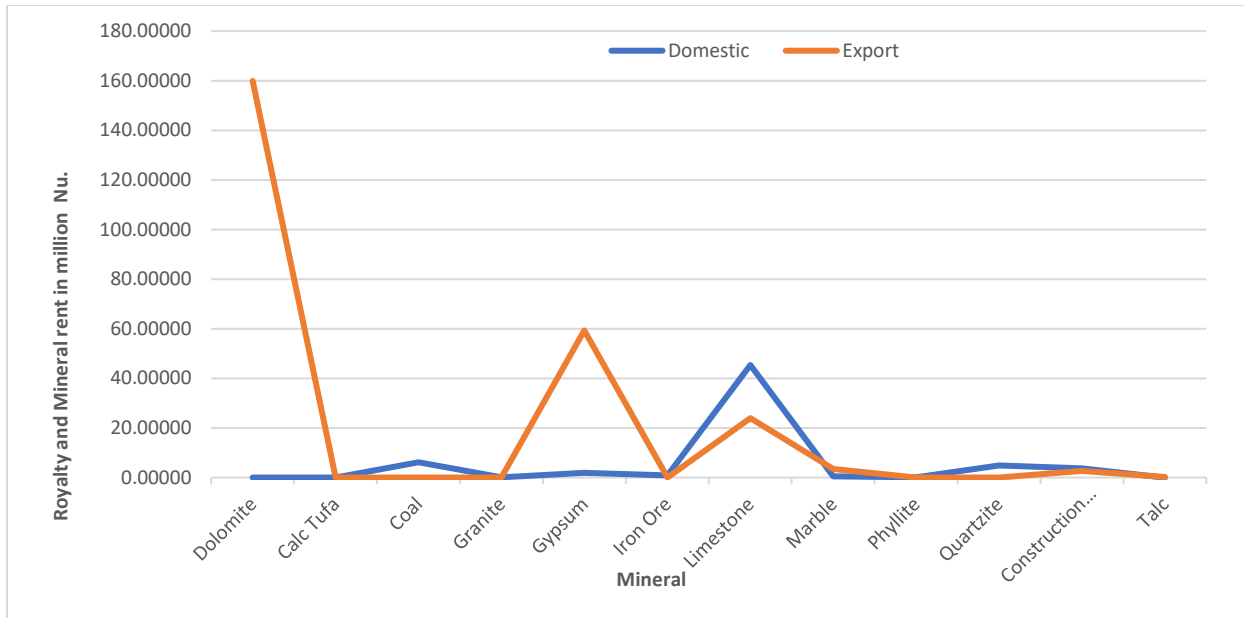


Figure 5. Royalty and mineral rent collected by sales of minerals in 2019

Royalty rates for Minerals

Until 2016, only unit-based royalty system was in practice. With the enactment of Revised Taxes and Levies Act of Bhutan 2016, the country has adopted an Ad Valorem royalty system for export of minerals. However, the domestic royalty is levied on unit-based system. Royalty of minerals for domestic market is incentivized to promote and sustain in-country mineral-based industry and infrastructure development. The existing rates of Royalty and mineral rent for domestic and export of minerals are shown in Table 3 and Table 4, respectively. The Royalty contribution to national exchequer from financial year 2014-15 to 2018-19 is shown in Figure 7. The increasing trend in the Royalty contribution over the period is mainly due to the introduction of Ad Valorem Royalty system. The Ad Valorem Royalty rates are levied on

Minimum Floor Price (MFP) established at the country exit point or invoiced value, whichever is higher. The existing MPF for different minerals is shown in Table 5.

Broader Economic Impact

Mining sector generates business opportunities such as hiring of machineries and trucks, supply of good and services, and opportunity for downstream industries. The GDP contribution from mining sector for last five years is shown in Figure 8. The GDP from mining sector is reported from the number of mines and stone quarries in the country excluding GDP contribution from sectors such as mineral based industries.

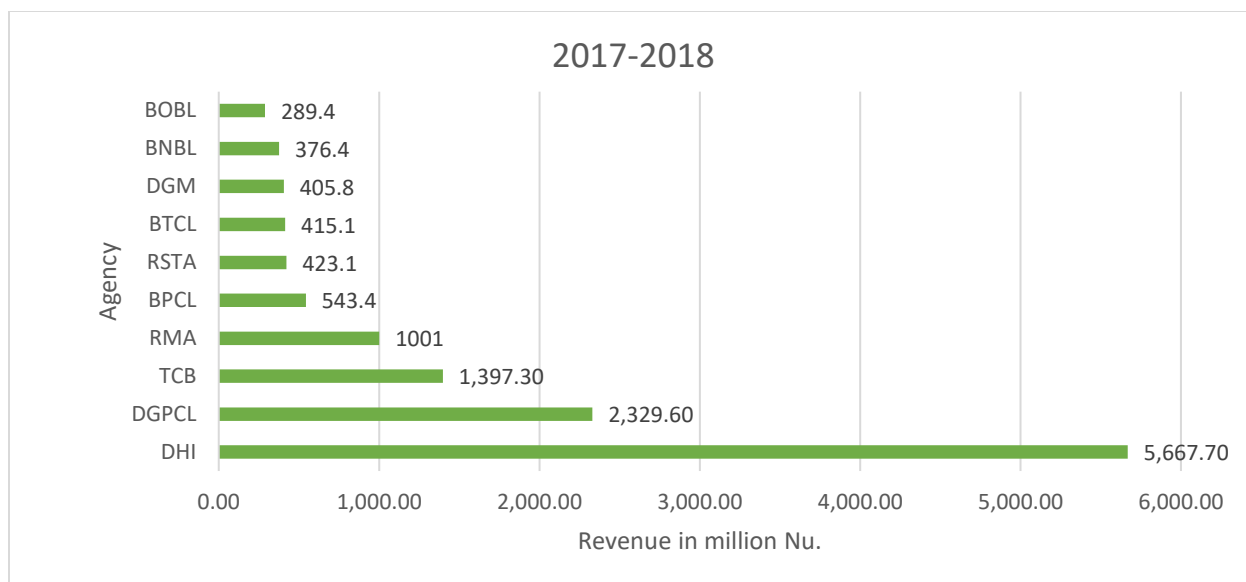


Figure 6. Major revenue contributors in 2017-18

Table 3. Existing Royalty and mineral rent rates for domestic sale

Domestic Royalty and Mineral Rent						
Sl. No.	Type of Mineral	Grade	Unit of Measure	Royalty (Nu.)	Mineral Rent (Nu.)	Total
1	Dolomite	All grade	MT	40	10	50
2	Limestone	All grade	MT	34	8.5	42.5
3	Marble	All grade	MT	34	8.5	42.5
4	Granite	All grade	MT	2.2	0.55	2.75
5	Construction stones	All grade	MT	2.2	0.55	2.75
6	Gypsum	All grade	MT	50	5	55
7	Talc	All grade	MT	40	10	50
8	Phyllite	All grade	MT	4	0.55	4.55
9	Quartzite	All grade	MT	30	5	35
10	Coal	All grade	MT	50	5	55
11	Iron Ore	All grade	MT	20	5	25
12	Shale	All grade	MT	34	8.5	42.5
13	Clay	All grade	MT	2.2	0.55	2.75

Table 4. Existing Royalty and mineral rent rates for mineral export

Ad Valorem Royalty and Mineral Rent for Export of minerals						
Type of Mineral	Grade	Unit of Measure	Minimum Floor Price (MFP) in Nu.	Royalty (%)	Mineral Rent (%)	Remarks
Dolomite	Powder (white)	MT	1200	6.5	<i>Amount equivalent to 10% of projected export Royalty or Domestic Royalty, whichever is higher</i>	
	Powder (Low grade black)	MT	550			
	Dolo-dust (low grade)	MT	450			
Limestone/ Marble	Lumps	MT	2330	8		
	Powder	MT	2700			
Construction stone	Boulder (Larger than 40mm)	MT	410	2		
	40mm	MT	540			
	30mm	MT	600			
	20mm	MT	625			
	10mm	MT	450			
	Dust	MT	300			
Gypsum	All grade	MT	1850	8	Export to India/ Nepal	
	All grade	MT	2735		Export to Bangladesh	
Talc	All grade	MT	3300	6.5		
Phyllite	All grade	MT	610	3.5		
Ferro-Silicon Grade Quartzite (Undersize)	30mm	MT	600	7		
	20mm	MT	625			
	10mm	MT	450			
	Dust	MT	300			
	Non-sorted	MT	500			
Coal	All grade	MT	8000	7		

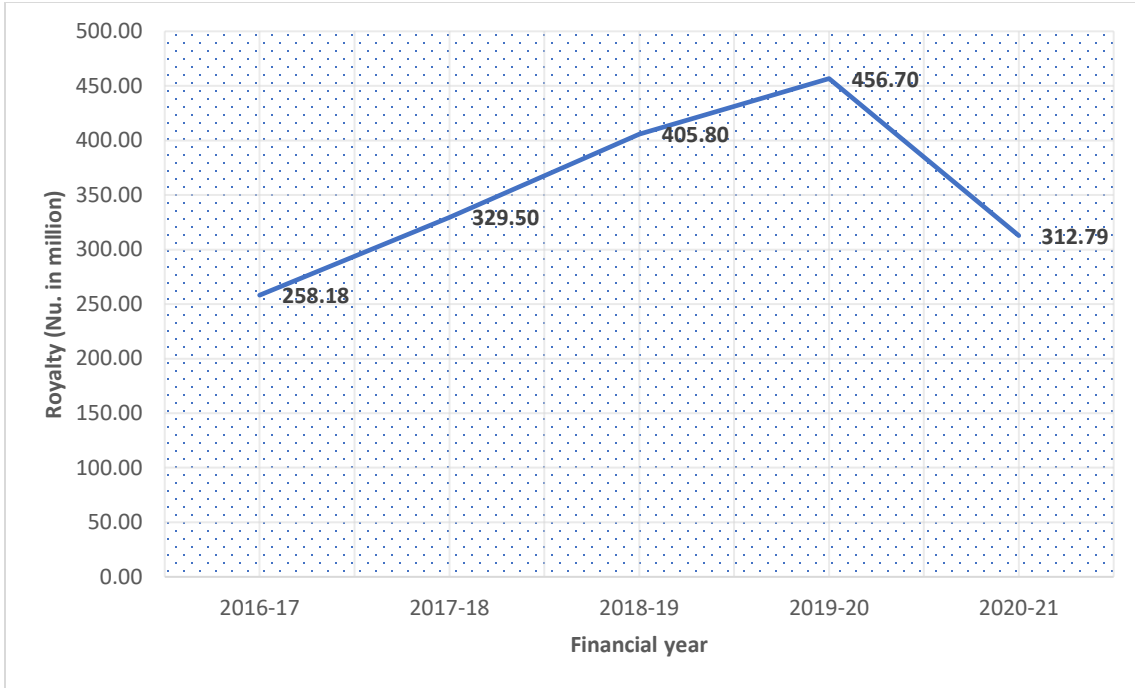


Figure 7. Royalty contribution to National exchequer from 2014-15 to 2018-19

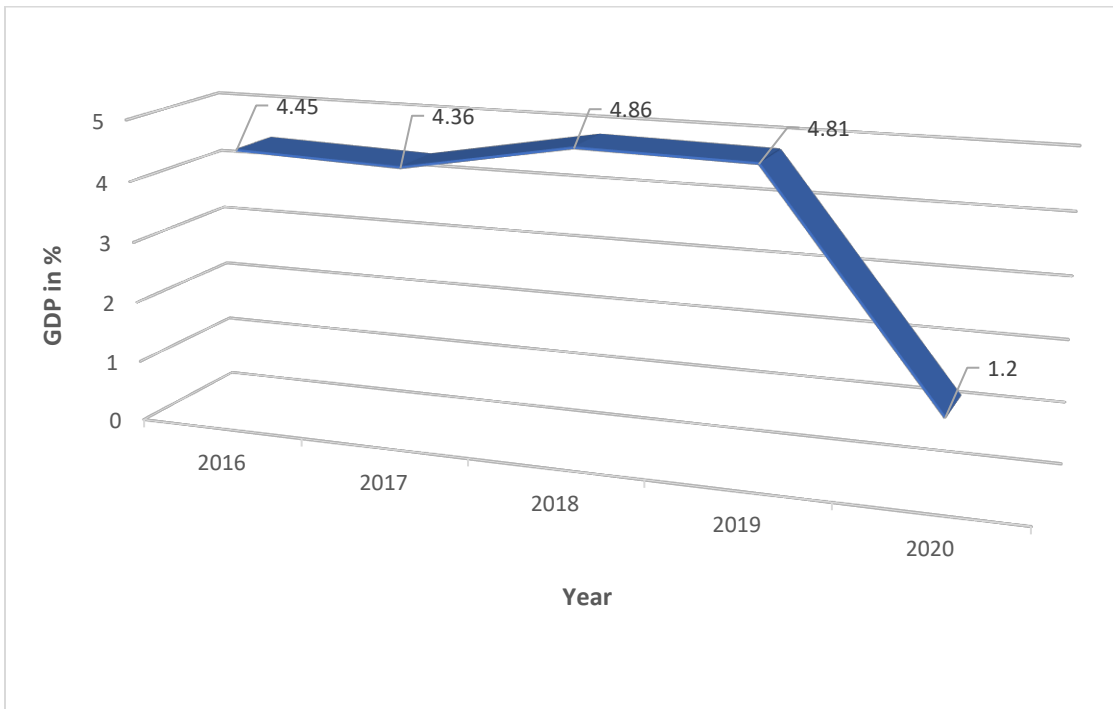


Figure 8. GDP contribution from Mining sector from 2015 to 2020

Table 5. Existing MFP for different minerals

Sl. No.	Mineral	Categories	Country	Rate (Nu.)
1	Dolomite	Lumps & Chips (White)	-	1070
		Powder (White)	-	1350
		Powder (Low grade black)	-	550
		Dolomite Dust (Low grade)	-	450
2	Limestone/Marble	Lumps	India	1860
		Lumps	Bangladesh	2440
		Power	India	2325
		Powder	Bangladesh	2800
3	Talc	Lumps	-	3300
		Powder	-	3545
4	Gypsum	All grade	India	2455
			Nepal	2150
			Bangladesh	2680
5	Coal	All grade	-	8000
6	Fero-silicon grade quartzite (Undersize)	30mm	-	620
		20mm	-	685
		10mm	-	525
		Dust (smaller than 10mm)	-	300
		Un sorted	-	500
7	Construction Materials	Boulders (larger than 40mm)	-	480
		40mm	-	555
		30mm	-	620
		20mm	-	680
		10mm	-	525
		Dust (smaller than 10mm)	-	300
8	Phyllite	All grade	-	610

Mineral Based Industry

The mineral based industries are directly dependent on mining sector for supply of raw materials. The government prioritize allocation of mines as captive to mineral based industry to maximize the benefit to the nations. Some of mines which are leased as captive mines in Bhutan are gypsum for Plaster of Paris (POP) factory, limestone for cement industry, quartzite

(high grade) for Ferro- silicon factory, granite for granite factory (for producing slab), and marble for powdering unit (for manufacturing wall putty). The mineral and mineral based products have become the most important an export commodity. The export data of 2020 shows that most of top ten commodities are mineral and mineral based products (Table 6).

Table 6. Top ten commodities export in 2020

Sl. No.	Commodity	Value in million Nu.
1	Containing by weight more than 55% of silicon	15,280,963,288.00
2	Boulders	2,483,869,290.00
3	Ferro-Silico-Manganese	2,271,386,480.00
4	Neither crushed nor ground	1,713,225,312.00
5	Portland pozzolana cement	1,497,888,432.00
6	Dolomite, not calcined or sintered, chips	1,399,490,693.00
7	Pebbles, gravel, broken or crushed stone, of a kind commonly used for concrete	1,194,313,489.00
8	Gypsum; anhydrite	872,979,685.00
9	Dolomite, not calcined or sintered, lumps and slabs	724,741,790.00
10	Ordinary Portland cement	719,786,023.00

Employment from Mining Sector

In addition to economic development, mining sector also provides job opportunity to the job seekers, addressing unemployment issues in the nation. Total jobs opportunities created from the mining sector for the year 2021 is 1612 of which 1366 are men and 246 are women as shown

in Figure 9. These numbers are ones that are directly employed in mining only. There are other employments involved in transportation of minerals from source to market. Further, minerals-based industries also provide job opportunity.

Reference

- Ministry of Finance. (2021). Bhutan Trade Statistics*
- Ministry of Finance. (2017-2018). National Revenue Report.*
- Ministry of Finance. (2016-2017). Revised Taxes and Levies Act of Bhutan.*
- National Statistics Bureau. (2021). National Accounts Report.*
- National Statistics Bureau. (2021). Statistical Yearbook of Bhutan.*
- Royal Government of Bhutan. (2016). Economic Development Policy.*
- Royal Government of Bhutan. (2017). Mineral Development Policy.*
- Royal Government of Bhutan. (1995). Mines and Minerals Management Act.*
- Royal Government of Bhutan. (2022). Mines and Mineral Management Regulations*

OVERVIEW OF GEMSTONES IN BHUTAN

Ugyen Namdol¹

What is a gemstone?

A gemstone may loosely be defined as a valuable piece of stone that can be used in jewelry. It may be a mineral such as rubies and emeralds, certain rocks like lapis lazuli and opal and occasionally organic materials such as amber and pearl. Gemstones are widely divided into two categories, precious stones which include diamonds, emeralds, sapphires and rubies. The remaining is collectively grouped under semi-precious stones.

Unlike other minerals, gemstones do not occur as ore deposit and tend to be scattered sparsely throughout a rock unit or crystallized as small aggregates in veins and cavities. To put it into perspective, the average grade of the richest diamond kimberlite pipes in Africa is about 1 part diamond in 40 million parts "ore." And rarity is one main factor that give gemstones their value.

Which factors determine the formation of gemstones?

The main factors required for gemstones depend upon availability of ingredients, temperature, pressure, time and space.

1. Ingredients – the composition of the source material determines which

minerals may form; to form tourmaline, boron must be available in the source; and the element beryllium is required to form the mineral beryl.

2. Temperature - At a higher temperature, a solution can hold more minerals in suspension. As the temperature drops, the amount of solid ingredients it can hold in suspension also decreases. When that happens, mineral crystals form. In fact, different minerals in the same solution will crystallize at different temperatures. For example, corundum might crystallize first. As the same solution continues to cool, topaz might form next, and finally quartz.
3. Pressure - It takes the proper combination of pressure and temperature for minerals to crystallize. For instance, diamond and graphite are polymorphs formed under different temperature-pressure (T-P) conditions. Diamonds form deep within the earth at depths of about 150-200 km where the temperature is 900-1300⁰ C and pressure as high as 45-60 kilo bars (source: Cape Town Diamond Museum) while graphite forms at lower T-P.
4. Time and space – Minerals need time to form large crystals. Also, the right combination of ingredients, heat, and pressure must last long enough for the

¹ Ugyen Namdol, Senior Geologist, Department of Geology and Mines, Thimphu, Bhutan.
B.Sc Geology, Osmania University, India, Email: unamdol@moea.gov.bt

minerals to crystallize. For example, obsidian (Figure 1) is an igneous rock which is formed when magma reaches the earth's surface and immediately cools in a matter of seconds which doesn't allow the formation of crystals and form glass instead.



Figure 1. Obsidian with no mineral crystals - instead a glassy texture. (Source: geology.com)

The minerals also need space to grow into large, well-developed crystals, which is crucial to a gemstone's value. When there is no space for crystals to grow, they form clustered masses without definite crystal habit.

Where can we find gemstones?

Most gemstones are found in igneous rocks and alluvial gravels, but sedimentary and metamorphic rocks also contain gemstones. Generally, gemstones are often associated with certain geological settings, but many kinds of gems occur in more than one environment. For example, garnet can be found in metamorphic rocks as well as in igneous settings.

Most gemstones are formed deep beneath the earth and are brought to the surface by

various processes. Gemstones like diamond are formed deep in the earth and brought to the surface by explosions of molten rock, and therefore, it is less likely to find such stones in Bhutan. Minerals like tourmaline and aquamarine, recrystallized slowly from hot fluids and gases as they cooled and solidified, far below the surface of earth. Others formed from liquids filtered into cracks and pockets in rock, like varieties of opal and quartz. Some, like garnet, formed when rocks were heated and pressurized by tectonics, and combined to form new minerals.

Geological environments in Bhutan which hosts gemstones:

Bhutan may not be very rich in gemstones like many other countries, mainly owing to the geological setting, but we do find some semi-precious gemstones in the country. The main rock types or geological setting that hosts these stones are described below.

a. Pegmatites:

Pegmatites are coarse-grained intrusive igneous rock body, occurring as dikes and sills, or veins. These rocks are usually rich in uncommon minerals and contain very coarse mineral crystals. In Bhutan, large pegmatite bodies are often associated with massive granite bodies. We find garnets, beryl and tourmaline in such formation.

- i. Tourmaline is a gemstone found in a wide variety of colors, which is one major factor that determines its worth. In Bhutan, we commonly come across a black (due to iron), opaque variety known as schorl, which is also the most common variety of tourmaline (Figure 2). It is not

used in jewelry but is popular in the field of healing stones. It is mainly found in pegmatites which host large individual crystals with well-developed crystal habit.



Figure 2. Schorl crystals in pegmatites with the lighter minerals' feldspar and quartz. (Source: DGM, MoEA)

- ii. Aquamarine is the blue variety of the mineral Beryl. Beryl comes in different colors, the most valuable being the green variety – Emerald. Emerald is considered a precious gemstone while aquamarine is a semi-precious gemstone despite being the same mineral. The classification of gemstones into precious and semi-precious stones took place as far back as in the 1800s and still hasn't seen much changes. The classification doesn't have any scientific backing and are frequently challenged by gemologists and the wider audience alike.

In Bhutan, aquamarine is also found in granites and granitic pegmatites (Figure 3). Most of the aquamarines encountered by the department were opaque to clouded, possess well developed hexagonal crystals and appreciable size. Transparent variety of the

stone with a strong blue color is considered more valuable.



Figure 3. Beryl (aquamarine) with well-formed hexagonal prism embedded in granite pegmatite. (Source: DGM, MoEA)

b. Metamorphic rocks:

These are rocks that have been altered by heat, pressure, and interaction with solutions. As discussed above, these are factors that are necessary in the formation of gemstones. In Bhutan, the dominant rock types are metamorphic rocks formed during the uplift of the Himalayas. The most common valuable mineral formed in these rocks in the country are Garnet and Kyanite, found mainly in gneiss, mica schist and amphibolite bodies.

- i. The garnets found in Bhutan are the almandine-pyrope variety, which is the most common variety of the gemstone. The color ranges from brownish red to purplish red, opaque and comes in varying sizes (Figure 4). The garnets form well developed, dodecahedron (12 faces) crystals and occur as porphyroblasts in the schist, gneiss and amphibolites.



Figure 4. Almandine-Pyrope garnet with well-developed crystal habit in varying sizes. (Source: DGM, MoEA)

- ii. Kyanite is another mineral found in metamorphic rocks like schist and gneiss that have been subjected to high pressure. Some varieties of kyanite may be considered valuable gemstones while most are not even in the semi-precious gemstones category.



Figure 5. Blue, bladed Kyanite crystal specimen. (Source: DGM, MoEA)

Kyanite derives its name from the Greek word kyanos which means ‘blue’ as it is the most common color for the mineral. The

kyanite found in Bhutan is commonly blue in color and exhibit the typical bladed crystal habit (Figure 5). Kyanite is mainly popular in the field of meditation and healing stones.

c. Veins and cavities in rocks:

As discussed under factors determining growth of minerals, space is one major requirement to get crystals of large size and well-developed habit. Fractures in the rock formation allow hydrothermal fluids to deposit minerals in these breaks which crystallize over time to large size. If the fracture is wide enough, very large crystals can form.



Figure 6. A smoky quartz cluster specimen. (Source: DGM, MoEA)

Quartz is one mineral that forms in this manner, and geodes of minerals like amethyst or chalcedony also form through a similar process.

d. Stream gravels:

When a primary gemstone deposit is weathered or eroded, more durable gemstones such as diamond, corundum and garnet may be transported by water and accumulated later in a secondary gravel deposit like along a river or in a delta. Such rich concentrations of gemstones are often called gem pockets and are convenient targets during mineral fossicking.

other semi-precious stones were mainly encountered during geological mapping.

Recently, the department has drawn the objective to map the occurrences of precious and semi-precious stones during the Toposheet wise geological mapping of the country, and therefore, the mineral information on such stones is expected to improve in the future.

Conclusion

The mineral information on precious and semi-precious gemstones in Bhutan is still very limited as no detailed prospecting has been carried out by the department. This is mainly due to lack of economic potential of such stones in the country. Garnets have been explored in the past for use as abrasives, and

References

Clark, D. *Gem Formation: How are Gemstones Created?* International Gem Society. <https://doi.org/https://www.gemsociety.org/article/gem-formation/>

Precious & Semi-Precious Gemstones: Explanation & Difference. (2022, October 25). *How to Find Rocks.* <https://howtofindrocks.com/precious-and-semi-precious-gemstones/>

SYLLABUS. (n.d.). <https://nature.berkeley.edu/>. <https://nature.berkeley.edu/classes/eps2/wisc/Lect1b.html>

TOPOSHEET WISE MAPPING MASTER PLAN 2021

Yonten Jamtsho ¹

Introduction

Bhutan is geographically located in the south-eastern part of Himalaya between the geo-coordinates of latitudes 26° N and 29° N, and longitudes 88° E and 93° E. It was formed during the Himalaya Orogenic process by the collision (continent to continent collision) of Indian plate and Eurasian plate which began 50 million years ago and the process is still continuing. As a result, numerous thrust faults, both active and inactive, have been formed in the country. These thrust fault zones are considered geologically fragile and unstable and are more susceptible to geo-hazards.

Geological Survey of India (GSI), Bhutan Unit from early 1960s to 1990s has extensively mapped the country on various scales. With limited accessibility, they have mapped only the accessible parts of the country on 1:50,000 scale. Similarly, with the institutionalization of the Department of Geology and Mines (DGM), the Department has taken the task of mapping the country.

Geoscience and Mineral Division (GMD) carries out regional mapping as one of the important activities of the Department since the initiation of Systematic Geological Mapping on Toposheet wise from the 9th Five Year Plan. Based on previous reports and data available in the Department's

Library, DGM and GSI has mapped only 19,359 sq.km (50%) of the total area on a 1:50,000 scale. For this purpose, Toposheet-wise Geological Mapping on 1:50,000 scale Master Plan 2021 has been prepared to guide and prioritize the unmapped areas of Bhutan.

Toposheet Maps

The established systematic method of carrying out geological mapping is based on the existing grid system developed by National Land Commission Secretariat (NLCS) known as Toposheet Map. Bhutan is divided into 77 grids with the grid dimension 15 s x 15 s ($\approx 25 \times 25 \text{ km}^2$) (Figure 1).

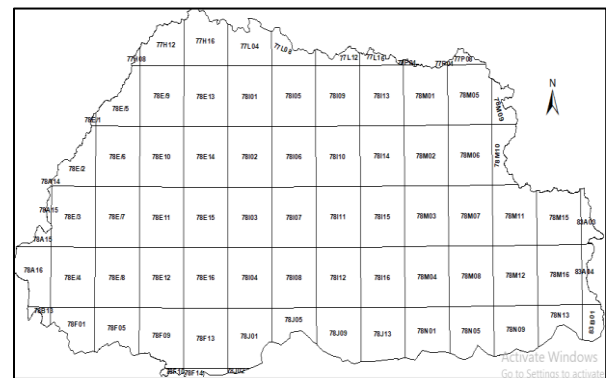


Figure 1. Map of Bhutan showing the Toposheet grid.

¹ Yonten Jamtsho, Senior Geologist, Department of Geology and Mines, Thimphu, Bhutan
B.Sc Geology, Osmania University, India, Email: yontenj@moea.gov.bt

National Level Coverage of Geological Mapping on 1:50,000 scale

Bhutan’s total area is 38,394 sq.km (*Land use and land cover of Bhutan 2016, DoFPS, MoAF*). Geological Survey of India, Bhutan Unit (GSI) initiated Geological Mapping on the 1:50,000 scale as early as the 1960s but the systematic geological mapping on Toposheet wise was started from the 9th Five Year Plan. As of June 2021, 19,359 sq.km (≈50%) of the total area is mapped on a 1:50,000 scale by DGM and GSI as shown in Figure 2, 3, 4, 5 and 6.

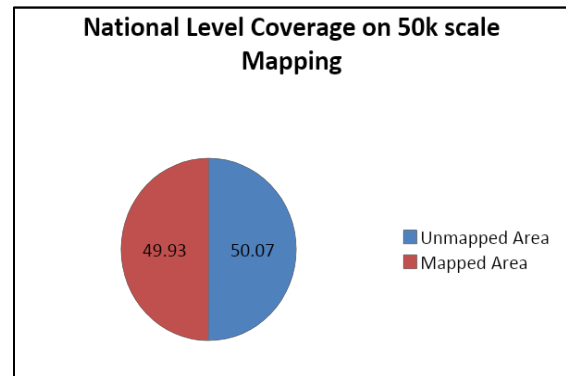


Figure 2. National Level Coverage of Geological Mapping on 1:50,000 scale in %

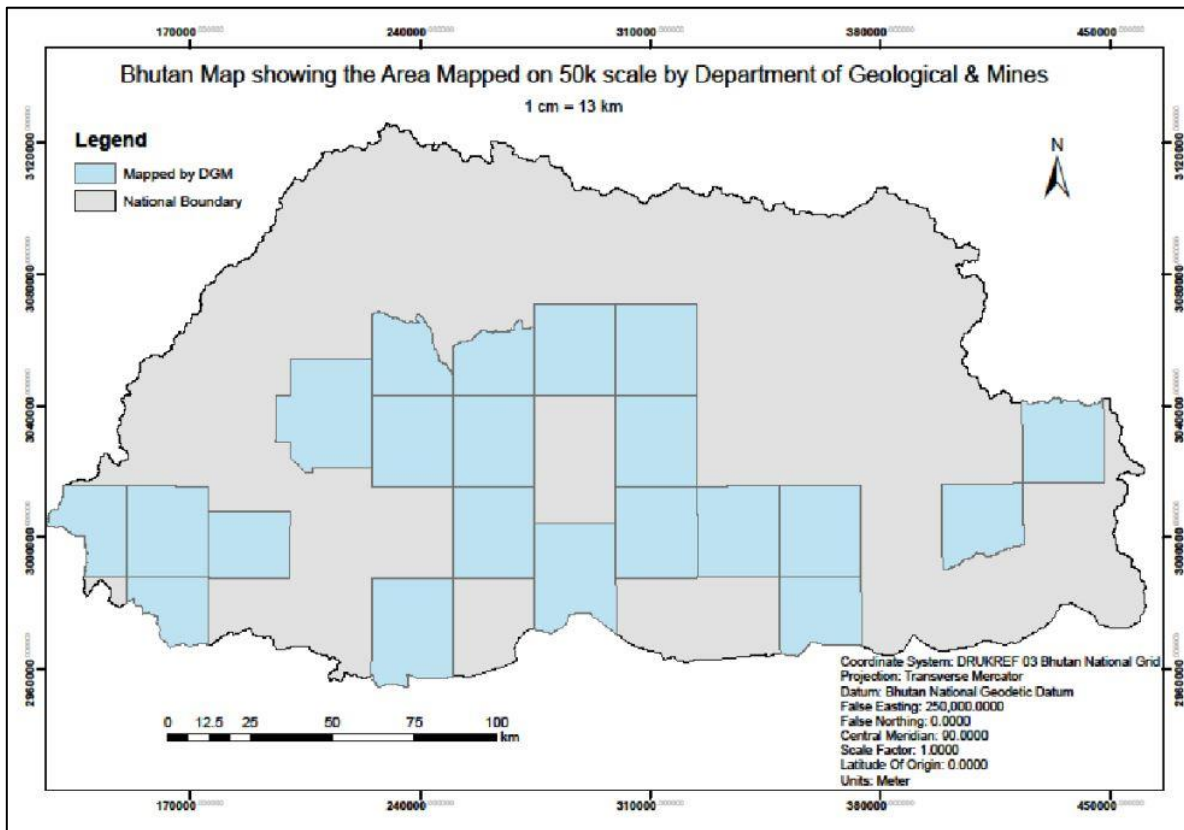


Figure 3. Bhutan Map showing the area mapped on 1:50,000 scale by Department of Geology and Mines

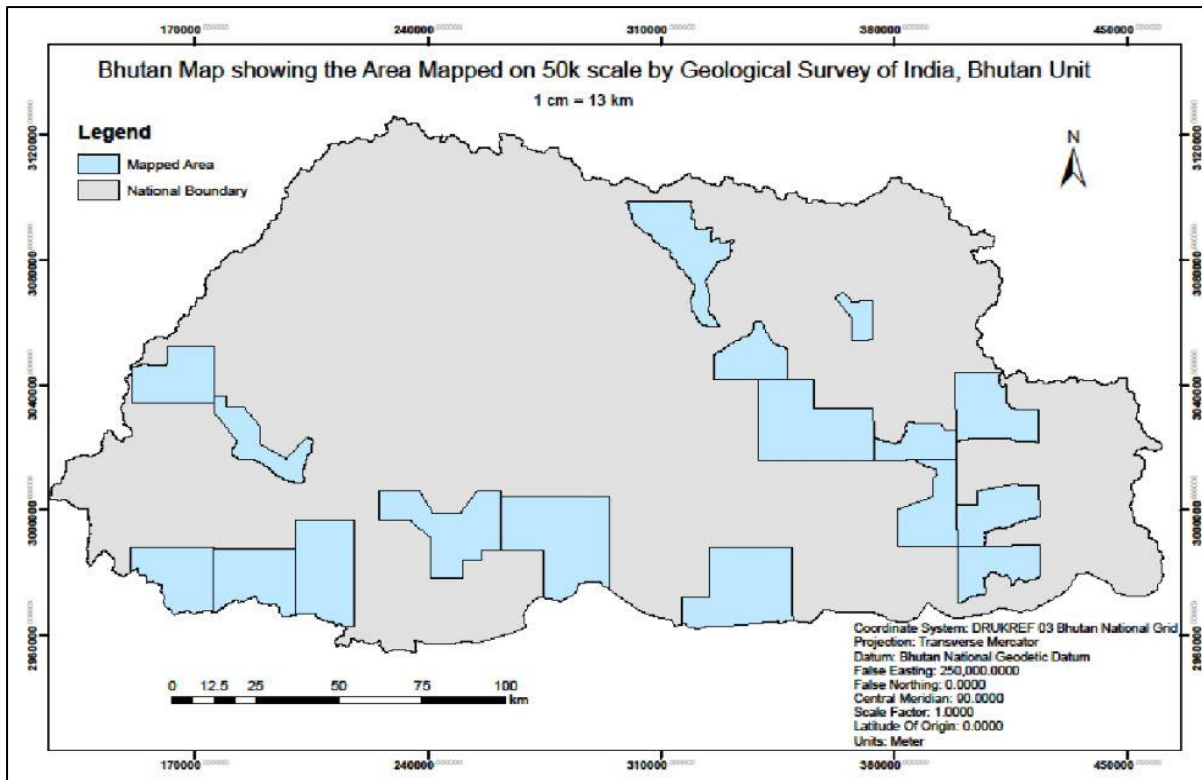


Figure 4. Bhutan map showing the area mapped on 1:50,000 scale by Geological Survey of India, Bhutan Unit

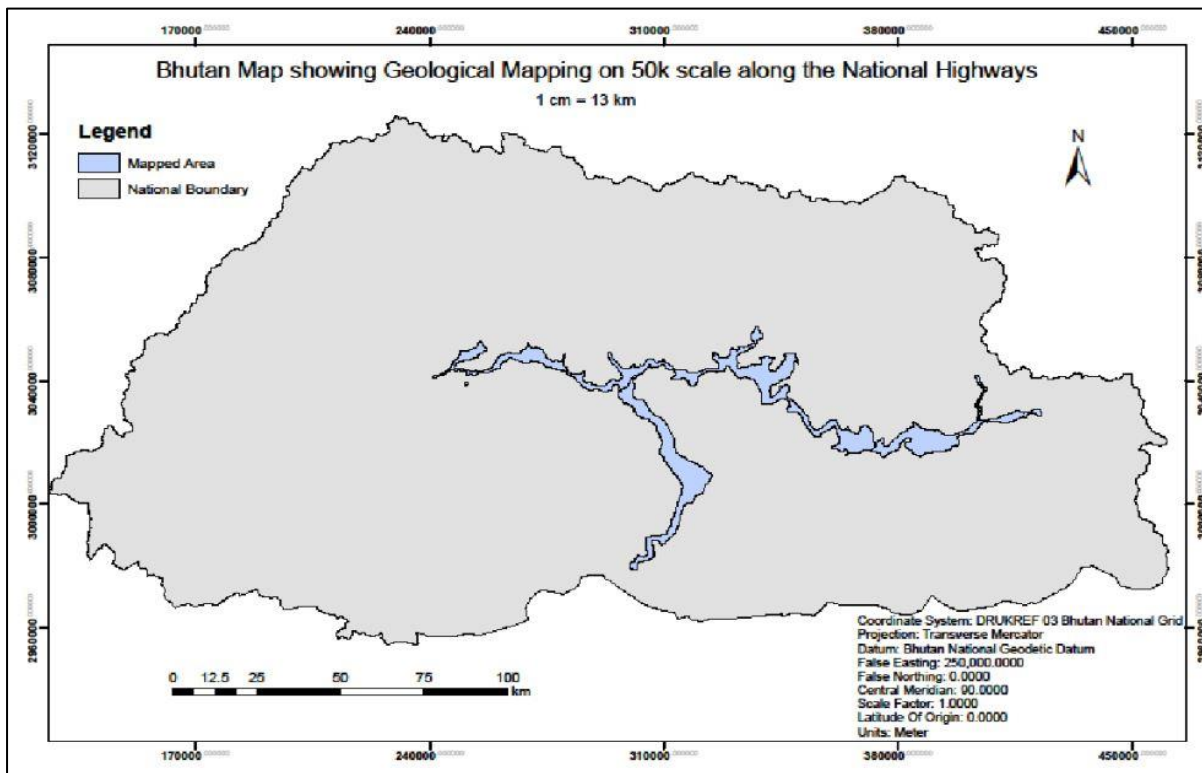


Figure 5. Bhutan Map showing geological mapping on 1:50,000 scale along the national highways by DGM & GSI

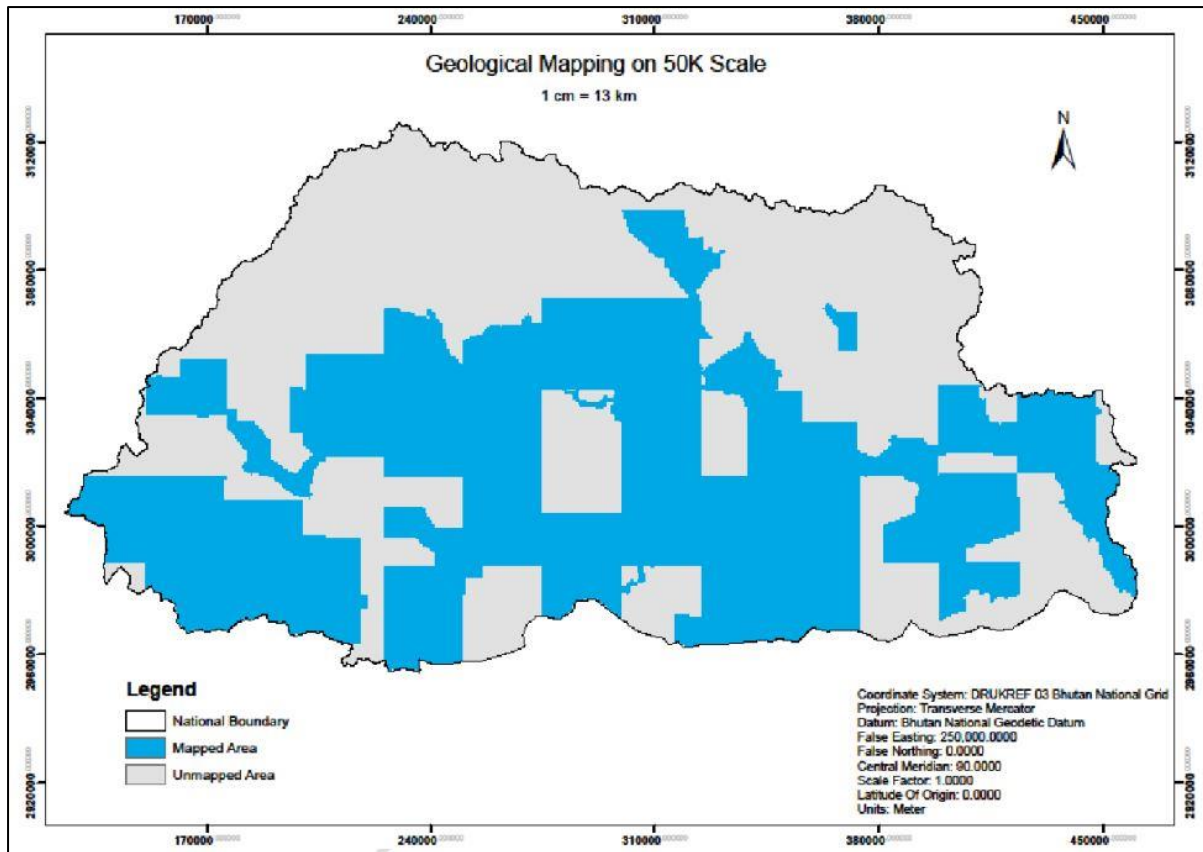


Figure 6. Bhutan Map showing combined geological mapping completed on 1:50,000 scale by DGM & GSI

Dzongkhag Level Coverage of Geological Mapping on 1:50,000 scale

Toposheet-wise Geological Mapping on the 1:50,000 scale was carried out in 19 Dzongkhags except Gasa. Statistically, none of the Dzongkhags are mapped 100%. As of fiscal year 2020-21, 13 Dzongkhags are mapped more than 50% of the total area and the rest of the Dzongkhags are mapped less than half of its total area. Based on the graph shown in Figure. 7 and 8, Wangdue Phodrang (2,439 km²) has the maximum area coverage followed by Zhemgang (2,094 km²).

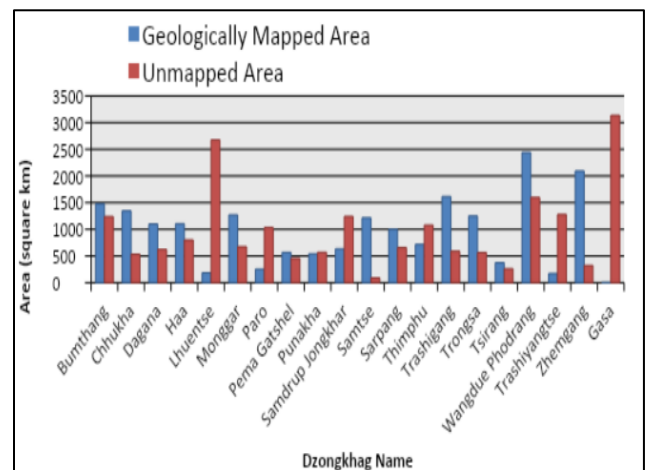


Figure 7. Bhutan Map showing Dzongkhag wise geological mapping completed on 1:50,000 scale

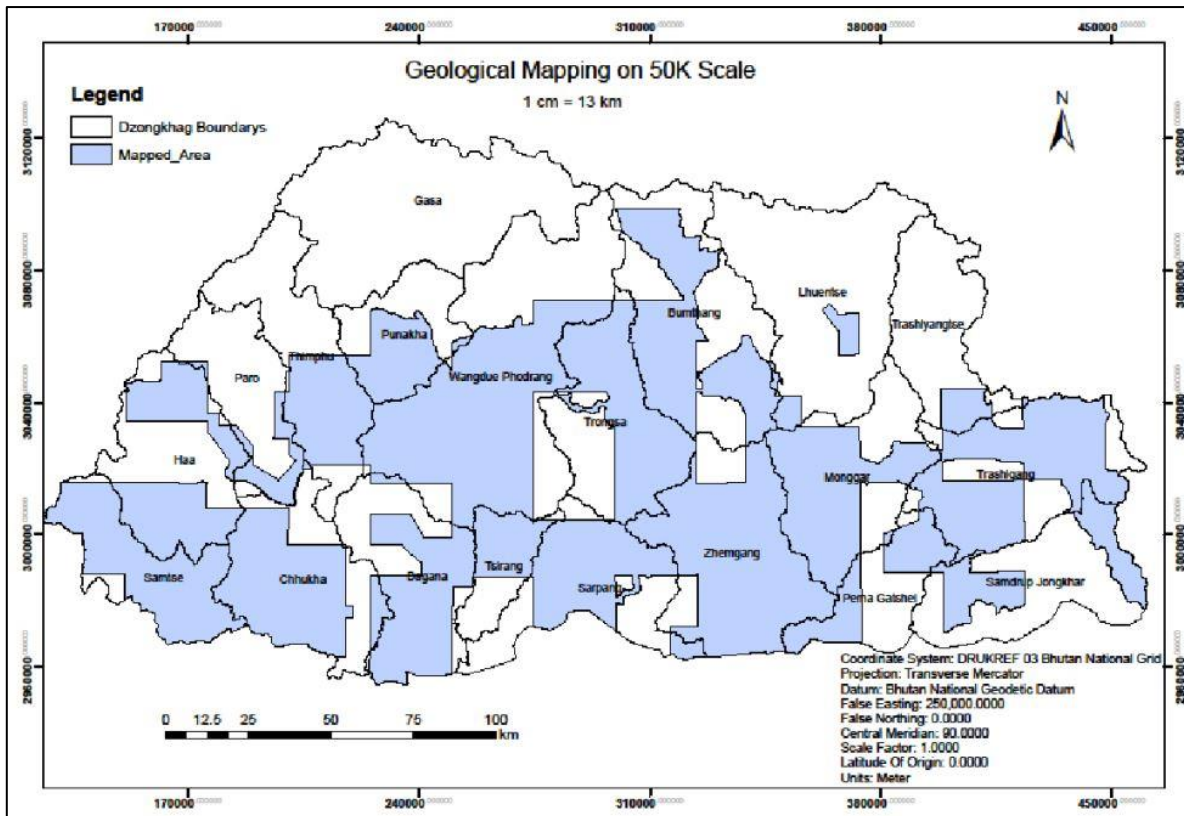


Figure 8. Graph showing the coverage of areas of each Dzongkhag

Methodology

Toposheet-wise geological mapping on 1:50,000 scale was conducted based on the mineral potentiality and the existing available information; other considerations include the unmapped toposheet, and continuity of the previous year's explored toposheet. Though these criteria are useful in the selection of toposheet for the geological mapping, it does not give the concrete rationale behind the selection. Therefore, with the development of this master plan it will provide a series of information on which Toposheet to be mapped.

Multi Criteria Analysis (MCA) Method is adopted for the selection of the Toposheet maps. It helps to select the most suitable location first based on the following sets of

criteria that influences each other and those that are independent in selection.

Evaluation Criteria for Toposheet Master Plan

The following are the parameters used for analysis while using the Multi Criteria Analysis (MCA) method (Table 1).

i. Unexplored/Unmapped Toposheet

This data is used as the primary criteria with the main objective of mapping the whole country on 1:50,000 scale. The unmapped toposheet has the maximum influence in the MCA method and accords an overall weightage of 52%.

ii. Regional Geology

Regional Geological data are very useful which gives general information on the lithology, structural, geomorphology and

mineral occurrences. Based on the existing data and information, it is evident that certain minerals (such as limestone, dolomite, coal, gypsum, talc and high-grade quartzite in lesser Himalaya and Sub-Himalaya) are concentrated in certain geological formations. Therefore, regional geological information is used in MCA method with the maximum priority to the Lesser Himalaya, Paro Formation followed by Chekha formation and Greater Himalaya Zone.

iii. Metallic Mineral

Currently Bhutan does not have huge metallic mines but few small-scale mining such as iron is carried out for domestic supply. The number of Metallic Mineral locations (Atlas of Mineral Resources of the ESCAP Region, Volume 8) are reported to have occurred in the country. Therefore, the available data is also used as MCA criteria with the maximum consideration given to iron ore deposit.

iv. Non-metallic Mineral/Industrial Minerals

The number of mineral-based industries in the country such as cement industries, calcium carbide industries and ferro-silicon factories use the raw materials from within the country. To keep these industries running, a continuous supply of raw materials is very important. Therefore, the existing non-metallic information is used in MCA method with substantial weightage.

v. Elevation

Physiographically, Bhutan Himalaya is divided into three major zones from south to north as Himalayan foothills, Inner Himalayas and the Greater Himalayas. The elevation ranges from less than 100 m in the

south to more than 7,000 m in the north. These broad ranges in elevation make the geological mapping challenging especially those areas which are located in the higher elevation.

vi. Infrastructure Development

Hydropower is one the major contributor of Bhutan's economy and currently, Bhutan has five operational hydropower plants which harness fraction of our country's potential to power generation. Bhutan has identified a number of hydropower sites (Power System Master Plan 2040) for future development. The identified location and sites are also considered for MCA method.

vii. Accessibility

Bhutan has been connected by roads in every corner over the years. However, there are still many areas which are not connected by road, and accessibility is considered as one of the main factors for mining to be economic. Therefore, road data is used for MCA.

viii. Protected Area

Bhutan is known for its diverse ecological settings, and currently more than half of the country's total area falls under reserved area as protected areas or network of biological corridors. To maintain sustainable economic growth through preservation and conservation of the natural environment, certain weightage is considered while performing MCA method.

Table 1. Evaluation criteria and weightage of MCA method

Sl.No	Criteria	Sub Criteria	Weightage	
1	Unmapped Area	Mapped Area	0	52%
		Unmapped Area	1	
2	Regional Geology	Sub-Himalaya, Lesser Himalaya, Paro Formation	3	11%
		Chekha Formation	2	
		Greater Himalaya	1	
3	Non-metallic Mineral	Asbestos, Sapphire/ruby,	1	8%
		Sand, Clay, Slate,	2	
		Beryl, Granite, Graphite	3	
		Calc-tufa, Quartzite, Coal	4	
		Dolomite, Gypsum, Limestone, Marble, Talc	5	
4	Metallic Mineral	Gold, Silver,	1	8%
		Copper, Lead -Zinc, Tungsten	2	
		Pyrite, Iron	3	
5	Elevation	> 4500m	1	8%
		3500 - 4500m	2	
		< 2500m	3	
6	Accessibility	>3.5km	1	5%
		2.5 - 3.5km	2	
		< 2.5km	3	
7	Protected Area	National Park, Wildlife Sanctuary and Reserve	1	4%
		Biological Corridors	2	
		Unprotected Area	3	
		No	0	
8	Future Infrastructure Development	Low Density	1	4%
		Medium Density	2	
		High Density	3	

Result and Analysis

Various parameters essential as a deciding factor for Geological Mapping have been integrated and analyzed using MCA method. The following toposheet map of Bhutan along with the rank is obtained as a result as shown in Figure 9 and Table 2.

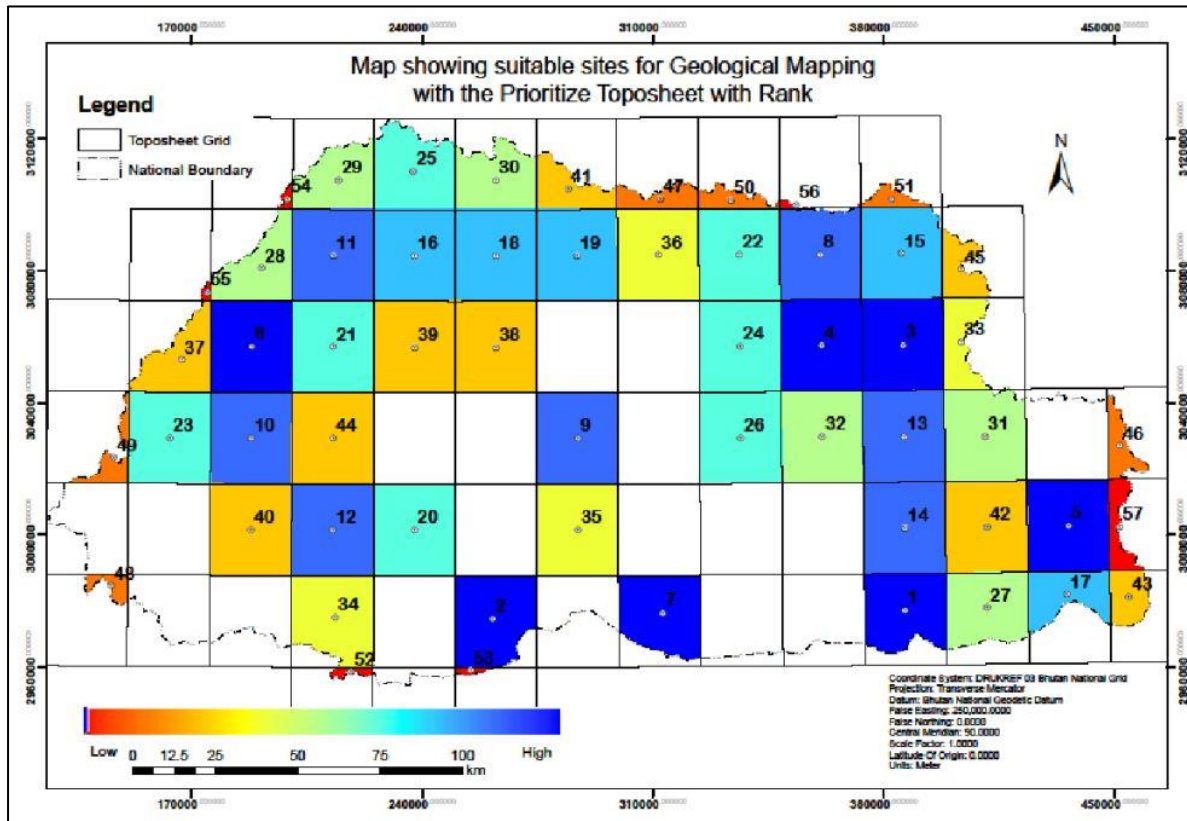


Figure 9. Map showing suitable site for geological mapping along with ranking

Table 2. Analytical result of toposheet along with a rank

Sl. No	Toposheet No.	Rank
1	78N05	1
2	78J01	2
3	78M06	3
4	78M02	4
5	78M16	5
6	78E/07	6
7	78J09	7
8	78M01	8
9	78I07	9
10	78E/08	10
11	78E/10	11
12	78E/13	12
13	78M07	13
14	78M08	14
15	78M05	15
16	78E/14	16
17	78N13	17
18	78I01	18
19	78I05	19

Sl. No	Toposheet No.	Rank
20	78E/17	20
21	78E/11	21
22	78I13	22
23	78E/04	23
24	78I14	24
25	77H16	25
26	78I15	26
27	78N09	27
28	78E/06	28
29	77H12	29
30	77L04	30
31	78M11	31
32	78M03	32
33	78M10	33
34	78F09	34
35	78I08	35
36	78I09	36
37	78E/03	37
38	78I02	38

Sl. No	Toposheet No.	Rank
39	78E/15	39
40	78E/09	40
41	77L08	41
42	78M12	42
43	83B01	43
44	78E/12	44
45	78M09	45
46	83A03	46
47	77L12	47
48	78B13	48
49	78A15	49
50	77L16	50
51	77P08	51
52	78F10	52
53	78J02	53
54	77H08	54
55	78E/02	55
56	77P04	56
57	83A04	57

Conclusion:

- Toposheet Mapping Master Plan has been developed using the Multi Criteria Analysis (MCA) method in ArcGIS. It helps to select the most suitable location first based on the following sets of criteria that influences each other and those that are independent in selection.
- This Master Plan is subjected to revision based on change in parameters and weightage.

References

Chang, K. T. (2008). Introduction to geographic information systems (Vol. 4). Boston: McGraw-Hill.

Publication of Geological Reports in DGM Library.

LANDSLIDE INVENTORY OF 15 DZONGKHAGS

Rinzin Wangmo¹

General Idea on landslide Mapping

Landslide Mapping is the process of documenting information about a landslide, in both large and small scale to analyze the risk and vulnerability of a slide in an area to provide mitigation measures. Although there are many types of maps used to show how vulnerable and dangerous landslides are, the most significant ones are given below:

Landslide Inventory Map: It displays the sites of each landslide as well as its historical movement, size, extent, and geological conditions. Generally, this map will provide the basic information on the landslide distribution of the country in a small scale and act as a building block to proceed further in vulnerability and risk assessment.

Landslide Susceptibility Map: It gives the future likelihood of landslide and its risk in the area, utilizing the basic information from the inventory map and collecting additional data like slope steepness, rock, and soil strength. The susceptibility map is done on a large scale and is more advanced.

Landslide Hazard Map: It uses information from the susceptibility map and extra comprehensive data to show the possibility of a landslide occurrence, the level of hazard, and the probable landslide extension in that specific location.

Landslide Risk Map: It gives information on the landslide potentiality and the extent of possible loss to people and properties. It utilizes the data collected in the Hazard map with the analysis of possible consequences.

Why Landslide Inventory?

Bhutan is a small country located between the two giants. Owing to its young and fragile nature, the country confronts many issues and difficulties, largely brought on by geohazards like landslides, earthquakes, and other natural disasters. Geohazard like landslides have caused significant problems in the country. However, there is no concrete landslide database to assist relevant stakeholders and agencies in analyzing and understanding the extent of risk.

In this regard, the Department has been carrying out Landslide Inventory mapping for the past 10 years. The main objective of this study is to identify critical landslides through remote sensing and ground-truthing and create a base map consisting of all the essential information on the landslides. These particulars will further assist in creating a susceptibility and hazard map that will allow respective personnel to understand the risk and vulnerability, the landslide will cause.

¹ Rinzin Wangmo, Geologist, Department of Geology and Mines, Thimphu, Bhutan.
B.Sc Geology, Osmania University, India, Email: rwanmo@moea.gov.bt

Methodology

In order to create an effective Inventory Map of the country, it is ideal to have a valid and uniform procedure to collect data. Generally, the inventory procedure is divided into two stages:

1. Desktop Study

The following activities fall under the desktop study:

I: Data extractions

Data was extracted from JAXA ALOS, AVINIR-2 data using Digital Image Processing (DIP) software, and from Land use and Land Cover Assessment data (LULC2016) published by Forest Resources Management Division, Department of Forests and Park Services (DoFPS). It was then converted to kml/kmz file.

II: Data Validation

The First-Hand Validation was done using a time series satellite imagery, Toposheet Data (1:50,000 scale maps), and other GIS processes. It also includes additional data from the Department of Roads (DoR), basic information from LG personnel, and past events and news from social media.

III: Selection of potentially critical landslides using Google Imagery

In this stage a team of experts sits together to identify critical landslides, based on the criteria listed below:

- i. Roads (including farm roads)
- ii. Settlement
- iii. Cultivation land

- iv. River (with stream orders, perennials, non-perennials)
- v. High tension lines
- vi. Important infrastructures and institutions
- vii. Proposed and existing hydro-power plants

IV: Selection of potentially critical landslides using multiple criteria in GIS

In this stage, critical landslides are selected based on the number of households affected. Only those landslides, where there are ten or more residences within its 1 km radius and may or may not contain high tension transmission lines, are chosen for field validation

2. Field Validation and Landslide Inventory

The field validation involves collecting the location of the landslide, validating its activity, and characteristics associated with the landslide. For this purpose, Brunton compass, handheld GPS, geological hammer, Google image map, plastic bags, digital camera, field notebook, and handheld lens were used. Local people were consulted to further understand the history of the slides. To maintain uniformity of data collection, a datasheet is prepared to collect data in the field.

3. Engineering Geological and Geotechnical observations of Critical areas

Besides gathering information on the location and characteristics of the critical landslides, seepages and lithological data of the area

were recorded. The colour, dip direction and amount, strike trend, joint set of the rock, joint gap width, and degree of weathering were observed and collected for the outcrop encountered in the area. Soil samples collected from the critical landslide areas were analyzed in the geotechnical lab of the department.

Inventory Statistics

1. Desktop Study

Although a total of 1,781 landslide points were extracted from the LULC 2016 data, a total of 267 landslide points were considered for field validation based on the criteria for selection of potentially critical landslides (Figure 1).

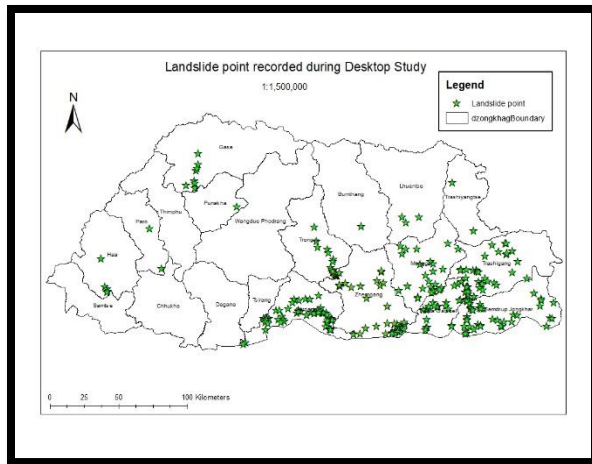


Figure 1. Landslide point recorded during desktop study

2. Field Validation

A total of 104 landslides were validated during the field study (Figure 2).

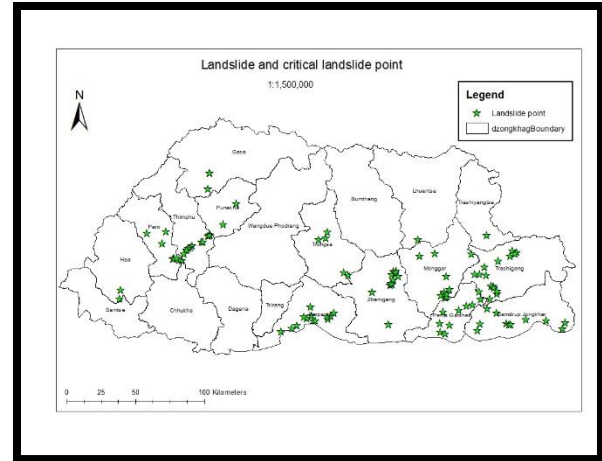


Figure 2. Landslide point recorded during field validation

Through analysis of the data, the following observations were made (Figure 3):

1. A large number of landslides have occurred in the southern and eastern parts of the country mainly due to poor geological and structural conditions combined with high precipitation.
2. Although natural factors can trigger landslides, it is often the anthropogenic factors such as poor drainage system, steep slope cuts and other developmental activities which aggravates slope stability.
3. 70% of landslides had no mitigation measures in place, whereas 30% had mitigations in place such as artificial walls, reforestation, and bioengineering.
4. Despite the fact that landslides have been an ongoing issue, many were left without proper mitigation measures and this could further cause greater risk and impact to the country.

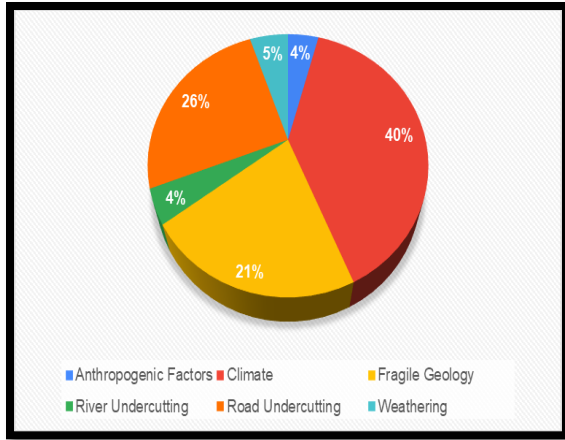


Figure 3. Factors triggering slope failure

3. Critical Landslides

Out of the 104 landslides validated, a total of 16 landslides have been identified as a critical landslide (Table 1; Figure 4) based on the following criteria:

1. Status of the landslide;
2. Size of the landslide;
3. Proximity to settlements and infrastructures;
4. Past damages and destruction caused by the landslide.
5. Probable impact the landslide might cause based on its past history.

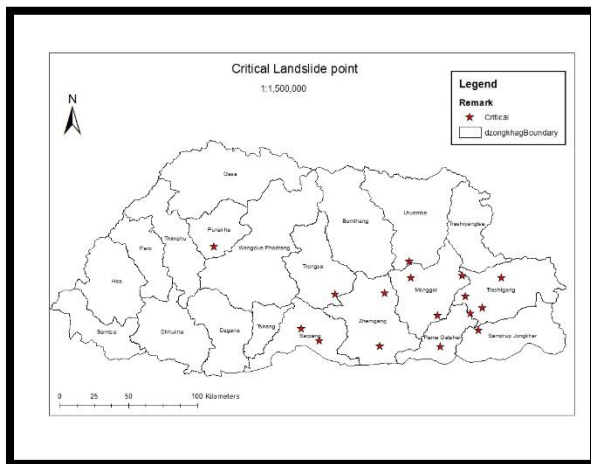


Figure 4. Critical Landslide point

Table 1. Critical landslide count

Sl.no	Dzongkhag	No. of Critical Landslide
1	Trongsa	1
2	Zhemgang	2
3	Sarpang	2
4	Trashigang	4
5	Mongar	3
6	Samdrup Jongkhar	1
7	Pema Gatshel	1
8	Lhuntse	1
9	Punakha	1

Constraint

Landslide inventory is a challenging activity but the data recorded from this activity can be used as a base map for further disaster related analysis and to provide the basic information of landslide distribution in the country. Detecting and accessing landslides in the field involves great risk and difficulties depending on the site. Some of the major constraints/limitation faced during the field study are as follows:

1. Desktop Study:

- Data availability:** Insufficient data greatly hinders the data processing and analysis to generate quantitative output.
- Software:** Although there are existing softwares like ArcGIS, QGIS, and R-studio that are generally used in mapping,

there is a need for more advanced software like Scoops3D that can make data processing and analysis more effective.

2. Field Validation:

- i. **Inaccessibility:** Some landslides are difficult to validate due to inaccessibility issues such as steep topography, thick vegetation or impermissible areas. Additionally, it is difficult to obtain historical data since the slide areas are distorted by various natural and anthropogenic factors.
- ii. **Risk to one's life:** Slide areas are often adorned with overlying boulders and loose debris. Although certain safety gears like helmets and goggles are used, there is still risk to those personnel validating the slide area.
- iii. **Time Constraints:** Each slide generally takes about 30 - 45 minutes to collect basic information of the slide area. Including travel time (both on foot and on vehicle), a maximum of 5 to 6 slides can be covered in a day.

Conclusion

Landslide inventory map is an essential type of mapping which provides basic and concise information on landslide distribution. Albeit being a challenging, risky and difficult activity with many limitations, the department has undertaken the Landslide Inventory of 15 Dzongkhag as one of the annual field activities from 16th March till

16th June 2022. A total of 267 landslides were recorded during desktop study which was then used as a reference during the field validation. 104 landslides were documented during the field validation out of which 16 landslides were identified as critical landslide.

Most of landslides were observed to be caused by climatic factors and further triggered by anthropogenic factors like unplanned constructions, steep road cuts and deforestation. Although a few landslides have been controlled through proper mitigations, majority have been left vulnerable without proper mitigation thus increasing the risk associated with slope failure.

Way Forward

The Landslide Inventory Map series is designed to understand the landslide distribution and their attributes. This information can be used for strengthening disaster resilient development, sustainable land-use planning and risk reduction in the country. The existing landslide inventory map shall be updated periodically in the future.

Reference

- Froude, M.J. and Petley, D.N. (2018). Global fatal landslide occurrence from 2004 to 2016. Nat. Hazards Earth Syst. Sci., 18, pp.2161- 2181.*
- Greewood, L.V., Argles, T.W., Parrish, R.R, Harris, W. and Warren, C. (2015). The Geology and Tectonics of Central Bhutan.*
- Sato, S., Chettri, J.K. and Ghaley, K.S. (2003). Geological Mapping on the Topo-Sheet No.78I/6, Wangdue Phodrang and Trongsa Area.*
- Singh, A.K. (2009). Causes of slope instability in the Himalayas. Disaster Prevention and Management, 18(3), pp.283-298.*
- Wangmo, N. and Chettri, L.K. (2014). Report on Inventory of Landslides and Field Verification under Chhukha Dzongkhag.*

OVERVIEW OF GEO-CHEMICAL LABORATORY

Ugyen Dorji¹, Radha Devi Sharma²

Introduction

The Chemical Laboratory Section is a unit under the Geoscience & Mineral Division (GMD), Department of Geology and Mines (DGM). The lab was set up in 1986, to provide basic laboratory support for the DGM's activities in mineral exploration and mapping. However, with the growing demand for laboratory services, the chemical laboratory has expanded its scope of services to private and public.

The Chemical laboratory has the following three sub-units:

- Sample processing unit
- Wet chemical lab
- Instrumentation lab

Roles & Responsibilities

Chemical laboratory is responsible for generating laboratory analytical data of rock and mineral samples by employing classical (gravimetric & volumetric) and instrumental methods, to support the following activities:

- Mineral prospecting and exploration
- Geological mapping
- Compliance monitoring of mines (captive mines) through sampling and lab analysis

- Testing of private samples

Analytical Instrument/Equipment

Analytical instruments and equipment available with the chemical laboratory are:

- Atomic Absorption Spectrophotometer (flame) (Figure 1)
- Flame Photometer (Figure 2)
- Multi-parameter meter (Figure 3)
- Microwave digestion unit
- Muffle furnace
- Digital weighing balance
- Hot air oven



Figure 1. Atomic Absorption Spectrometer

¹ Ugyen Dorji, Chief Chemist, Department of Geology and Mines, MoEA, Thimphu, Bhutan
Master of Environmental Science, University of Wollongong, Australia, Email: udorji@gmail.com

² Radha Devi Sharma, Assistant Chemist, Department of Geology and Mines, MoEA, Thimphu, Bhutan
B.Sc. Mathematic & Chemistry, Sherubtse College, RUB. Email: rdsharma@moea.gov.bt

General Information

Sample Type

Metallic and non-metallic minerals (industrial minerals) analyzed in the chemical laboratory are iron ore, base metals (trace metals), limestone, marble, dolomite, quartzite, gypsum, pyrite, phyllite, talc, graphite and coal.

Sample Quantity

The minimum quantity of sample required for analysis is as provided in the Table 1.

Table 1. Sample quantity

Sl. No	Sample Type	Quantity (Kg & lit)
1	Rock & mineral sample	3-5 kg/sample
2	Water sample	2 lit/sample

Turnaround Time (TAT)

Sample analyses are performed on a “First Come, First Served basis”. Lab reports are normally made available to clients within 7 working days from the receipt date of samples. However, sometimes the sample turnaround time (TAT) is affected due to large sample backlog resulting from sample reanalysis, instrument breakdown, water problem and engagement in urgent ad-hoc works.

In such cases, applicants are informed well in advance.



Figure 2. Flame photometer



Figure 3. pH meter

Analytical Services

- Determination of major & minor oxide composition in rock & mineral samples (%) – (SiO₂, acid insoluble (A.I.), Al₂O₃, Fe₂O₃, CaCO₃, MgCO₃, moisture & loss on ignition (LOI)(%).
- Determination of trace metals in geological samples (*ppm level*) – Cu, Pb, Zn, Fe, Mn, Co, Mg, Ca, Ni, Na & K.
- Proximate analysis – moisture content, volatile matter, ash content and fixed carbon (%).
- Determination of trace elements in water sample - *pH, conductivity, temperature, Ca, Mg, Na, K, SO₄, Cl, HCO₃, TDS, TS, TSS*).

Sample Test Charges & Revenue

The private samples are charged at a minimal rate to cover the costs of chemicals, reagents and other administrative costs incurred for the analysis of samples.

With the approval of the Ministry of Finance (MoF), DGM has revised the Lab Test Rates of 2010. The revision has come into effect from 1st of December 2021. The revised rates are as provided in the Table 2.

Table 2. Revised test rates, 2021

Sl. No	Description	Test rate/sample (Nu)
1	Complete chemical analysis of rock and mineral (major, minor and trace elements)	3000
2	Major oxide determination in rock and mineral samples (5 major oxides)	2000
3	Coal & Graphite (proximate analysis)	1500
4	Water analysis	1500

The revenue generated through test charges of private samples from 2010 to 2021 is shown in Figure 4.

As per the annual revenue graph (2010-2021), the maximum revenue generated is Nu. 0.336 m (2011) and minimum is Nu. 0.038 m (2018). The average annual revenue generated for the last 12 years is Nu. 0.093 m.

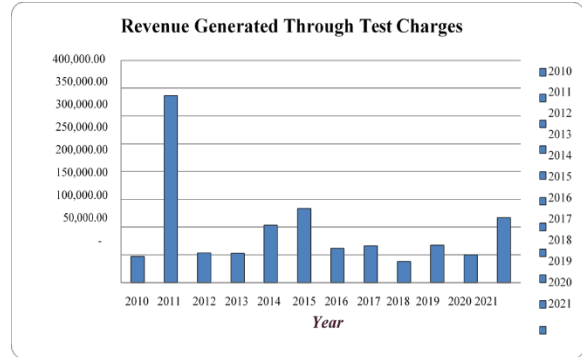


Figure 4. Revenue Graph (2010-2021)

Chemical Lab Services & Mines Administration System (MAS)

DGM has developed an online system called “Mines Administration System” (MAS). Like other services of the department, individual(s)/company(s) can avail chemical laboratory services through the MAS. Applicants can register into the system and select the required chemical lab services from the list of services available under the geoscience/chemical laboratory.



Sample Payment

The online sample payment system is not available at the moment, due to non-existence of online gateway payment services. Therefore, the mode of payment shall remain like before. After making the payment, the applicant is required to upload the receipt copy in the system for the analysis of the samples.

Sample Packaging

Samples must be properly packed in airtight polyethylene bags and plastic bottles, to prevent cross contamination of different samples. Every sample has to be individually packed and labeled with proper sample identification number while submitting to the laboratory without which the samples will not be accepted.

Sample Retention

Powdered samples (-100 mesh) are retained with the chemical laboratory for a period of 100 days from the date of submission of the test reports. However, the water samples are discarded right after the analysis is completed.

Contact Person(s) for Chemical Laboratory Section, DGM.

1. *Head, Chemical Laboratory Section, Geoscience & Mineral Division, DGM. (Ext: 217, 323096)*
2. *Chemist, Chemical Laboratory, Geoscience & Mineral Division, DGM. (Ext: 218, 323096)*